Design and Development of Fiber Optic Sensors for Quality Evaluation of various Liquid and Gaseous Media

Thesis submitted to

Cochin University of Science and Technology

in partial fulfillment of the requirements

for the degree of

Doctor of Philosophy

by

LINESH J.

INTERNATIONAL SCHOOL OF PHOTONICS
COCHIN UNIVERSITY OF SCIENCE AND TECHNOLOGY
COCHIN 682022

May 2014

Design and Development of Fiber Optic Sensors for Quality Evaluation of various Liquid and Gaseous Media

Ph.D. Thesis in the field of Photonics

Author

Linesh J.
Research Scholar
International School of Phonics
Cochin University of Science and Technology
Kochi - 682022
Email: lineshnair80@gmail.com

Research Advisor:

Dr. V P N Nampoori
Emeritus Professor,
International School of Phonics,
Cochin University of Science and Technology,
Cochin-682 022, Kerala, India
Email: nampoori@gmail.com

International School of Phonics
Cochin University of Science and Technology
Kochi - 682022

May 2014

Dedicated to My Parents,
and Teachers

Certificate

     This is to certify that the thesis entitled **"Design and Development of Fiber Optic Sensors for Quality Evaluation of various Liquid and Gaseous Media"** submitted by Mr. Linesh J., is an authentic record of research work carried out by him under my guidance and supervision in partial fulfillment of the requirement of the degree of Doctor of Philosophy of Cochin University of Science and Technology, under the Faculty of Technology and has not been included in any other thesis submitted previously for the award of any degree.

Kochi – 682022
05th May- 2014

                                                 Prof. (Dr.) V P N Nampoori
                                                     (Supervising Guide)

Declaration

I, Linesh J., do hereby declare that the thesis entitled **"Design and Development of Fiber Optic Sensors for Quality Evaluation of various Liquid and Gaseous Media"** is a genuine record of research work done by me under the supervision of Prof. V. P. N. Nampoori, Emeritus Professor, International School of Photonics, Cochin University of Science and Technology, Kochi–22, India and it has not been included in any other thesis submitted previously for the award of any degree.

Cochin 682022
05th May- 2014   **Linesh J.**

List of publications

International Journals:

1. **J Linesh**, K Sudeesh, P Radhakrishnan V P N Nampoori, "*Liquid Level SensorUsing Etched Silica Fiber*", Microwave. Opt. Technol. Lett. **52** (4), 883-885 (2010).

2. **J. Linesh**, T. M. Libish, M. C. Bobby, P. Radhakrishnan and V. P. N. Nampoori, "*Periodically Tapered LPFG for Ethanol Concentration Detection in Ethanol-Gasoline Blend*", Sensors & Transducers Journal, **125** (2), 205-212 (2011).

3. **J Linesh**, K Sudeesh, T M Libish, P Radhakrishnan and V P N Nampoori, "*Optical fiber sensor to determine critical mole fractions of alcohol-water binary mixtures*", Proc. of SPIE, **8173,** 81731U1-7 (2011)

4. **J Linesh**, T M Libish, M C Bobby, P Radhakrishnan and V P N Nampoori, "*Comparison of Thermal and Refractive index Sensitivity of Symmetric and Antisymmetric modes of Long Period Fiber Gratings*, AIP Conf. Proc., **1391**, 397-399 (2011)

5. T. M. Libish, **J. Linesh**, P. Biswas, S. Bandyopadhyay, K. Dasgupta and P. Radhakrishnan, "*Fiber Optic Long Period Grating Based Sensor for Coconut Oil Adulteration Detection***,** Sensors & Transducers Journal, **114** (3), 102-111 (2010).

6. T. M. Libish, **J. Linesh**, P. Biswas, S. Bandyopadhyay, K. Dasgupta and P. Radhakrishnan, "*Detection and analysis of paraffin oil adulteration in coconut oil using fiber optic long period grating sensor*", Optik, **122**, 1939– 1942 (2011).

7. T. M. Libish, **J. Linesh**, M. C. Bobby, P. Biswas, S. Bandyopadhyay, K. Dasgupta, P. Radhakrishnan, "*Fiber optic sensor for the adulteration detection of edible oils*", Optoelectron. Adv. Mater. Rapid Commun., **5** (1), 68-72(2011).

8. T. M. Libish, M. C. Bobby, **J.Linesh**, P. Biswas, S. Bandyopadhyay, K. Dasgupta, P. Radhakrishnan, "*The effect of grating period on refractive index sensitivity of long period gratings written in hydrogen loaded SMF-28 fiber*", J. Optoelectron. Adv. Mater., **13** (5), 491-496 (2011).

9. T. M. Libish, **J. Linesh**, M. C. Bobby, B. Nithyaja, S. Mathew, C. Pradeep and P. Radhakrishnan, "*Glucose Concentration Sensor Based on Long Period Grating Fabricated from Hydrogen Loaded Photosensitive Fiber*", Sensors & Transducers Journal, **129** (6), 142-148 (2011).

10. P.P.Anish, **J.Linesh** ,T.M.Libish ,S.Mathew ,P.Radhakrishnan, "*Design and development of diaphragm based EFPI pressure sensor*", Proc. of SPIE, **8173,** 81731V1-6 (2011).

11. Dibin Mary George, **J Linesh** and P Radhakrishnan, "*Design and Simulation of a Polymer Planar-Lightwave- Circuit Type 1X 32 Optical Power Splitter*", AIP Conf. Proc., **1391**, 467-469 (2011).

12. Libish T. M., Bobby M. C., **Linesh, J**., Nampoori, V. P. N., Radhakrishnan P, "Experimental analysis on the response of long period grating to refractive indices higher and lower than that of fiber cladding", Microwave. Opt. Technol. Lett, **54** (10), 2356-2360 (2012).

13. T M Libish, M C Bobby, **J Linesh**, S Mathew, C Pradeep, V P N Nampoori, P Biswas, S Bandyopadhyay, K Dasguptaand P Radhakrishnan, "Detection of adulteration in virgin olive oil using a fiber optic long period grating based sensor", *Laser Phys.* **23**, 045112 (2013).

International Conference:

1. **J Linesh**, K Sudeesh, A V Arun Babu, P K Shabeeb, V P N Nampoori, "*Imaging Of Corrugated Surface Using Tapered Optical Fiber*", International Conference on Fiber Optics and Photonics (PHOTONICS-2008), Dec 2008, IIT Delhi.

2. **J Linesh**, K Sudeesh, T M Libish, P Radhakrishnan and V P N Nampoori, "*Optical Fiber Sensor to Determine Critical Mole Fractions Of Alcohol-Water Binary Mixtures*", International Conference on Fiber Optics and Photonics (PHOTONICS-2010), Dec 2010, IIT Guwahati..

3. **J Linesh**, T M Libish, P Radhakrishnan and V P N Nampoori, "*LPFG Based Sensor to Monitor Ethanol Concentration in Ethanol Petrol Blend*", International Conference on Fiber Optics and Photonics (PHOTONICS-2010), Dec 2010, IIT Guwahati..

4. **J Linesh**, T M Libish, P. Biswas, S. Bandyopadhyay, K. Dasgupta, P. Radhakrishnan and V P N Nampoori, "*Effect Of Etching on the Refractive Index and Temperature Sensitivity of a Fiber Bragg Grating*", International Conference on Fiber Optics and Photonics (PHOTONICS-2010), Dec 2010, IIT Guwahati.

5. **J Linesh**, Dibin M G, T M Libish, Bobby M, P Radhakrishnan and V P N Nampoori, "*Optical Fiber Sensor to Determine Critical Micelle Concentration of Binary Mixtures of tert -Butyl Alcohol and Water*", International Conference on Contemporary Trends in Optics and Optoelectronics, Jan 2011, IIST Thiruvananthapuram.

6. **J Linesh**, T M Libish, Bobby Mathews, P Radhakrishnan and V P N Nampoori, "*Comparison of CO_2 and UV Inscribed LPFG for Ethanol Concentration Detection in Ethanol Blended Petrol*", International Conference on Contemporary Trends in Optics and Optoelectronics, Jan 2011, IIST Thiruvananthapuram.

7. **J Linesh**, T M Libish, M C Bobby, P Radhakrishnan and V P N Nampoori, "*Comparison of Thermal and Refractive index Sensitivity of Symmetric and Antisymmetric modes of Long Period Fiber Gratings*", Proceedings of International Conference on Light (optics'11), NIT Calicut, India, May 23-25, 2011.

8. A.V. Suresh Kumar, **J. Linesh**, P.P. Anish, K.M. Shafi and P. Radhakrishnan, *All Silica EFPI Fiber Sensor for Temperature Measurement*", International Conference on Sensors and Related Networks (SENNET'09), Dec 2009, VIT University, Vellore.

9. Anish P P, **J Linesh**, T M Libish, S Mathew and P Radhakrishnan , *"Design andDevelopment of Diaphragm-Based EFPI Pressure Sensor"*, International Conference on Fiber Optics and Photonics (PHOTONICS-2010).

10. T.M.Libish, **J.Linesh**, P.P.Anish, P.Biswas, S.Bandyopadhyay, K.Dasgupta and P.Radhakrishnan, *"Adulteration Detection Of Coconut Oil Using Long Period Fiber Grating",* International Conference on Fiber Optics and Photonics (PHOTONICS-2010), Dec 2010, IIT Guwahati.

11. T M Libish, **J Linesh**, Bobby Mathews, C.Pradeep and P Radhakrishnan, *"Fiber optic sensor for the adulteration detection of edible oils"*, International Conference on Contemporary Trends in Optics and Optoelectronics, Jan 2011, IIST Thiruvananthapuram.

12. Dibin Mary George, **J Linesh** and P Radhakrishnan, *"Design and simulation of a Polymer Planar-Lightwave-Circuit Type 1× 32 Optical power splitter"*, Proceedings of International Conference on Light (optics'11), NIT Calicut, India, May 23-25, 2011.

13. Bobby Mathews C, T. M. Libish, **J. Linesh**, P. Biswas, S. Bandyopadhyay, K. Dasgupta, P.Radhakrishnan, "A Long Period Grating based Biosensor for the Detection and Estimation of Cholesterol", International Conference on Fiber Optics and Photonics (Photonics 2012), IIT Madras, India, 2012

National Conference:

1. **J.Linesh**, V.K.Jayasree, K.S.Beena, V.P.N.Nampoori, *"Optic Fiber based Sensor to study Clay Consolidation"* DAE- BRNS National Laser Symposium (NLS)-2007, Dec 2007, MS University Baroda.

2. **J Linesh**, K Sudeesh, S. Mathew, V P N Nampoori, *"A Fiber optic probe to studyproperties of binary liquid mixtures"*, DAE- BRNS National Laser Symposium (NLS)-2009, Jan 2010, BARC, Mumbai.

3. **J Linesh**, K J Thomas, K Sudeesh, V P N Nampoori, *"Fiber Optic Temperature sensor based on Periodically tapered long period grating"*, DAE- BRNS National Laser Symposium (NLS)-2009, Jan 2010, BARC, Mumbai.

4. **J Linesh**, T M Libish, P Radhakrishnan and V P N Nampoori, *"Comparative Study of Long-Period Gratings Written Using an Electric Arc and CO_2 Irradiation for Ethanol Concentration Detection in Petrol"*, DAE- BRNS National Laser Symposium (NLS)-2010, Dec 2010, RRCAT, Indore.

5. **J Linesh**, T M Libish, Bobby Mathews, P Radhakrishnan and V P N Nampoori, *"Fiber Optic Sensor for Adulteration Detection in Ethanol*

Blended Petrol", 20th Swadeshi Science Congress, Nov 6-8, 2010, Central Marine Fisheries Research Institute (CMFRI), Kochi.

6. **J Linesh**, M C Bobby, T M Libish, P Radhakrishnan and V P N Nampoori, "Fiber Optic Alcometer Using Pva/Chitosan Polymer Blend", XXXVI OSI Symposium on Frontiers in Optics and Photonics (FOP11), December 3-5, 2011, IIT Delhi

7. **J Linesh**, Bejoy Varghese, T M Libish, M C Bobby, P Radhakrishnan and V P N Nampoori, *"Fiber optic humidity sensor based on TiO2 blended PVA coating"*, DAE-BRNS National Laser Symposium (NLS-21)-2012, February 6-9, 2013, BARC Mumbai.

8. **J Linesh,** T M Libish, M C Bobby, P Radhakrishnan and V P N Nampoori, *"Fiber Optic Alcometer using TiO$_2$ blended Chitosan/PVA polymer composite"*, XXXVII National Symposium of Optical Society of India, 23-25 Jan 2013, Pondicherry University, Puducherry

9. **J Linesh**, T M Libish, M C Bobby, P Radhakrishnan and V P N Nampoori, "Fiber Optic Alcometer using TiO2 blended Chitosan/PVA polymer composite" 22nd Swadeshi Science Congress, Nov 6-8 2012, Central Plantation Corps Research Institute (CPCRI), Kasargod

10. S P Sithara, Lyjo K Joseph, **J Linesh**, B Nithyaja, P Radhakrishnan, V P N Nampoori, ***"Thermal Characterization Of Ba3dyta3o12 Ceramic By Photoacoustic Technique"***, DAE- BRNS National Laser Symposium (NLS)-2008, Jan 2009, Laser Science and Technology Center (LASTEC), Delhi.

11. Mathew S, **Linesh. J**, Arif P. Ahamed,V P N Nampoori , C P Girijavallabhan, *"Effect of doping of Manganese on spectral properties of ZnS nanoparticles"*, DAE- BRNS National Laser Symposium (NLS)-2009, Jan 2010, BARC, Mumbai.

12. Lyjo K. Joseph, K. R. Dayas, **J. Linesh,** V. P. N. Nampoori ,P. Radhakrishnan, *"Thermal diffusivity measurement using photothermal technique- Fractal approach"*, DAE- BRNS National Laser Symposium (NLS)-2009, Jan 2010, BARC, Mumbai.

13. Lyjo K. Joseph, K. Sudeesh, M. N. Muralidharan, **J. Linesh**, V. P. N. Nampoori, P. Radhakrishnan, *"Thermal characterization of rare earth doped sol gel glasses using photoacoustic method"*, DAE- BRNS National Laser Symposium (NLS)-2009, Jan 2010, BARC, Mumbai.

14. P P Anish, **J Linesh**, T M Libish, Bejoy Varghese and P Radhakrishnan, *"A Metal Diaphragm Based Fiber Optic EFPI Temperature Sensor"*, DAE-BRNS National Laser Symposium (NLS)-2010, Dec 2010, RRCAT, Indore.

15. T.M.Libish, **J.Linesh**, P.P.Anish, S Mathew, V P Nampoori and P.Radhakrishnan, *" Fiber Optic Sensor for Detection of Adulteration in Sunflower Oil"*, DAE- BRNS National Laser Symposium (NLS)-2010, Dec 2010, RRCAT, Indore.

Acknowledgement

I wish to place on record my sincere and heartfelt thanks to my supervising guide Prof. V P N Nampoori, Professor Emeritus, International School of Photonics, CUSAT, Cochin-22, for his invaluable guidance, precious suggestions, critical assessment and constant encouragement which culminated in this thesis. His unwavering support throughout the research period as well as his pain-staking effort in reviewing the thesis is greatly appreciated.

I would like to express my sincere gratitude to Prof. P Radhakrishnan, Professor, International School of Photonics, CUSAT, Cochin-22, for his suggestions, encouragement and moral support during the years of my PhD.

My sincere thanks goes to Prof. C P G Vallabhan, Prof. V M Nandakumaran, Dr. Kailasnath, Dr. Sheenu Thomas and all other teachers of both ISP and CELOS for the support provided during the tenure of the research programme.

I would like to place on record my immense gratitude and appreciation to Mr. Libish T M, Mr. Sudeesh K, Mr. Bejoy Varghese, Mr. Mathew S, Dr. Lyjo K Joseph, Dr. Manu P. John, Dr. Rajesh S, Mr. Thomas K J, Dr. Sony T George, Mr. Bobby Mathews, Mr. Pradeep Chandran, Ms Dibin Mary George and other colleagues for infusing their constant motivation and support during the entire period of this work.

The helpful suggestions and assistance extended by all the office staff, librarian and my fellow researchers at the International School of Photonics are gratefully acknowledged.

I would like to mention that this thesis would not have been possible without the continuous support and love of my father Sri. Janardanan M K and Mother Smt. Thankamani K N. I profusely thank my sister for all her kindness, and encouragement.

Finally I wish to offer my regards to all the unmentioned people, who supported me in any respect during the completion of my thesis.

Linesh J

Preface

Adulteration refers to mixing other matter of an inferior and sometimes harmful quality with a superior one of the same kind. Adulteration can be categorized into two separate groups namely, incidental and intentional adulteration. Incidental adulteration occurs when foreign substances are added due to ignorance, negligence or improper facilities. Intentional adulteration, better known as economic adulteration, involves the deliberate addition of inferior materials to enhance appearance qualities and value for economical gain. Incidental and intentional adulteration of air, food and fuel are common in every society and to check the adulteration effectively, it is necessary to monitor the quality at the distribution point itself. The equipment for this purpose should be inexpensive, portable and easy to use while the measurement method should be quick and capable of providing test result within a very short time. Fiber optic sensors are an ideal choice for quality evaluation due to their well-known characteristics such as compactness, high sensitivity, in situ measurements, and immunity to external electromagnetic interference.

Fiber optic sensors of various configurations like intrinsic, extrinsic, intensity modulated, grating based, Fabry Perot cavity based etc were successfully developed by various authors for quality evaluation of different substances. This work aims at the design and fabrication of fiber optic sensors for checking the quality of liquid media like alcohol water mixture and ethanol blended petrol. The amount of humidity in ambient air is an important parameter to be measured and the development of fiber optic sensor for measuring the quality of air is reported. The thesis is divided into six chapters as follows

Chapter 1 gives a brief introduction to fiber optic sensors. Various techniques used for the fabrication of fiber optic sensors, a brief review of their applications and latest developments in the field are discussed.

Chapter 2 is devoted to the design and development of an extrinsic fiber optic sensor for determining quality of alcohol water mixtures. The fabrication and principle of operation of the etched silica fiber probe is explained. The sensor works on the principle of formation of Hydrogen bonding network created between alcohol and water molecules in the mixture. Different binary mixtures of alcohols like methanol-water, ethanol-water, 2-propanol-water and tert-butyl alcohol-water mixtures were studied and analyzed. The critical alcohol mole fractions obtained using the fiber optic probe for methanol, ethanol, 2-propanol and tert-butanol agrees well with literature values. Aqueous solutions of alcohols have found widespread use in several sectors like beverage industries, personal care products, food additives and chemical industries. The designed sensor can be effectively used to detect concentration of alcohols in their binary mixture with water. Since extrinsic modulation is used, the fiber sensor has its own disadvantages and such problems can be improved by using a wavelength modulated sensor like long period fiber gratings. The next chapter describes the fabrication of long period fiber gratings.

Chapter 3 discusses the basic theory related to long-period fiber gratings and the different mechanisms involved in the formation of thermal induced gratings. The fabrication of asymmetric long period fiber gratings (LPFG) in SMF 28 using fusion splicer and CO_2 laser is then elaborated along with the possible mechanisms of grating formation. The refractive index and temperature sensitivities of the fabricated LPFG's is shown in the chapter and are compared with that of a standard UV fabricated LPFG. The temperature response shown by the arc induced periodically tapered LPFG's

indicates that it can be used as temperature insensitive refractive index sensor. Moreover for many telecommunications applications spectral stability is of prime importance, and an LPFG with temperature insensitive attenuation band is an attractive feature.

Chapter 4 is devoted to the application of fabricated LPFG's in determining the quality of ethanol blended petrol. The basic theory related to the refractive index sensitivity of long-period fiber gratings is presented along with the response of the fabricated LPFG's namely UV, electric arc and CO_2 induced long period fiber gratings towards ambient refractive indices. Besides being insensitive to temperature, the arc induced LPFG shows better sensitivity among the three LPFG's in determining purity of ethanol blended petrol. The bare LPFG has limitations in sensing different parameters and the use of suitable coating materials can further diversify its application area.

Chapter 5 discusses the development of suitable polymer coatings for fiber optic hygrometer. The design and fabrication of fiber optic humidity sensors using polymers like poly vinyl alcohol and chitosan blended poly vinyl alcohol as hygrosensitive coatings are explained. The hygroscopic properties of PVA, chitosan and TiO_2 are discussed and the preparation polymer coatings are explained. Blending of chitosan in PVA helps to improve its mechanical strength and the available hydrophilic head groups per unit volume. Blending of titanium dioxide too increases hydrophilic heads and the humidity sensitivity of TiO_2 blended chitosan/PVA coating and TiO_2 blended pure PVA coating is discussed.

Finally the general conclusions and future work is presented in **Chapter 6**

CONTENTS

Chapter I

Introduction to Fiber Optic Sensors

1.1 Introduction

An optical fiber is defined as a flexible optically transparent fiber, usually made of glass or plastic, through which light can be transmitted by successive internal reflections. The history of light guidance starts with the experiment by Daniel Colladon and Jacques Babinet in 1841 [1]. In their experiment they demonstrated that a jet of water can guide light waves through it. John Tyndall included a demonstration of it in his public lectures and also wrote about the property of total internal reflection in an introductory book about the nature of light in 1870. During the early half of 20th century, experiments were carried out using bent glass rod to guide light but leakage of optical power was the hurdle. The solution to this problem was solved by Brian O'Brien, Haay Hopkins and Narinder Kapany in 1950 by proposing a lower refractive index coating termed as cladding to the waveguide [1]. The serious problem faced during that period was related to the absorption of light by glass and the attenuation in glass fibers was around 1000 dB/Km.

In 1965 Charles K Kao and George Hockham concluded that the loss in optical fibers is merely due to absorption by impurities and the fundamental limitation for glass light attenuation is below 20 dB/km, which is a key threshold value for optical communications [2]. This conclusion opened an intense race to find low-loss materials and suitable fibers for reaching such criteria which laid the groundwork for high-speed data communication in the Information Age. In 2009 The Royal Swedish Academy of Sciences awarded the Nobel Prize in Physics to Charles K Kao *"for groundbreaking achievements concerning the transmission of light in fibers for optical communication"*[3]. The fiber loss gradually got reduced and in 1970 Corning introduced the 20 dB/Km loss fiber making the optical fibers usable for communication purpose. The first generation optical communication used 850 nm light with a loss of 22dB/Km which then migrated to second generation where 1310 nm was used with 0.5dB/Km loss. Now we are in the third generation fiber optic communication where 1550

nm wavelength is used with loss in the range of 0.2 dB/Km, which is close to the theoretical limit based on Rayleigh scattering in an amorphous glass material [4]. Optical fibers provide unmatched transmission bandwidth, but light propagates 31% slower in a silica glass fiber than in vacuum. Wide-bandwidth signal transmission with low latency is emerging as a key requirement in a number of applications, including the development of future exascale supercomputers, financial algorithmic trading and cloud computing. The research today is focused on the development of hollow-core photonic-bandgap fibers which can significantly reduce fiber latency due to air guidance. Recently a fundamentally improved hollow-core photonic-bandgap fiber that provides a loss of 3.5 dB km−1 with a wide bandwidth of 160 nm was reported to transmit 37 × 40 Gbit s−1 channels at a 1.54 μs km−1 faster speed than a conventional fiber [5].

The field of fiber optic technologies has undergone tremendous growth and advancement and has revolutionized the telecommunications industry by providing high performance and reliable telecommunication links. The costs of laser diodes and optical fibers have drastically reduced along with the evolution of the technology. In parallel with these developments, fiber optic sensor [6-10] technology has undergone tremendous growth using the technologies associated with the optoelectronic and fiber optic communications industry. Over the past decades fiber optic sensors for the measurement of strain [11], temperature [12], pressure [13], velocity [14,15], magnetic field [16], electric current [17], acoustic signal [18] chemical and biological parameters[19-22]etc. have been reported. Though fiber optic sensors excel in performance, they face the problem of competing with the well-established conventional sensor technologies which provide adequate and reliable performance at low cost. However they have found excellent applications in harsh environment defined by high temperature, high pressure, corrosive/erosive, and strong electromagnetic interference, where conventional electronic sensors do not have a chance to survive. In some applications the ability to efficiently multiplex fiber sensors may be the criterion used to select fiber sensors over other technologies.

Fiber Optic sensors have inherent advantages such as immunity to electromagnetic interference (EMI), lightweight, small size, high sensitivity, multiplexing capability and large bandwidth over other technologies. Due to these inherent advantages fiber optic sensors have an edge over electronic

sensors and various ideas have been proposed and various techniques have been developed for various measurands and applications. A vide variety of sensors were reported during the past decades for sensing various physical and chemical parameters. Though some types of optical fiber sensors have been commercialized, only a limited number of techniques and applications have been commercially successful.

This chapter describes the structure and light guiding mechanism of optical fibers. The general principle of operation of fiber optic sensors is discussed. Various schemes used in fiber optic sensing technology to convert the measuring parameter into corresponding variation of optical properties are presented along with their merits and demerits. This chapter also presents a brief review about fiber optic sensors reported during the past decades in the area of quality evaluation.

1.2. Optical Fiber

A typical communication optical fiber is a cylindrical optical waveguide as shown in figure 1.1(a), consisting of a number of layers namely core, cladding, buffer and jacket. The outer layers, typically made of polymer or plastic materials, are the buffer and jacket and are for the purpose of reinforcing the mechanical strength. The center layer is made of doped glass and is the core of the fiber where most of the light energy is confined. The cladding layer is made of fused silica glass and has a refractive index (n_{cl}) less than that of the core (n_{co}). Thus light is guided inside the core as a result of total internal reflection (TIR) at the core-cladding interface [23,24].
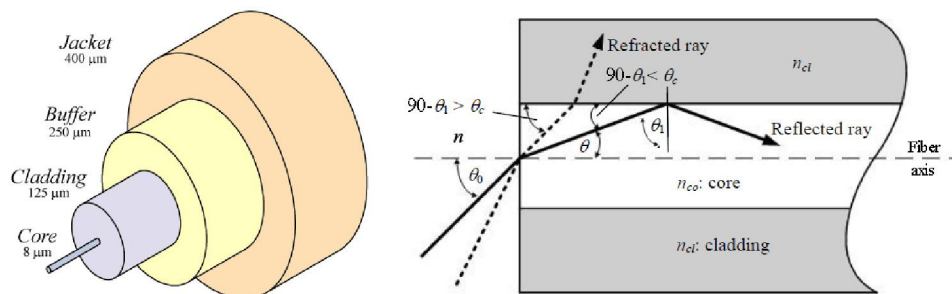
Figure 1.1 a) Structure of Optical Fiber b) Ray-optics representation of light propagation mechanisms in an ideal step-index optical fiber

If a beam of light is incident on the end face of a fiber within the angular cone specified by an entrance (or acceptance) angle θ_0, the light is confined to the core material by virtue of total internal reflection from the core-cladding interface [24], as shown in Figure 1.1(b). From elementary optics, total internal reflection is only supported in the fiber if the angle that the ray makes with the core-cladding interface is greater than the critical angle θ_c. By applying Snell's law to the air-fiber face boundary, the maximum entrance angle θ_0 can be deduced as

$$n\sin\theta_0 = \sqrt{n_{co}^2 - n_{cl}^2} \qquad (1.1)$$

where n is the refractive index of air.

The value on the left hand side of equation 1.1 is defined as the numerical aperture (NA) of the fiber. Since it is related to the maximum acceptance angle, numerical aperture defines the light gathering capability of the fiber.

Thus $\qquad NA = \sqrt{n_{co}^2 - n_{cl}^2} \qquad (1.2)$

1.2.1 Mechanism of Light Guidance and Fiber Modes

The basic mechanism by which light is transmitted through an optical fiber is total internal reflection (TIR). The simplest approach in analyzing light confinement is using geometrical optics. When a light ray incidents on the boundary of an optically denser medium (refractive index n_{co}) that separates it from a rarer medium (refractive index n_{cl}, $n_{co} > n_{cl}$) at an angle greater than the critical angle (θ_c) it will be totally internally reflected back to the denser medium itself. Thus light coupled to the core gets confined in it due to total internal reflection at the core cladding boundary.

Although it would seem possible for all light rays to propagate along the fiber if they are incident at an angle θ_1 ($\pi/2$-angle of incidence θ) from the core-cladding interface, where $\theta_1 < \theta_c$, this is not the case because the phase of the light wave also needs to be considered [24]. The phase that results after the wave has undergone two reflections from the core-cladding interface must be an integer multiple of the incident phase. If this condition is not satisfied, the wave will interfere destructively with itself and ultimately cease to propagate, thus restricting the light to certain discrete ray paths within the core. The total phase shift consists of two components namely the

shift in phase due to the distance traversed by the light wave and the Goos-Hanchen shift due to reflection from the dielectric (core-cladding) interface [23,24].

The phase change due to the former effect can be formulated from

$$\Delta = k_{co}S \tag{1.3}$$

where k_{co} is the propogation constant in the medium of refractive index n_{co} and S is the distance the wave travels in the material.

Since the free space propagation constant $k = k_{co}/n_{co} = 2\pi/\lambda$

$$\Delta = n_{co}kS = n_{co}2\pi S/\lambda \tag{1.4}$$

The Goos-Hanchen shift arising from a single reflection is calculated using the following expression [24]

$$\Delta_{G-H} = 2\tan^{-1}\frac{\sqrt{n_{co}^2\cos\theta - n_{cl}^2}}{n_{cl}\sin\theta} \tag{1.5}$$

As shown in figure 1.2, consider two rays, ray1 and ray2, associated with the same wave that is incident on the material interface at an angle $\theta < \pi/2-\theta_c$. The condition required for wave propagation is that all points on the same wave front must be in phase. This means that the phase change occurring for ray1 when traveling from point A to point B minus the phase change occurring for ray2 while traveling from point C to D must be an integer multiple of 2π. If S_1 is the distance between A and B and S_2 that between C and D, then from figure 1.2

$$S_1 = d/\sin\theta \tag{1.6}$$

where d is the radius of the fiber

$$S_2 = AD\cos\theta = (AE-AS)\cos\theta \tag{1.7}$$

$$S_2 = (d\tan(90-\theta) - d\tan\theta)\cos\theta = (\cos^2\theta - \sin^2\theta)\, d/\sin\theta \tag{1.8}$$

5
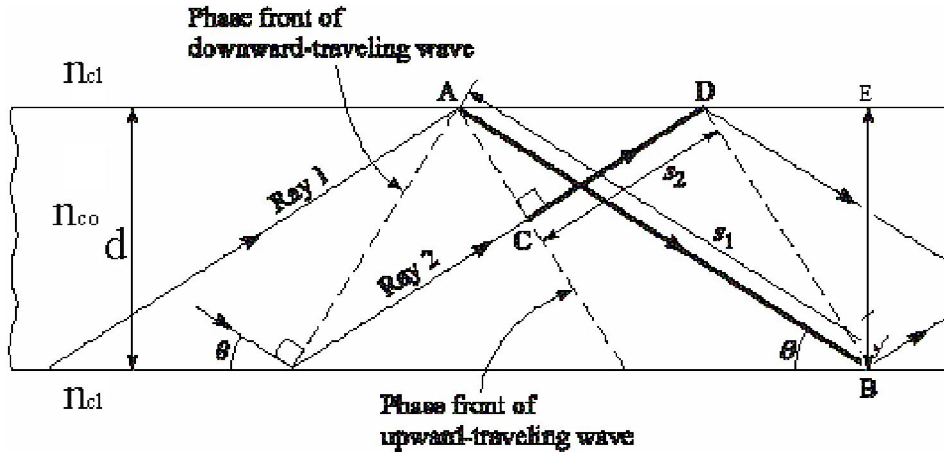
Figure 1.2 Light wave propagating along a fiber waveguide

Also ray1 undergoes two reflections and hence Goose-Hanchen shift occurs two times. Hence the requirement for wave propogation can be written as

$$\frac{2\pi n_{co}}{\lambda}(s_1 - s_2) + 2\Delta_{G-H} = 2\pi m \tag{1.9}$$

where m=0,1,2,3,…

Substituting for S_1, S_2 and Δ_{G-H} from equations 1.6, 1.8 and 1.5 into 1.9, equation can be reduced as

$$\tan\left(\frac{\pi n_{co} d \sin\theta}{\lambda} - \frac{\pi m}{2}\right) = \frac{\sqrt{n_{co}^2 \cos^2\theta - n_{cl}^2}}{n_{co}\sin\theta} \tag{1.10}$$

where the integer *m* denotes a discrete ray at an angle θ that is allowed for wave propagation. Thus only waves that have those angles θ which satisfy the condition in equation 1.10 will propagate in the waveguide.

Thus only light rays with discrete angles of incidence are allowed to propagate in the core region, each of which is associated with a specific fiber mode. An optical field distribution, or mode, corresponding to the minimum allowed ray angle (i.e. m=0) is called the fundamental mode, while all other guided modes (for which m ≥1) are higher-order modes. The larger the inclination angle θ at the core-cladding interface, the higher the order of the mode [24].

Guided modes obey electromagnetic wave theory and typically consist of a set of electromagnetic field configurations that form a standing-

wave pattern in a direction transverse to that of the fiber axis. Maxwell's equations in a linear, isotropic dielectric material having no currents and free charges are given below.

$$\nabla . \overline{D} = 0 \tag{1.11}$$

$$\nabla . \overline{B} = 0 \tag{1.12}$$

$$\nabla \times \overline{E} = -\frac{\partial \overline{B}}{\partial t} \tag{1.13}$$

$$\nabla \times \overline{H} = \frac{\partial \overline{D}}{\partial t} \tag{1.14}$$

where ε is the permittivity and μ is the permeability of the medium. The electric flux and magnetic flux are given by D=εE and B=μH

By taking the curl of these equations, the wave equations for the electromagnetic fields are obtained as

$$\nabla^2 E = \mu\varepsilon \frac{\partial^2 E}{\partial t^2} \tag{1.15}$$

$$\nabla^2 H = \mu\varepsilon \frac{\partial^2 H}{\partial t^2} \tag{1.16}$$

Here ∇^2 is called the scalar Laplacian and the choice of coordinate system is critical in solving the wave equation. If a cylindrical coordinate system {r,ɸ,z} with the z axis lying on the axis of the wave guide is defined for a cylindrical fiber, then the solutions of the wave equations take the form

$$E = E_0(r,\phi)e^{j(\omega t - \beta z)} \tag{1.17}$$

$$H = H_0(r,\phi)e^{j(\omega t - \beta z)} \tag{1.18}$$

which are harmonic in time t and coordinate z. The parameter β is the z component of the propagating mode while E and H gives the electric and magnetic filed distributions of the mode.

As discussed using ray theory, the electric field distribution has a peak value corresponding to points where two positive wave fronts interfere constructively, and a trough is formed for constructive interference between negative phase fronts [23]. Destructive interference occurs when positive and negative phase fronts cause total field cancellation at a certain point. Thus a standing wave is formed in the transverse direction that varies periodically along the fiber's axis. This standing wave has a period corresponding to the wavelength given by [23]

7

$$\lambda_0 = \frac{\lambda}{n_{co}\cos\theta} = \frac{2\pi}{\beta} \tag{1.19}$$

Fiber modes traveling in the positive *z*-direction, composed of light of a single angular frequency ω (and wavelengthλ), have a spatial and time dependence proportional to $e^{j(\omega t - \beta z)}$. The fiber optic axial propagation constant β– the component of *k* in the *z* direction is given by [24]

$$\beta = kn_{co}\cos\theta \tag{1.20}$$

Due to the restriction on the inclination angle θ, the propagation constant β also has a discrete set of solutions, and is denoted as an eigenvalue. This constant is thus an indication of whether or not the mode propagates in the core of the fiber or not. A mode remains guided if [24]

$$kn_{cl} < |\beta| < kn_{co} \tag{1.21}$$

The wave equations in cylindrical coordinates are obtained by substituting the general solution in the wave equations. The equations thus obtained are

$$\frac{\partial^2 E_z}{\partial r^2} + \frac{1}{r}\frac{\partial E_z}{\partial r} + \frac{1}{r^2}\frac{\partial^2 E_z}{\partial \phi^2} + q^2 E_z = 0 \tag{1.22}$$

$$\frac{\partial^2 H_z}{\partial r^2} + \frac{1}{r}\frac{\partial H_z}{\partial r} + \frac{1}{r^2}\frac{\partial^2 H_z}{\partial \phi^2} + q^2 H_z = 0 \tag{1.23}$$

where $q^2 = \omega^2 \varepsilon\mu - \beta^2 = k^2 - \beta^2$

These two equations contain either E_z or H_z. This implies that the longitudinal components of E and H are uncoupled and can be chosen arbitrarily provided that they satisfy equations 1.22 and 1.23. However, coupling of E_z and H_z is required by the boundary conditions of the electromagnetic field components. If there is no coupling then mode solutions can be obtained in which either E_z or $H_z = 0$.When $E_z = 0$ modes are called transverse electric or TE modes and when $H_z = 0$, they are called transverse magnetic or TM modes. Hybrid modes exist if both E_z and H_z are non zeros and are designated as HE or EH modes depending whether H_z or E_z makes a larger contribution to the transverse field. The two lowest order modes are designated by HE_{11} and TE_{01}.

The wave equations can be solved using the variable separable method. The solution of the equation is of the form [24]

$$E_z = AF_1(r)F_2(\phi)F_3(z)F_4(t) \tag{1.24}$$

8

Since the wave is sinusoidal in time and propogates along the z direction, time and z - dependant factors are given by

$$F_3(z)F_4(t) = e^{j(wt-\beta z)} \tag{1.25}$$

Because of the circular symmetry of the waveguide, each field component must not change when the co-ordinate ϕ is increased by 2π. Thus we assume

$$F_2(\phi) = e^{jv\phi} \tag{1.26}$$

where the constant 'v' is an integer and can be positive or negative. Substituting these in wave equation for E_z we will get

$$\frac{\partial^2 F_1}{\partial r^2} + \frac{1}{r}\frac{\partial F_1}{\partial r} + \left(q^2 - \frac{v^2}{r^2}\right)F_1 = 0 \tag{1.27}$$

This is a differential equation for Bessel function. An exactly identical equation can be derived for H_z as well. Equation 1.27 is solved for the regions inside the core and outside the core. For the inside region the solutions for the guided modes must remain finite as r→0, whereas outside, the solutions must decay to zero as r → ∞.

Thus for r < a (radius of the fiber), the solutions are Bessel functions of first kind of order v.

$$E_z(r<a) = AJ_v(ur)e^{jv\phi}e^{j(wt-\beta z)} \tag{1.28}$$

$$H_z(r<a) = BJ_v(ur)e^{jv\phi}e^{j(wt-\beta z)} \tag{1.29}$$

where $u^2 = k_{co}^2 - \beta^2$ and $k_{co} = 2\pi n_{co}/\lambda$ and A and B are arbitrary constants. Outside the core, the solutions are given by modified Bessel functions of the second kind, $K_v(wr)$, where $w^2 = \beta^2 - k_{cl}^2$ and $k_{cl} = 2\pi n_{cl}/\lambda$. The expression for E_z and H_z outside the core are given by [24]

$$E_z(r>a) = CK_v(wr)e^{jv\phi}e^{j(wt-\beta z)} \tag{1.30}$$

$$H_z(r>a) = DK_v(wr)e^{jv\phi}e^{j(wt-\beta z)} \tag{1.31}$$

where C and D are arbitrary constants.

From the definition of modified Bessel function, it is seen that $K_v(wr)$→e^{-wr} as wr→∞. The modified Bessel function decays exponentially with respect to r. Hence $K_v(wr)$ must go to zero as r→∞.

The field distributions in the core and cladding regions have the same form and the electric field pattern corresponds to a non-uniform wave travelling along the z-direction. It is a standing-wave pattern in the fiber core and a

decaying field in the cladding region. This decaying field in the cladding is called evanescent wave.

Figure 1.3 shows the field patterns of several of the lower order transverse electric (TE) modes in a dielectric slab waveguide, and their evanescent field tail in the cladding. The order of a mode is equal to the number of field zeroes across the guide.
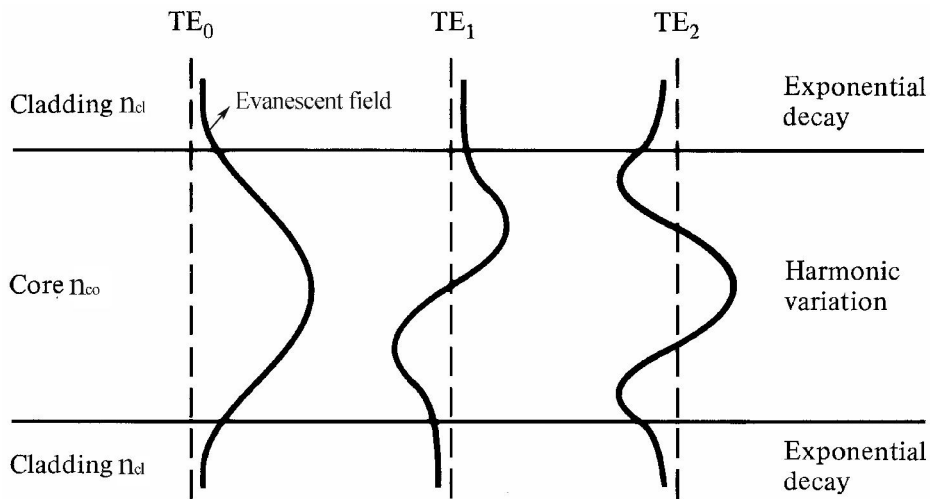
Figure 1.3 Transverse electric (TE) modes in a dielectric slab waveguide

Thus along with the guided modes, evanescent radiation modes or leaky modes also propagate along the optical fiber. One situation in which these modes occur is the case where a cladding mode no longer undergoes total internal reflection at the cladding-external boundary as a result of the index of refraction of the surrounding medium being greater than that of the cladding material. Leaky modes cause continuous power diffusion from the core to the cladding but are usually attenuated after propagating for short distances only [24], thus they do not diminish the optical power in the waveguide as a whole to a great extent.

Apart from these modes, there exists a continuum of (unguided) radiation modes as a result of light waves that no longer adhere to the critical angle condition for total internal reflection at the core-cladding boundary. Such modes undergo refraction from the core to the cladding, where they are often

trapped as a result of the abrupt cladding-ambient interface to form cladding modes. Once generated, cladding modes travel alongside the guided core modes in the optical fiber. Subsequently, mode coupling occurs because the electric field distributions of both types of modes penetrate the material on either side of the core-cladding interface. This mainly results in power being lost from the guided core modes into the cladding. A lossy coating around the cladding serves to attenuate cladding modes, thus limiting the amount of optical power leaking out of the core.

1.2.2 Weakly guiding approximation and Linearly Polarized (LP) modes

The electromagnetic field expressions for the guided modes are rather complicated to derive and hence a simpler method for obtaining the fiber modes is required. An assumption is made that will simplify analysis to a great extent – the weakly guiding fiber approximation [24], first introduced by Gloge in 1971 [25]. This approximation technique assumes that the difference in refractive index between the core of the fiber and cladding material is very small, typically of the order of one percent (n_{co}-n_{cl} <<1) . Technically speaking, the weakly guiding approximation neglects the longitudinal components of the electric and magnetic fields , resulting in linearly polarised (LP) 'pseudo-modes' [24]. This terminology has been applied because the waves described by these simplified solutions propagate at small angles to the fiber axis and are essentially polarised in a single direction, transverse to the fiber axis. In this scheme for the lowest order modes, each LP_{0m} mode is derived from an HE_{1m} mode and each LP_{1m} mode comes from TE_{0m}, TM_{0m}, and HE_{0m} modes. Thus the fundamental LP_{01} mode corresponds to an HE_{11} mode. Figure 1.4 shows the electric field amplitude profiles for all the guided modes (LP_{lm}) of a fiber with a step index profile. The two colors indicate different signs of electric field values. The fundamental or lowest-order mode (LP_{01}) has an intensity profile which is similar to that of a Gaussian beam. In general, light launched into a multimode fiber will excite a superposition of different modes, which can have a complicated shape.

11

l = 0, m = 1	l = 1, m = 1	l = 2, m = 1	l = 0, m = 2
l = 3, m = 1	l = 1, m = 2	l = 4, m = 1	l = 2, m = 2
l = 0, m = 3	l = 5, m = 1	l = 3, m = 2	l = 1, m = 3
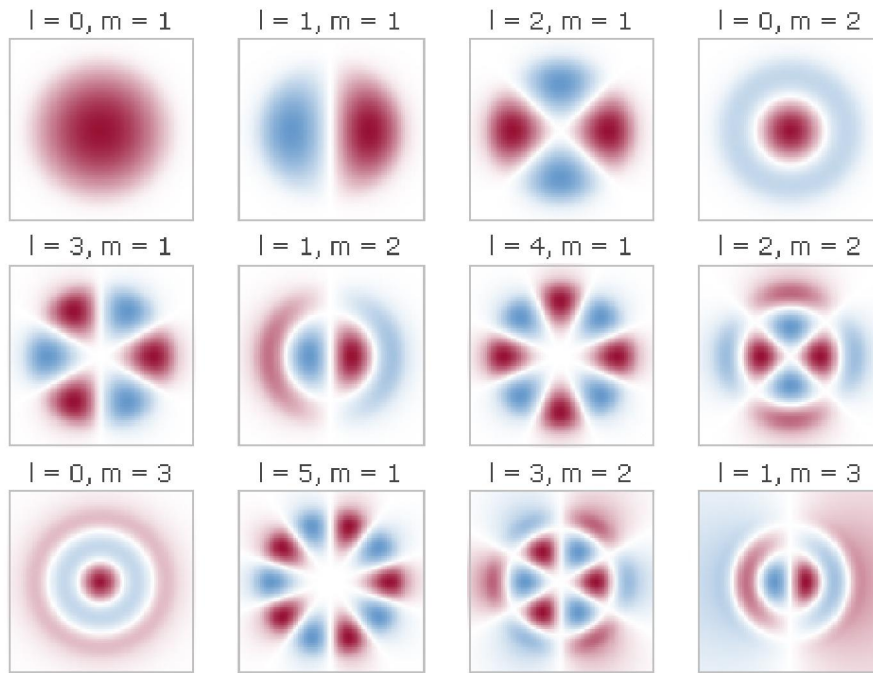
Figure 1.4 Electric field amplitude profiles for the guided modes
(LP_{lm}) of a step index fiber

1.2.3. Single mode fiber and Normalized frequency

A core mode remains guided as long as β satisfies the condition given in equation 1.21. The boundary between truly guided modes and leaky modes is defined by the cutoff condition $β=n_{cl}k$. Another parameter connected with the cutoff condition is called the normalized frequency or V parameter/number defined by [24]

$$V = \frac{2\pi a}{\lambda}\sqrt{n_{co}^2 - n_{cl}^2} = \frac{2\pi a}{\lambda}NA \qquad (1.32)$$

where a is the radius of the fiber core

This is a dimensionless number that determines how many modes a fiber can support. Except for the fundamental or lowest order mode (LP_{01}) each mode can exist only for values of V that exceed a certain limiting value. The modes are cutoff when $β=n_{cl}k$, and this occurs when V≤2.405. The fundamental mode has no cutoff and ceases to exist only when the core diameter is zero. This is the principle on which single mode fibers are

12

constructed, which guides only the fundamental mode. As per equation 1.32, V parameter can be reduced by reducing numerical aperture (NA) and/or radius of the core 'a'. Single mode fibers are fabricated by letting the core diameter to be a few wavelengths (usually 8-12 μm) and by having small index differences between the core and the cladding.

The V number can also be used to calculate the number of modes M in a multimode fiber and is given by [24]

$$M=V^2/2 \tag{1.33}$$

1.3. Fiber Optic Sensors

The general structure of an optical fiber sensor system is shown in Figure 1.5. It consists of an optical source, optical fiber, sensing or modulator element, an optical detector and processing electronics. Optical sources used for fiber optic sensing are light emitting diodes (LED) and lasers while photodiodes are mainly used as detectors. The sensing area converts the measurands into corresponding optical signals and the detected variation is processed using instruments like oscilloscope, Optical Spectrum Analyzers (OSA), Optical Time Domain Reflectometer (OTDR) etc.
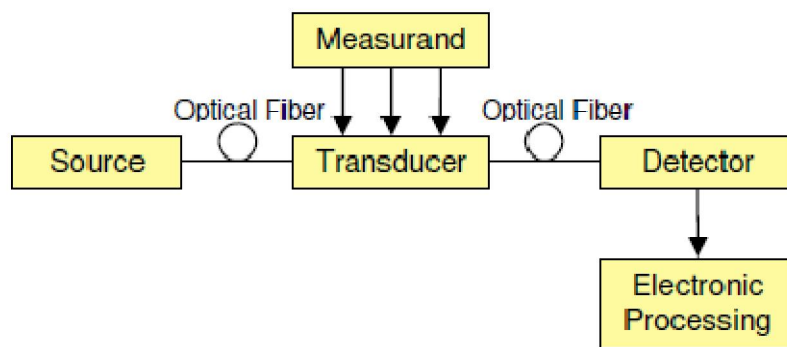
Figure 1.5 Fiber Optic Sensor system

In terms of the parameters like sensing location, the operating principle and the application, fiber optic sensors can be classified into various groups. Based on the sensing location, a fiber optic sensor can be classified as *extrinsic or intrinsic*. In an extrinsic fiber optic sensor [26-28], the fiber simply acts as a means of getting the light to the sensing location and then to

13

the detector. In the sensing zone the properties of light is changed using various physical and chemical techniques. Chemical agents like dyes can be used to change of the properties of the light in the presence of measurands or a physical deformation proportional to the measurands can change the coupled light intensity.

In the case of intrinsic fiber optic sensors, the internal property of optical fiber itself converts the environmental changes into a modulated light signal. This modulation of light signal can be in the form of intensity, phase, frequency or polarization [6-10, 26].

Based on the operating principle or the light modulation process, a fiber optic sensor can be classified as ***intensity, phase, frequency, or polarization*** modulated sensor [6-10]. All these parameters can be transformed as functions of external perturbations. The external perturbations can be sensed by measuring these parameters and their changes.

1.3.1 Intensity modulated Fiber Optic Sensors

Intensity-based fiber optic sensors rely on generating a loss or gain to the transmitted optical power proportional to the measurands. They are made by using a transducer to convert the measurand into a factor which causes attenuation of the signal. There are a variety of mechanisms like microbending loss, attenuation and evanescent fields to produce a change in the optical intensity guided by an optical fiber proportional to the measurand[6- 10]. These types of fiber optic sensors possess inherent advantages like simplicity of implementation, low cost, multiplexing capability, and ability to perform as real distributed sensors. There are also some limitations like unwanted power variation in the system due to connections at joints, splices, micro bending loss, macro bending loss, mechanical creep and many other factors.

Evanescent field is the exponentially decaying field in the lower index region of a waveguide and ***Evanescent wave*** sensor is the one that utilizes the light energy which leaks from the core into the cladding. They are probably the most studied and developed intrinsic sensor subfamily [29-60]. The sensing region is made by stripping the cladding from a section of the fiber. A light source having a wavelength that can be absorbed by the measurands is transmitted through the fiber and detected at the other end.

The resulting change in light intensity is a measure of the measurand concentration [39]. The cladding can also be made sensitive to specific organic vapors [35] or the cladding of the optical fiber can be replaced along a small section by a sensitive material [30,31,33]. Any change in the optical or structural characteristic of the coating material due to the presence of the measurands generates a change in the effective index of the optical fiber.

Generally fibers have a cladding made of silica, which is difficult to remove or modify. A remedy is to polish the fiber to eliminate the cladding [40-42] or using chemical etching where the optical fiber is soaked in hydrofluoric acid solution [31,43,44]. Plastic cladded fibers (PCS) are an easy alternative where the cladding can be easily removed either mechanically or with non hazardous solvents such as acetone [45-48].
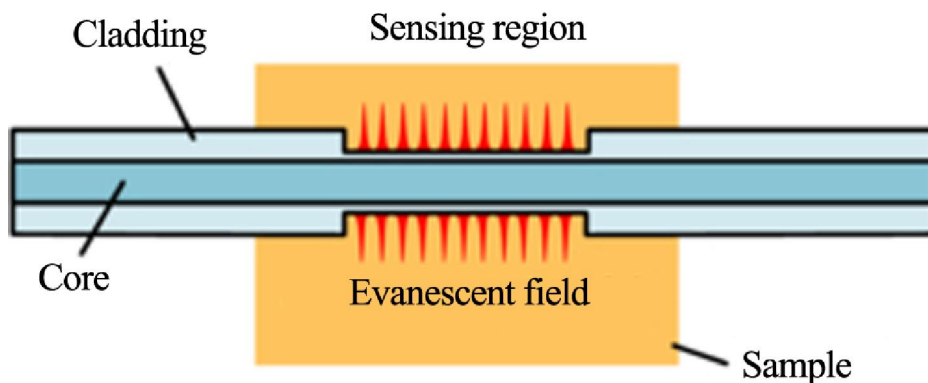
Figure 1.6 Evanescent wave Fiber Optic Sensor System

Once the cladding is removed or modified the sensing material has to be fixed onto the fiber core surface. To achieve this analyte is dissolved in a chemical solution and the fiber is dipped into it several times, known as dip coating [49,50]. Another method of coating sensitive material is using sol-gel solutions. Since the sol-gel solution is in liquid phase, the sensing material is added to it and then the fiber is dipped into the mixture. After drying the deposition, an optically uniform porous matrix doped with the analyte fixed onto the fiber is achieved [35,43, 51-57]. Langmuir-Blodgett technique is another available deposition procedure. The process is based on the

15

deposition of layers with hydrophobic and hydrophilic behavior, yielding a homogeneous structure formed by bilayers [58,59].

1.3.2. Wavelength Modulated Fiber Optic Sensors

Wavelength modulated sensors use changes in the wavelength of light for detection. Fluorescence sensors and fiber grating sensors are examples of wavelength-modulated sensors. The most widely used wavelength based sensor is the fiber grating sensor and are generally of two types namely Fiber Bragg Grating (FBG) and Long Period Fiber Grating (LPFG) based sensors. In the case of Bragg gratings (FBG) the change is in the reflection and transmission spectrum, while the variation occurs in the transmission wavelength in the case of long period fiber a grating (LPFG)

1.3.2.1. Fluorescence sensors

These sensors are based on the spontaneous light emission of a fluorophore when it is excited with light at a wavelength located in the absorption spectral region of such fluorophore. The change in the emission of the dye when it interacts with the measurands is used as the sensing response. Different schemes have been proposed for fluorescent based fiber optic sensors and the most popular schemes are fluorescence intensity sensors, fluorescence lifetime sensors and fluorescence phase-modulation sensors [61-65].

1.3.2.2. Fiber Gratings

Fiber grating was first reported by Hill et al [66] in 1978 at the Canadian Communications Research Centre (CRC) and was an outgrowth of research investigating in nonlinear properties of germania-doped silica fiber. It is a submicron periodical modulation of the refractive index of the fiber core coupling light from the forward-propagating mode to a counter propagating mode of the optical fiber [67-71] and is known as Fiber Bragg Grating (FBG). In the original experiments an intense Argon-ion laser (488nm) was launched into a germania-doped fiber and an increase in the reflected light intensity was noticed with the advancement of time. This light reflection was due to the formation of periodic refractive index modulation occurring in the fiber core due to the standing wave pattern formed by the laser reflected from the fiber end [68]. The technique of grating fabrication by side illumination was demonstrated by Meltz et al. [72] while a more

efficient and user-friendly method of grating fabrication using a phase mask has been demonstrated [73] in 1993. This enabled the fabrication of FBGs with high reproducibility and at a relatively low cost without affecting the physical characteristics of the host fiber.

Fiber gratings quickly transformed to a technology that currently plays a significant role in optical communications and sensor systems [74-80]. Structure of the grating can vary in terms of the refractive index, or the grating period and based on these features fiber gratings are divided into many namely Fiber Bragg Grating (FBG), Long Period Fiber Grating (LPFG), Chirped Fiber Grating, Tilted Fiber Bragg Grating (TFBG), Superstructure Bragg gratings (SBG) etc.

A **Fiber Bragg Grating (FBG)** has a short period on the scale of the optical wavelength (less than 1 μm) and under phase matching conditions, a fiber Bragg grating (FBG) couples the forward propagating core mode to the backward propagating core mode (Figure 1.7 a). FBG's are now commercially available and they have found key applications in many domains, such as optical add/drop multiplexers, wavelength-stabilized pump lasers, fiber lasers, WDM multiplexers, dispersion compensators, etc. In the area of fiber optic sensors FBGs are used as sensing heads for a large range of measurands like strain, temperature, vibration, pressure, acceleration, etc. The reasons for the impact of fiber Bragg gratings in sensing are multiple, and the most important one is the fact that the measurand information is encoded in the resonance wavelength of the structure. This brings up the properties of immunity to optical power fluctuations, avoids the need of recalibration procedures and provides natural identification of a particular sensor in a multiplexed sensing array [74-80].

If the grating period is much longer than the wavelength of light (100 μm to 1 mm), then it is called a **long-period fiber grating (LPFG)** and it can couple the forward propagating core mode to one or a few of the forward propagating cladding modes (figure 1.7b). After initials by Vengsarkar et al in 1996 [81], LPFGs have increasingly been applied in both telecommunications and sensing applications. In the communication field LPFGs are being used as band-rejection filters, source-noise suppressors and gain-equalising or gain-flattening filters for erbium-doped fiber amplifiers (EDFAs) [82-85]. Other communication applications include LPFGs employed as comb filters [86], wavelength-selective optical fiber polarizers

17

[87-90], add-drop couplers [91], components in wavelength division multiplexing (WDM) systems [92-94], or in all-optical switching [95], and for chromatic dispersion compensation [96]. Though long period fiber gratings (LPFG) lacks the ability of multiplexing, its high sensitivity to refractive index gives them an edge over fiber bragg gratings (FBG) in chemical and biochemical applications.

In a chirped fiber grating (figure 1.7c) the grating period is not uniform along the length and is achieved by varying the grating period, the average index, or both along the length of the grating. Chirp in gratings may take many different forms. The period may vary symmetrically, either increasing or decreasing in period around a pitch in the middle of a grating [97-98]. The reflection spectrum of a chirped fiber grating is wider compared to FBG and each wavelength component is reflected at different positions. This causes a delay time difference for different reflected wavelengths. Several techniques to impart chirp was reported namely, exposure to UV beams of non uniform intensity of the fringe pattern, varying the refractive index along the length of a uniform period grating, altering the coupling constant of the grating as a function of position, incorporating a chirp in the inscribed grating, fabricating gratings in a tapered fiber, applying a non uniform strain [99-101] etc. All these gratings have special characteristics, which are like signatures and may be recognized as special features of the type of grating. Chirped gratings have many applications and have found a special place in optics as a dispersion-correcting and compensating device. Ultralong, broad-bandwidth chirped gratings of high quality is used for high-bit-rate transmission in excess of 40 Gb/sec over 100 km [102]. Some of the other applications include chirped pulse amplification [103], chirp compensation of gain-switched semiconductor lasers [104], sensing [68,105], higher-order fiber dispersion compensation [106], ASE suppression [107], amplifier gain flattening [108], and band blocking and band-pass filters [109].

In standard FBGs, the grading or variation of the refractive index is along the length of the fiber (the optical axis) and perpendicular to the optical axis. In a *tilted FBG (TFBG),* the variation of the refractive index is at an angle to the optical axis leading to the occurrence of more complex mode coupling, as shown in Figure 1.7d. A tilted fiber grating can thus couple the forward propagating core mode to the backward propagating core mode and a backward propagating cladding mode and the angle of tilt has an

effect on the reflected wavelength, and bandwidth. TFBGs have found applications in the field of optical fiber communications and fiber sensing technology. In optical fiber communication TGBgs are used a gain flattening filters for erbium-doped fiber amplifiers (EDFAs) and wavelength division multiplexing (WDM) channel monitor. In sensing tilted fiber Bragg grating (TFBG) has been implemented as temperature-independent strain sensor [110-112], temperature independent external refractive index sensor [113-114] and bend sensor [115].
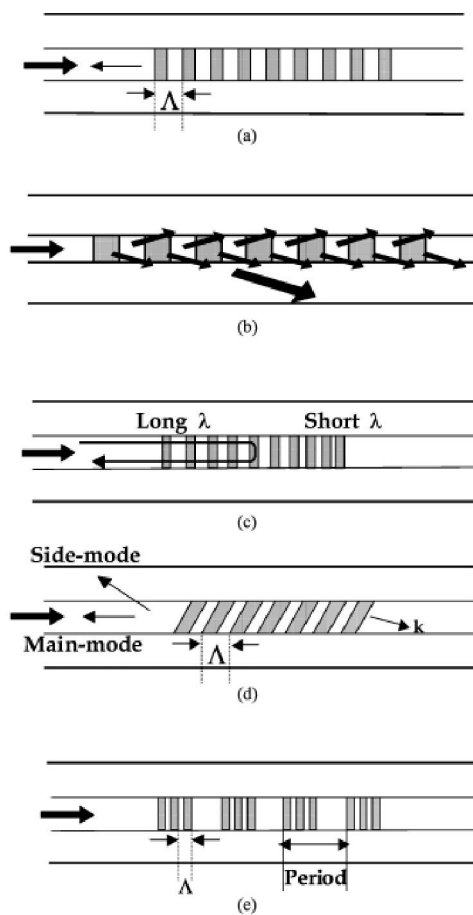
Figure 1.7 Different types of fiber gratings a) FBG b) LPFG
c) Chirped Fiber Bragg Grating d) TFBG e) SFBG

19

A *sampled fiber Bragg grating (SFBG) or superstructure Bragg grating (SBG's)* are structures for which parameters vary periodically along the length of the grating on a scale much larger than the wavelength of light. They are contra-directional coupling gratings foe which effective refractive index amplitude and/or phase is modulated through a long periodic structure (figure 1.7e). The special reflection characteristics of SFBGs make them very useful and attractive devices for optical communications and fiber sensors [116-117]. A sampled fiber grating can reflect several wavelength components with equal wavelength spacing.

1.3.3. Phase Modulated Fiber Optic Sensors

Phase modulated sensors use changes in the phase of light for detection. The measurands modulate the phase of the light wave passing through the fiber and this phase modulation is then detected interferometrically [6-10,118-127]. Mach-Zehnder and Michelson [118-119], Fabry-Perot [120-126], Sagnac [127] and grating interferometers [123, 126] are the most commonly used intereferometers. Fiber Fabry-Perot interferometric sensor (FFPI) is the commonly used interferometer based sensor and is classified into two categories namely Intrinsic Fabry-Perot interferometer (IFPI) sensor [121-122] and Extrinsic Fabry-Perot interferometer (EFPI) sensor [123-126]. In an EFPI sensor, the Fabry- Perot cavity is outside the fiber and Figure 1.8 shows a typical EFPI sensor using a capillary tube. Fiber guides the incident light into the Fabry Perot cavity and then collects the reflected light. In an IFPI sensor, the mirrors are constructed within the fiber. The cavity between two mirrors acts both as sensing element and waveguide and in this case, the light never leaves the fiber [121].
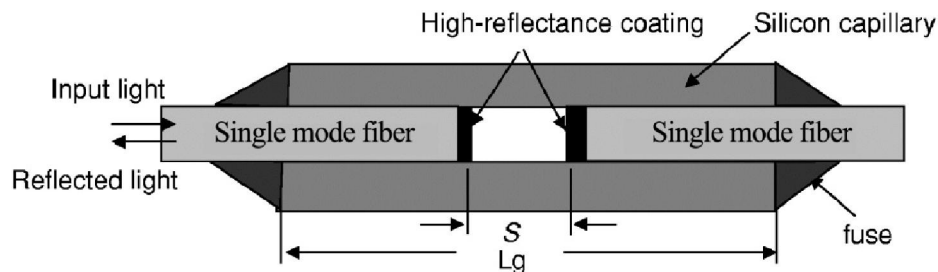
Figure 1.8 Typical EFPI sensor

1.3.4. Polarization Modulated Fiber Optic Sensors

The direction of the electric field portion of the light field is defined as its polarization state and the fiber optic sensors based on detection of change in induced phase difference between different polarization directions are termed as Polarization Modulated Fiber Optic Sensors. The refractive index of a fiber varies when it undergoes stress or strain and the induced refractive index change occurs in the direction of applied stress or strain. Thus an induced phase difference is created between different polarization directions and this phenomenon is called photoelastic effect. Therefore, by detecting the change in the output polarization state, the external perturbation can be sensed [9].

1.4 Fiber Optic Sensors in Quality evaluation

Quality is defined as the standard of something as measured against other things of a similar kind or in other words the degree of excellence of something. The definition of quality depends on the role of the people defining it and on the material on which it is defined. Some people view quality as "performance to standards" while some view it as "meeting the customer's needs" or "satisfying the customer." The difficulty in defining quality exists regardless of product, and this is true for both manufacturing and quality control organizations.

The evaluation of quality of a product is thus important in both the production side and consumer side. It can be either done manually or automatically and both methods have its own merits and demerits. Traditionally quality evaluation is done manually and it requires skilled operators and the process is time consuming. Moreover, the chances for human error are more in this process. On contrary automatic quality evaluation is fast, cost effective and accurate.

Sensors are the vital elements of such automatic quality evaluation systems where appropriate sensors with high sensitivity and resolution are a necessity and sensors based on various technologies have carved their niches in their areas. One of the major application area of fiber optic sensors is in monitoring the physical health of structures like buildings, bridges, tunnels, dams and heritage structures in real time. Concrete monitoring during setting, crack (length, propagation speed) monitoring, pre stressing monitoring,

spatial displacement measurement, neutral axis evolution, long-term deformation (creep and shrinkage) monitoring, concrete-steel interaction, and post-seismic damage evaluation are some of the civil engineering parameters measured using fiber optic sensors [128-131]. Twenty-six FBG strain sensors have been reported to be monitoring the Horsetail Falls Bridge in Oregom successfully for 2 years [132]. The bridge was originally built in 1914 and in 1998 it was strengthened by placing composite wraps over the concrete beams. Bragg grating strain sensors have been employed for monitoring the prestressing tendons of the Beddington Trail Bridge, Canada [133] and Tsing Ma Bridge in China [134]. Gebremichael et al. in 2005 have reported the use of 40 FBG sensors to remotely monitor the real-time strain on Europe's first all-fiber reinforced composite bridge, The West Mill Bridge [135]. In situ monitoring of strain data from the bridge and to analyze this data for assessment of its structural integrity, maintenance scheduling and validation of design codes are the main objective behind this study. Quality measurement of reinforced concrete beams instrumented with FBG sensors have been reported in literatures [136-140]. Bragg grating sensors have been used successfully to monitor the strain in concrete piles [141-144] and are essential since piles carry the weight of the foundation and transmit the load of the structure to the subsoil. Another area where quality monitoring is essential is the cement curing process which is affected by the water to cement ratio, the curing temperature, humidity and type of cement used. FBG strain sensors have been used to study early-age cement paste shrinkage [145] and the shrinkage and temperature change behavior of reactive powder concrete (RPC) in the early age was studied by Wong et al. [146]. M. Rajesh et. al [147] did studies on the setting characteristics of various grades of cement while plastic optical fibers were successfully used for cement setting studies by Andrea et.al [148].

Adulteration in food is a major area of concern and a fiber optic sensor for determining quality of coconut oil was reported by Sheeba et al [149]. An evanescent type fiber optic sensor using a side polished plastic clad silica fiber was used in their work. Altering the quality of fuels is another major problem faced world wide and fiber optic sensors were successfully developed to test the purity of petrol and diesel. [150-153]. While Mishra et.al [153] developed long period based sensor for identifying kerosene adulteration in petrol, a similar technique was utilized by Falate

22

et.al [151] for Biodiesel Quality Control. Fiber optic sensors supervised by artificial neural networks were demonstrated as integrate systems for smart sensing in fuel industry by Possetti et.al [152].

Another important area is contamination of water where authors have reported works on pH detection using optical methods [154-160]. Ganesh et.al [154] used a membrane made of cellulose acetate for reagent immobilization and congo red (pKa 3.7) and neutral red (pKa 7.2) as pH indicators while a sol–gel derived film doped with a pH indicator bromocresol purple (BCP) was reported by Burke et.al [160]. Long Period Fiber Gratings (LPFG) based in-fiber Mach–Zehnder interferometer for salinity measurement in a water solution was reported by Possetti et. al [161] and Samer et.al [162]. Ethanol concentration detection in alcohol beverages is another area where adulteration is common and an optical-fiber sensor using the fluorescence induced by a laser-diode-pumped Tm3+:YAG for determining water concentrations in ethanol–water and methanol–water mixtures was reported by Yokota et.al [163]. A fiber-optic sensor with a chitosan/poly(vinyl alcohol) blended membrane as the cladding was fabricated to determine ethanol in alcoholic beverages by Kurauchi et. al [164]

Quality of air depends on the concentration of many parameters and their measurement in various environments is a necessity. Humidity is one such parameter and its precise measurement is inevitable in various industrial and domestic environments and various authors have presented fiber optic sensors for humidity detection [165-171]. Long Period Fiber Grating based humidity sensor with PVA coating was reported by Venugopalan et. al [165-167] while Liwei Wang et. al [166] and Arregui et. al [169] used hydro gel as the sensitive material. An Optical fiber based humidity sensor using cobalt-polyaniline as sensitive cladding material was reported by Anu Vijayan et. al [171]. Measurement of ammonia concentration is important in industrial environments and Wenqing Cao et. al. [172] have developed an optical fiber based sensor system using sol-gel immobilized bromocresol purple (BCP). An ammonia sensor using a pH Indicator dye p-nitrophenol was reported by Arnold et.al. [173]. Fiber optic gas sensors were reported for the detection of Oxygen [174], carbon dioxide [175-177], hydrogen [178] and nitrogen dioxide [179-181]. Mahesh et.al.[175] have developed a carbon dioxide sensor for fermentation monitoring while Shelly et.al.[181] reported

a sensor with nanoporous structure for the selective detection of NO_2 in air samples.

Conclusions

In this chapter we discussed the basics of optical fiber and fiber optic sensor technology. The theory of light guiding in an optical fiber was explained along with various types of fiber sensor configurations, their advantages and disadvantages. Fiber sensors are being investigated for the past forty years and some of the findings related to their applications in quality evaluation of civil structures, liquids and air are discussed in this chapter.

References

1. V. P. N. Nampoori, "Dream Merchants-The Evolution of Fiber Optics", http://photonics.cusat.edu/Article1.html
2. K. C. Kao and G. A. Hockham, "Dielectric-fiber surface waveguides for optical frequencies", Proc. IEE **113**, 1151-1158 (1966)
3. Charles K. Kao, "Nobel Lecture: Sand from centuries past: Send future voices fast", Rev. Mod. Phys. **82**, 2299-2303 (2010)
4. K. Saito, M. Yamaguchi, H. Kakiuchida, A. J. Ikushima, K. Ohsono and Y. Kurosawa, "Limit of the Rayleigh scattering loss in silica fiber", Appl. Phys. Lett. **83**, 5175-5177 (2003)
5. F. Poletti, N. V. Wheeler,M. N. Petrovich,N. Baddela, E. Numkam Fokoua, J. R. Hayes, D. R. Gray, Z. Li, R. Slavík and D. J. Richardson, "Towards high-capacity fiber-optic communications at the speed of light in vacuum", Nature Photonics **7**, 279–284 (2013)
6. B Culshaw and J Dakin, Optical Fiber Sensors: Systems and Applications, (Artech House, Boston, 1989)
7. D A Krohn, Fiber Optic Sensors: Fundamental and Applications, (Instrument Society of America, Research Triangle Park, North Carolina, 1988).
8. E Udd, Fiber Optic Sensors: An Introduction for Engineers and Scientists, (Wiley, New York, 1991).
9. Francis To So Yu and Shizhuo Yin, Fiber Optic Sensors, (Marcel Dekker, Inc. New York, 2002).
10. B.D.Gupta, Gupta and Banshi Das, Fiber Optic Sensors: Principles and Applications (New India Publishing, New Delhi,2006)
11. Daru Chen, Weisheng Liu, Meng Jiang, and Sailing He, "High-Resolution Strain/Temperature Sensing System Based on a High-Finesse Fiber Cavity and Time-Domain Wavelength Demodulation", J. Lightwave Technol. **27**, 2477-2481 (2009)

12. N. Lagakos, J. A. Bucaro, and J. Jarzynski, "Temperature-Induced Optical Phase Shifts in Fibers," Appl. Opt. **20**, 2305-2308 (1981).

13. H. Y. Fu, H. Y. Tam, L. Y. Shao, X. Dong, P. K. A. Wai, C. Lu, and S. K. Khijwania, "Pressure sensor realized with polarization-maintaining photonic crystal fiber-based Sagnac interferometer," Appl. Opt. **47**, 2835-2839 (2008).

14. A. B. Tveten, A. Dandridge, C. M. Davis, and T. G. Giallorenzi, "Fiber Optic Accelerometer" Electron. Lett.**16**, 854-856 (1980).

15. V. Vali, R.W. Shorthill, "Fiber ring interferometer", Appl. Opt. **15**, 1099–1100 (1976).

16. Sven Kuehn, Fin Bomholt and Niels Kuste, "Miniature Electro-Optical Probe for Magnitude, Phase and Time-Domain Measurements of Radio-Frequency Magnetic Fields", (Asia-Pacific International Symposium on Electromagnetic Compatibility, Institute of Electrical and Electronics Engineers, New York, 2010)

17. A.H. Rose, Z.B. Ren, G.W. Day, "Twisting and annealing optical fiber for current sensors", J. Lightwave Technol. **14**, 2492–2498 (1996).

18. G.D. Peng, P.L. Chu, "Optical fiber hydrophone systems", in: F.T.S. Yu, S. Yin (Eds.), Fiber Optic Sensors (Dekker, New York, 2002).

19. Colette McDonagh, Conor S. Burke and Brian D. MacCraith, "Optical Chemical Sensors", Chem. Rev. **108**, 400-422 (2008).

20. Otto S. Wolfbeis, "Fiber-Optic Chemical Sensors and Biosensors", Anal. Chem.**78**, 3859-3874 (2006).

21. Otto S. Wolfbeis, "Fiber-Optic Chemical Sensors and Biosensors", Anal. Chem. **80**, 4269–4283 (2008).

22. M.D. Marazuela, M.C. Moreno-Bondi, "Fiber-optic biosensors—an overview", Anal. Bioanal. Chem. **372**, 664–682 (2002).

23. K Okamoto, Fundamentals of optical waveguides, (Academic Press. San Diego 2000).

24. G Keiser, Optical fiber communications. (3rd ed.). (McGraw-Hill, Singapore, 2000)

25. D Gloge, "Weakly guiding fibers", Appl.Opt. **10**, 2252-2258 (1971).

26. Culshaw B,Stewart G, Dong F, Tandy C, Moodie D, "Fiber optic techniques for remote spectroscopic methane detection-from concept to system realization". Sensor. Actuat. B-Chem. **51**, 25-37 (1998).

27. Stewart G, Tandy C, Moodie, D, Morante, M.A, Dong F, "Design of a fiber optic multi-point sensor for gas detection", Sensor. Actuat. B-Chem. **51**, 227-232 (1998).

28. Ho H.L, Jin W, Yu H.B, Chan K.C, Chan C.C, Demokan M.S, "Experimental demonstration of a Fiber-Optic Gas Sensor Network Addressed by FMCW", IEEE Photon. Tech. Lett. **12**, 1546-1548 (2000).

29. Tracey, P. M., "Intrinsic Fiber-Optic Sensors", IEEE Trans. Ind. Appl. **27**, 96-98 (1991)

30. Khijwania S.K, Gupta B.D, "Fiber optic evanescent field absorption sensor with high sensitivity and linear dynamic range", Opt. Commun.**152**, 259-262 (1998)

31. Khalil S, Bansal L, El-Sherif M, "Intrinsic fiber optic chemical sensor for the detection of dimethyl methylphosphonate", Opt. Eng. **43**, 2683-2688 (2004).

32. Dickinson T.A, Michael K.L, Kauer J.S, Walt D.R, "Convergent, Self-Encoded Bead Sensor Arrays in the design of an Artificial Nose", Anal. Chem. **71**, 2192-2198 (1999).

33. Yuan J, El-Sherif A, "Fiber-Optic Chemical Sensor Using Polyaniline as Modified Cladding Material", IEEE Sensor. J. **3**, 5-12 (2003).

34. Messica A, Greenstein A, Katzir A, "Theory of fiber-optic, evanescent-wave spectroscopy and sensors", Appl. Opt. **35**, 2274-2284 (1996).

35. Schwotzer G, Latka I, Lehmann H.,Willsch R, "Optical sensing of hydrocarbons in air or in water using UV absorption in the evanescent field of fibers", Sensor. Actuat. B-Chem. **38-39**, 150-153 (1997).

36. Shadaram M, Espada L, Garcoa F, "Modeling and performance evaluation of ferrocene-based polymer clad tapered optical fiber gas sensors", Opt. Eng. **37**, 1124-1129 (1998)

37. Barmenkov Y.O, "Time-domain fiber laser hydrogen sensor", Opt. Lett. **29**, 2461-2463 (2004).

38. Lacroix S, Bourbonnais R, Gonthier F, Bures J, "Tapered monomode optical fibers: understanding large power transfer" Appl. Opt. **25**, 4421-4425 (1986).

39. Willer U, Scheel D, Kostjucenko I, Bohling C, Schade W, Faber E, "Fiber-optic evanescent-field laser sensor for in-situ gas diagnostics", Spectrochim. Acta A **58**, 2427-2432 (2002).

40. Senosiain J, Díaz I, Gastón A, Sevilla J, "High Sensitivity Temperature Sensor Based on Side-Polished Optical Fiber", IEEE Trans. Instrum. Meas. **50**, 1656-1660 (2001).

41. Gastón A, Pérez F, Sevilla J, "Optical fiber relative-humidity sensor with polyvinyl alcohol film", Appl. Opt. **43**, 4127-4132 (2004)

42. Gastón A, Lozano I, Pérez F, Auza F, Sevilla J, "Evanescent Wave Optical-Fiber Sensing (Temperature, Relative Humidity and pH Sensors)", IEEE Sensor. J. **3**, 806-811 (2003).

43. Sumdia S, Okazaki S, Asakura S, Nakagawa H, Murayama H, Hasegawa T, "Distributed hydrogen determination with fiber-optic sensor", Sensor. Actuat. B-Chem. **108**, 508-514 (2005).

44. Segawa H, Ohnishi E, Arai Y, Yoshida K, "Sensitivity of fiber-optic carbon dioxide sensors utilizing indicator dye", Sensor. Actuat. B-Chem. **94**, 276-281 (2003).

45. Cherif K, Mrazek J, Hleli S, Matejec, V, Abdelghani, A Chomat M, Jaffrezic-Renault N, Kasik I, "Detection of aromatic hydrocarbons in air and water by using xerogel layers coated on PCS fibers excited by an inclined collimated beam", Sensor. Actuat. B-Chem. **95**, 97-106 (2003).

46. Malis C, Landl M, Simon P, MacCraith B.D, "Fiber optic ammonia sensing employing novel near infrared dyes" Sensor. Actuat. B-Chem. **51**, 359-367 (1998).

47. Potyrailo R.A, Hieftje G.M, "Oxygen detection by fluorescence quenching of tetraphenylporphyrin immobilized in the original cladding of an optical fiber", Anal. Chim. Acta. **370**, 1-8 (1998).

48. Okazaki S, Nakagawa H, Asakura S, Tomiuchi Y,Tsuji N, Murayama H, Washiya M, "Sensing Characteristics of an optical fiber sensor for hydrogen leak" Sensor. Actuat. B-Chem. **93**, 142-147 (2003).

49. Ho H.L, Jin W, Yu H.B, Chan K.C, Chan C.C, Demokan M.S, "Experimental demonstration of a Fiber-Optic Gas Sensor Network Addressed by FMCW", IEEE Photon. Tech. Lett. **12**, 1546-1548 (2000).

50. Scorsone E, Christie S, Persaud K.C, Simon P, Kvasnik F, "Fiber-optic evanescent sensing of gaseous ammonia with two forms of a new near-infrared dye in comparison to phenol red", Sensor. Actuat. B-Chem. **90**, 37-45 (2003).

51. Sekimoto S, Nakagawa H, Okazaki S, Fukuda K, Asakura S, Shigemori T, Takahashi S, "A Fiber-optic evanescent-wave hydrogen gas sensor using palladium-supported tungsten oxide", Sensor. Actuat. B-Chem. **66**, 142-145 (2000).

52. Jorge P.A.S, Caldas P, Rosa C.C, Oliva A.G, Santos J.L, "Optical fiber probes for fluorescente based oxygen sensing", Sensor. Actuat. B-Chem. **130**, 290-299 (2004).

53. Grant S.A, Satcher J.H. Jr, Bettencourt K, "Development of sol-gel-based fiber nitrogen dioxide gas sensors", Sensor. Actuat. B-Chem. **69**, 132-137 (2000).

54. Abdelghani A, Chovelon J.M, Jaffrezic-Renault N, Lacroix M, Gagnaire H, Veillas C, Berkova B, Chomat M, Matejec V, "Optical fiber sensor coated with porous silica layers for gas and chemical vapour detection", Sensor. Actuat. B-Chem. **44**, 495-498 (1997).

55. Abdelmalek F, Chovelon J.M, Lacroix M, Jaffrezic-Renault N, Matajec V, "Optical fiber sensors sensitized by phenyl-modified porous silica prepared by sol-gel", Sensor. Actuat. B-Chem. **56**, 234-242 (1999)

56. Bariain C, Matias I.R, Romeo I, Garrido J, Laguna M, "Detection of volatile organic compund vapors by using a vapochromic material on a tapered optical fiber", Appl. Phys. Lett. **77**, 2274-2276 (2000).

57. Bariain C, Matias I.R, Romeo I, Garrido J, Laguna M, "Behavioral experimental studies of a novel vapochromic material towards development of optical fiber organic compounds sensor", Sensor. Actuat. B-Chem. **76**, 25-31 (2001).

58. Hu W, Liu Y, Xu Y, Liu S, Zhou S, Zeng P, Zhu D.B, "The gas sensitivity of Langmuir-Blodgett films of a new asymmetrically substituted phthalocyanine", Sensor. Actuat. B-Chem. **56**, 228-233 (1999).

59. Bariain C, Matias I.R, Fernandez-Valdivielso C, Arregui F.J, Rodríguez-Méndez M.L, De Saja J.A, "Optical fiber sensor based on lutetium bisphthalocyanine for the detection of gases using standard telecommunication wavelengths", Sensor. Actuat. B-Chem. **93**, 153-158 (2003).

60. Gutierrez N, Rodríguez-Méndez M.L, De Saja J.A, "Array of sensors based on lanthanide bisphthalocyanine Langmuir-Blodgett films for the detection of olive oil aroma", Sensor. Actuat. B-Chem. **77**, 437-442 (2001).

61. Mitsubayashi K, Minamide T, Otsuka K, Kudo H, Saito H, "Optical bio-sniffer for methyl mercaptan in halitosis", Anal. Chim. Acta, **573**, 75-80.(2006).

62. Wolfbeis O.S, Kovacs B, Goswami K, Klainer S.M, "Fiber-Optic Fluorescence Carbon Dioxide Sensor for Environmental Monitoring", Mikrochim. Acta. **129**, 181-188 (1998).

63. Kim Y.C, Peng W, Banerji S, Booksh K.S, "Tapered fiber optic surface plasmon resonance sensor for analyses of vapor and liquid phases", Opt. Lett. **30**, 2218-2220 (2005)

64. O'Neal P.D, Meledeo A, Davis J.R, Ibey B.L, Gant V.A, Pishko M.V, Cote G.L, "Oxygen Sensor Based on the Fluorescence Quenching of a Ruthenium Complex Immobilized in a Biocompatible Poly(Ethylene Glycol) Hydrogel", IEEE Sensor. J. **4**, 728-734 (2004).

65. Grattan K.T.V, Zhang Z.Y, "Fiber Optic Fluorescence Thermometry", (Chapman & Hall: London, 1995).

66. K.O. Hill, Y. Fujii, D.C. Johnson, B.S. Kawasaki "Photosensitivity in optical fiber waveguides: application to reflection filter fabrication", Appl. Phys. Lett. **32** 647–649 (1978).

67. Raman Kashyap, "Fiber Bragg Gratings", (Academic Press, San Diego, USA 1999).

68. K.O. Hill and Gerald Meltz, "Fiber Bragg Grating Technology Fundamentals and Overview", J. Lightwave Technol. **15** ,1263-1276 (1997)

69. K.O. Hill, "Photosensitivity in Optical Fiber Waveguides: From Discovery to Commercialization", IEEE J. Sel. Top. Quantum Electron. **6**, 1186-1189 (2000)

70. Andreas Othonos, "Fiber Bragg gratings", Rev. Sci. Instrum. **68** ,4309-4341 (1997)

71. Turan Erdogan, "Fiber Grating Spectra", J. Lightwave Technol. **15**, 1277-1294 (1997)

72. G. Meltz, W.W. Morey, W.H. Glenn, Formation of Bragg gratings in optical fibers by a transverse holographic method", Opt. Lett. **14**, 823–825 (1989).

73. K. O. Hill, B Malo, F. Bilodeau, D. C. Johnson, and J. Albert, "Bragg gratings fabricated in monomode photosensitive optical fiber by UV exposure through a phase mask", Appl. Phys. Lett. **62**, 1035-1037(1993).

74. O. Frazao,L. A. Ferreira, F. M. Araujo, J. L. Santos, "Applications of Fiber Optic Grating Technology to Multi-Parameter Measurement", Fiber Integr. Opt. **24**, 227–244 (2005).

75. Giles, C. R. "Lightwave applications of fiber Bragg gratings", J. Lightwave Technol. **15**, 1391-1395 (1997)

76. Yun-Jiang Rao, "In-fiber Bragg grating sensors", Meas. Sci. Technol. **8** , 355–375 (1997)

77. A. D. Kersey, M. A. Davis, H. J. Patrick, M. LeBlanc, K. P. Koo, C. G. Askins, M. A. Putnam, and E. J. Friebele, "Fiber grating sensors," J. Lightwave Technol. **15**, 1442-1462 (1997).

78. Alan D. Kersey, Michael A. Davis, Heather J. Patrick, Michel LeBlanc, K. P. Koo, C. G. Askins, M. A. Putnam, and E. Joseph Friebele, "Fiber Grating Sensors", J. Lightwave Technol. **15**, 1442-1463 (1997)

79. Y.J. Rao, "Recent progress in applications of in-fiber Bragg grating sensors", Opt. Lasers Eng. **31**, 297-324 (1999)

80. Byoungho Lee, "Review of the present status of optical fiber sensors", Opt. Fiber Technol. **9**, 57-79 (2003)

81. Vengsarkar A.N., Lemaire P.J., Judkins J.B., Bhatia V., Erdogan T. and Sipe J.E, "Long-period fiber gratings as band-rejection filters". J. Lightwave Technol. **14**,58-65 (1996).

82. James S.W. and Tatam R.P., "Optical fiber long-period grating sensors: characteristics and applications", Meas. Sci. Technol. **14**, R49-R61 (2003).

83. Vengsarkar A.N., Pedrazzani J.R., Judkins J.B. and Lemaire P.J., "Longperiod fiber-grating-based gain equalizers", Opt. Lett. **21**,336-338 (1996).

84. Wysocki P.F., Judkins J.B., Espindola R.P., Andrejco M. and Vengsarkar A.M., "Broad-band erbium-doped fiber amplifier flattened beyond 40 nm using long-period grating filter", IEEE Photonics Technol. Lett. **9,** 1343-1345 (1997).

85. Frazão O., Rego G., Lima M., Teixeira A., Araújo F.M., André P., Da Rocha J.F.and Salgado H.M., "EDFA gain flattening using long-period fibergratings based on the electric arc technique", (Proceedings of the London Communications Symposium-LCS2001, 2001)

86. Gu X.J., "Wavelength-division multiplexing isolation fiber filter and light source using cascaded long-period fiber gratings", Opt. Lett. **23**, 509-510 (1998).

87. Ortega B., Dong L., Liu W.F., De Sandro J.P., Reekie L., Tsypina S.I., Bagratashvili V.N. and Laming R.I., "High-performance optical fiber polarizers based on long-period gratings in birefringent optical fibers", IEEE Photonics Technol. Lett. **9**,1370-1372 (1997).

88. Kurkov A.S., Douay M., Duhem O., Leleu B., Henninot J.F., Bayon J.F. and Rivoallan L., "Long-period fiber grating as a wavelength selective polarisation element", Electron. Lett. **33**, 616-617 (1997).

89. Kurkov A.S., Vasil'ev S.A., Korolev I.G., Medvedkov O.I. and Dianov E.M., "Fiber laser with an intracavity polariser based on a long-period fiber grating", Quantum Electron. **31**, 421-423 (2001).

90. Zhang L., Liu Y., Everall L., Williams J.A.R. and Bennion I., "Design and realization of long-period grating devices in conventional and high birefringence fibers and their novel applications as fiber-optic load sensors", IEEE J. Sel. Top. Quantum Electron. **5**, 1373-1378 (1999).

91. Chiang K.S., Liu Y., Ng M.N. and Li S., "Coupling between two parallel long-period fiber gratings", Electron. Lett. **36**, 1408-1409 (2000).

92. Laffont G. and Ferdinand P., "Fiber Bragg grating-induced coupling to cladding modes for refractive index measurements", Proc. SPIE **4185**, 326-329 (2000).

93. Lam P.K., Stevenson A.J. and Love J.D., "Bandpass spectra of evanescent couplers with long period gratings", Electron. Lett. **36**, 967-969 (2000).

94. Zhu Y., Lu C., Lacquet B.M., Swart P.L. and Spammer S.J., "Wavelength tunable add/drop multiplexer for dense wavelength division multiplexing using long-period gratings and fiber stretchers:, Opt. Commun. **208**, 337-344 (2002).

95. Eggleton B.J., Slusher R.E., Judkins J.B., Stark J.B. and Vengsarkar A.M., "All-optical switching in long-period fiber gratings", Opt. Lett. **22**, 883-885 (1997).

96. Das M. and Thyagarajan K. , "Dispersion compensation in transmission using uniform long period fiber gratings", Opt. Commun. **190,** 159-163 (2001).

97. Byron K. C., Sugden K, Bircheno T. and Bennion I., "Fabrication of chirped Bragg gratings in photosensitive fiber," Electron. Lett. **29**, 1659 (1993).

98. Parries M. C., Sugden K., Reid D. C. J., Bennion L, Molony A. and Goodwin M. J., "Very broad reflection bandwidth (44 nm) chirped fiber gratings and narrow-bandpass filters produced by the use of an amplitude mask," Electron. Lett. **30**, 891-892 (1994).

99. Stephens T, Krug P. A., Brodzeli Z., Doshi G., Ouellette R and Poladin L., "257 km transmission at 10 Gb/s in non dispersion shifted fiber using an unchirped

fiber Bragg grating dispersion compensator," Electron. Lett. **32**, 1559-1561 (1996).

100. Kashyap R., McKee P. R, Campbell R. J. and Williams D. L., "A novel method of writing photo-induced chirped Bragg gratings in optical fibers," Electron. Lett. **30**, 996-997 (1994).

101. Putnam M. A., Williams G. M. and Friebele E. J., " 'Fabrication of tapered, strain-gradient chirped fiber Bragg gratings," Electron. Lett. **31**, 309-310 (1995).

102. Loh W. H., Laming R. I., Robinson N., Cavaciuti A., Vaninetti, Anderson C. J., Zervas M. N. and Cole M. J., "Dispersion compensation over distances in excess of 500 km for 10 Gb/s systems using chirped fiber gratings," IEEE Photon. Technol. Lett. **8**, 944 (1996).

103. Boskovic A., Guy M. J., Chernikov S. V., Taylor J. R. and Kashyap R., "All fiber diode pumped, femtosecond chirped pulse amplification system," Electron.Lett. **31**, 877-879 (1995).

104. Gunning P., Kashyap R., Siddiqui A. S. and Smith K., "Picosecond pulse generation of <5 ps from gain-switched DFB semiconductor laser diode using linearly step-chirped fiber grating," Electron. Lett. **31**, 1066-1067 (1995).

105. M.G. Xu, L. Dong, L. Reekie, J.A. Tucknott and J.L. Cruz, "Temperature-independent strain sensor using a chirped Bragg grating in a tapered optical fiber", Electron.Lett. **31**, 823 – 825 (1995).

106. Williams J. A. R., Bennion I. and Doran N. J. "The design of in-fiber Bragg grating systems for cubic and quadratic dispersion compensation," Opt. Commun.,**116**, 62-66 (1995).

107. Fairies M. C., Ragdale G. M. and Reid D. C. J., "Broadband chirped fiber Bragg grating filters for pump rejection and recycling in erbium doped fiber amplifiers," Electron. Lett. **28**, 487-489 (1992).

108. Kashyap R., Wyatt R. and McKee P. F, "Wavelength flattened saturated erbium amplifier using multiple side-tap Bragg gratings," Electron. Lett. **29**, 1025-1027 (1993).

109. Zhang I., Sugden K, Williams J. A. R. and Bennion I., "Postfabrication exposure of gap-type bandpass filters in broadly chirped fiber gratings," Opt. Lett. **20**, 1927-1929 (1995).

110. Kang S C, Kim S Y, Lee S B, Kwon S W, Choi S S and Lee B, "Temperature-independent strain sensor system using a tilted fiber Bragg grating demodulator", IEEE Photon. Technol. Lett. **10,** 1461–1463 (1998).

111. Chen C, Xiong L, Jafari A and Albert J, "Differential sensitivity characteristics of tilted fiber Bragg grating sensors", Proc. SPIE. **6004,** 6004–6013 (2005).

112. Chen X, Zhou K, Zhang L and Bennion I, " In-fiber twist sensor based on a fiber Bragg grating with 81 degrees tilted structure", IEEE Photon. Technol. Lett. **18,** 2596–2604 (2006).

113. Laffont G and Ferdinand P, "Tilted short-period fiber-Bragg-grating-induced coupling to cladding modes for accurate refractometer", Meas. Sci. Technol. **12,** 765–770 (2001)

114. Chan C F, Chen C, Jafari A, Laronche A, Thomson D J and Albert J, "Optical fiber refractometer using narrowband cladding mode resonance shifts", Appl. Opt. **46,** 1142–1149 (2007)

115. Baek S, Jeong Y and Lee B, "Characteristics of short-period blazed fiber Bragg gratings for use as macro-bending sensors", Appl. Opt. **41,** 631–636 (2002)

116. Frazao O, Romero R, Rego G, Marques P V S, Salgado H M and Santos J L, "Sampled fiber Bragg grating sensors for simultaneous strain and temperature measurement", Electron. Lett. **38** 693–695 (2002)

117. Neil J. Baker, Ho W. Lee, Ian C. M. Littler, C. Martijn de Sterke, Benjamin J. Eggleton, Duk-Yong Choi, Steve Madden and Barry Luther-Davies, "Sampled Bragg gratings in chalcogenide (As_2S_3) rib-waveguides", Opt. Express **14**, 9451-9459 (2006)

118. Zhaobing Tian, Scott S-H. Yam and Hans-Peter Loock, "Single-Mode Fiber Refractive Index Sensor Based on Core-Offset Attenuators", IEEE Photon. Tech. Lett. **20**, 1387-1389 (2008).

119. T. Allsop, R. Reeves, D. J. Webb, and I. Bennion, "A high sensitivity refractometer based upon a long period grating Mach–Zehnder interferometer", Rev. Sci. Instrum. **73**, 1702-1705 (2002)

120. Yuan-Tai Tseng, Yun-Ju Chuang, Yi-ChienWu, Chung-Shi Yang, Mu-ChunWang and Fan-Gang Tseng, "A gold-nanoparticle-enhanced immune sensor based on fiber optic interferometry", Nanotechnology **19**, 345501(1-9) (2008)

121. Christopher J Tuck, Richard Hague and Crispin Doyle, "Low cost optical fiber based Fabry–Perot strain sensor production", Meas. Sci. Technol. **17 ,**2206–2212 (2006)

122. Tao Wei, Yukun Han, Yanjun Li, Hai-Lung Tsai, and Hai Xiao, "Temperature-insensitive miniaturized fiber inline Fabry-Perot interferometer for highly sensitive refractive index measurement", Opt. Express **16**, 5764-5769 (2008).

123. Yun-Jiang Rao, "Recent progress in fiber-optic extrinsic Fabry–Perot interferometric sensors", Opt. Fiber Technol. **12**, 227–237 (2006

124. Vikram Bhatia, Kent A Murphy, Richard 0 Claus, Mark E Jones, Jennifer L Grace, Tuan A Tran and Jonathan A Greene, "Multiple strain state measurements using conventional and absolute optical fiber-based extrinsic Fabry-Perot interferometric strain sensors", Smart Mater. Struct. **4,** 240-245 (1995)

125. Vikram Bhatia, Kent A Murphy, Richard 0 Claus, Mark E Jones, Jennifer L Grace, Tuan A Tran and Jonathan A Greene, "Optical fiber based absolute extrinsic Fabry–P´erot interferometric sensing system", Meas. Sci. Technol. **7 ,**58–61 (1996).

126. Yun-Jiang Rao, Zeng-Ling Ran, Xian Liao, and Hong-You Deng, "Hybrid LPFG/MEFPI sensor for simultaneous measurement of high-temperature and strain", Opt. Express **15**, 14936-14941(2007).

127. A. N. Starodumov, L. A. Zenteno, D. Monzon and E. De La Rosa, "Fiber Sagnac interferometer temperature sensor", Appl. Phys. Lett. **70** ,19-21 (1997).

128. F. Ansari, "State-of-the-art in the applications of fiber-optic sensors to cementitious composites", Cem. Concr. Compos. **19**, 3–19 (1997).

129. R.C. Tennyson, A.A. Mufti, S. Rizkalla, G. Tadros, B. Benmokrane, "Structural health monitoring of innovative bridges in Canada with fiber optic sensors", Smart Mater. Struct. **10**, 560–573 (2001).

130. Y.B. Lin, C.L. Pan, Y.H. Kuo, K.C. Chang, "Online monitoring of highway bridge construction using fiber Bragg grating sensors", Smart Mater. Struct. **14**, 1075–1082 (2005).

131. Y.B. Lin, J.S. Lai, K.C. Chang, L.S. Li, "Flood scour monitoring system using fiber Bragg grating sensors", Smart Mater. Struct. **15**, 1950–1959 (2006).

132. W.L. Schulz, J.P. Conte, E. Udd, J.M. Seim, "Static and dynamic testing of bridges and highways using long-gage fibre Bragg grating based strain sensors", Proc. SPIE **4202**, 79 (2000).

133. R. Maaskant, A.T. Alavie, R.M. Measures, G. Tadroos, S.H. Rizkalla, A. Guha-Thakurta, "Fiber optic Bragg grating sensors for bridge monitoring", Cem. Concr. Compos. **19**, 21–33 (1997).

134. T.H.T. Chan, L. Yu, H.Y. Tam, Y.Q. Ni, S.Y. Liu, W.H. Chung, L.K. Cheng, "Fiber Bragg grating sensors for structural health monitoring of Tsing Ma bridge: background and experimental observation", Eng. Struct. **28**, 648– 659 (2006).

135. Y.M. Gebremichael, W. Li, W.J.O. Boyle, B.T. Meggit, K.T.V. Grattan, B. McKin- ley, G.F. Fernando, G. Kister, D. Winter, L. Canning, S. Luke, "Integration and assessment of fibre Bragg grating sensors in an all-fibre reinforced polymer composite road bridge", Sens. Actuators A **118**, 78–85 (2005).

136. Y.B. Lin, K.C. Chang, J.C. Chern, L.A. Wang, "The health monitoring of a pre-stressed concrete beam by using fiber Bragg grating sensors", Smart Mater.Struct. **13**, 712–718 (2004).

137. M.H. Maher, E.G. Nawy, "Evaluation of fiber optic Bragg grating strain sen-sors in high strength concrete beams", in: F. Ansari (Ed.), Applications of FiberOptic Sensors in Engineering Mechanics, (ASCE-EMD, ASCE, New York, 1993)

138. M.A. Davis, D.G. Bellemore, A.D. Kersey, "Distributed fiber Bragg grating strainsensing in reinforced concrete structural components", Cem. Concr. Comp. **19**, 45–57 (1997).

139. J.S. Leng, G.C. Mays, G.F. Fernando, "Structural NDE of concrete structures using protected EFPI and FBG sensors", Sens. Actuators A **126**, 340–347 (2006).

140. W. Chung, D. Kang, "Full-scale test of a concrete box girder using FBG sensing system", Eng. Struct. **30**, 643–652 (2008).

141. G. Kister, D. Winter, R.A. Badcock, Y.M. Gebremichael, W.J.O. Boyle, B.T. Meg-gitt, K.T.V. Grattan, G.F. Fernando, "Structural health monitoring of a composite bridge using Bragg grating sensors. Part 1. Evaluation of adhesives and pro- tection systems for the optical sensors", Eng. Struct. **29**, 440–448 (2007).

142. H.N. Li, D.S. Li, G.B. Song, "Recent applications of fiber optic sensors to health monitoring in civil engineering", Eng. Struct. **26**, 1647–1657(2004).

143. G. Kister, D. Winter, J. Leighton, R.A. Badcock, P.D. Tester, S. Krishnamurthy, W.J.O. Boyle, K.T.V. Grattan, G.F. Fernando, "Methodology and integrity moni-toring of foundation concrete piles using Bragg grating optical fibre sensors", Eng. Struct. **29** 2048–2055 (2007).

144. W. Lee, W.J. Lee, S.B. Lee, R. Salgado, "Measurement of pile load transfer using the fiber Bragg grating sensor system", Can. Geotech. J. **41**, 1222–1232 (2004).

145. V. Slowik, E. Schlattner, T. Klink, "Experimental investigation into early age shrinkage of cement paste by using fibre Bragg gratings", Cem. Concr. Comp. **26**, 473–479 (2004)

146. A.C. Wong, P.A. Childs, R. Berndt, T. Macken, G.D. Peng, N. Gowripalan, "Simul-taneous measurement of shrinkage and temperature of reactive powderconcrete at early age using fibre Bragg grating sensors", Cem. Concr. Comp.**29**, 490–497. (2007).

147. M. Rajesh, K. Geetha, M. Sheeba, P. Radhakrishnan, C.P.G. Vallabhan and V.P.N. Nampoori, "A fiber optic smart sensor for studying the setting characteristics of various grades of cement", Opt. Lasers Eng. **44**, 486–493 (2006)

148. P.S. Andréa, Humberto Varum, Paulo Antunes, Licínio Ferreira and M.G. Sousa, "Monitoring of the concrete curing process using plastic optical fibers", Measurement **45**, 556–560 (2012).

149. M Sheeba, M Rajesh, C P G Vallabhan, V P N Nampoori and P Radhakrishnan, "Fiber optic sensor for the detection of adulterant traces in coconut oil", Meas. Sci. Technol. **16**, 2247-2250 (2005)

150. R. Falate, R.C. Kamikawachi, M. Müller, H.J. Kalinowski, J.L. Fabris, "Fiber optic sensors for hydrocarbon detection", Sens. Actuators, B **105**, 430–436 (2005)

151. R Falate, K Nike, Pedro Ramos da Costa Neto, Eduardo Caçao Jr., Marcia Muller, Hypolito Jose Kalinowski and Jose Luis Fabris, "Alternative Technique For Biodiesel Quality Control Using An Optical Fiber Long period Grating Sensor", Quim. Nova **30**, 1677-1680 (2007)

152. G R C Possetti, L C Cocco, C I Yamamoto, L V R de Arruda, R Falate, M Muller and J L Fabris, "Application of a long-period fiber grating-based transducer in the fuel industry", Meas. Sci. Technol. **20**, 034012(1-9) (2009)

153. V Mishra, S C Jain, N Singh, G C Poddar and P Kapur," Fuel Adulteration Detection using Long Period Fiber Grating Sensor Technology", Indian J. Pure Ap. Phy. **46**, 106-110 (2008)

154. A. Balaji Ganesh, T. K. Radhakrishnan, "Fiber-Optic pH Sensor Fiber Integrated Opt. **25**, 403–409 (2006)

155. Wolthuis, R., D. McCrae, E. Saaski, J. Hartl, and G. Mitchell. "Development of medical fiber-optic pH sensor based on optical absorption", IEEE Trans. Biomed. Eng. **39**, 531-535 (1992).

156. Lin, J., and D. Liu. "An optical pH sensor with a linear response over a broad range", Anal. Chim. Acta. **408**, 49-54 (2000).

157. Delana, A. N., M. V. Schiza, and S. M. Angel, "Multilayer sol-gel membranes for optical sensing applications: Single layer pH and dual layer CO2 and NH3 sensors", Talanta **58**, 543-551 (2002).

158. Jin, J., and Z. Rosenzweig. "Fiber optic pH/Ca2+ fluorescence microsensor based on spectral processing of sensing signals", Anal. Chim. Acta. **397**, 93-98 (1999).

159. John, E. L., and S. S. Saavedra. "Evanescent sensing in doped sol-gel glass films", Anal.Chim. Acta **285**, 265-269 (1994).

160. C S Burke, L Polerecky and B D MacCraith, "Design and fabrication of enhanced polymer waveguide platforms for absorption-based optical chemical sensors", Meas. Sci. Technol. **15**, 1140–1145 (2004)

161. G R C Possetti, R C Kamikawachi, C L Prevedello, M Muller, and J L Fabris, "Salinity measurement in water environment with a long period grating based interferometer", Meas. Sci. Technol. **20**, 034003 (1-6) (2009)

162. Samer K. Abi Kaed Bey , Cathy Chung Chun Lam, Tong Sun, Kenneth T.V. Grattan, "Chloride ion optical sensing using a long period grating pair", Sens. Actuators, A **141**, 390–395(2008)

163. Masayuki Yokota and Toshihiko Yoshino, "An optical-fiber water-concentration sensor using Tm3+:YAG fluorescent light", Meas. Sci. Technol. **11**, 152–156 (2000)

164. Yoshiaki Kurauchi , Takayuki Yanai, Naoyoshi Egashira and Kazuya Ohga, "Fiber-Optic Sensor with a Chitosan/Poly(vinyl alcohol) Cladding for the Determination of Ethanol in Alcoholic Beverages", Anal. Sci. **10**, 213-217 (1994)

165. T. Venugopalan, Teck L. Yeo, Tong Sun, and Kenneth T. V. Grattan, "LPG-Based PVA Coated Sensor for Relative Humidity Measurement", IEEE Sens. J. **8**,1093-1098 (2008)

166. LiweiWang, Yang Liu, Min Zhang, Dongsheng Tu, Xianhui Mao and Yanbiao Liao, "A relative humidity sensor using a hydrogel-coated long period grating", Meas. Sci. Technol. **18**, 3131–3134 (2007)

167. T. Venugopalan, T. Sun, K.T.V. Grattan, "Long period grating-based humidity sensor for potential structural health monitoring", Sens. Actuators, A **148**, 57–62 (2008)

168. Ainhoa Gaston, Fatima Perez, and Joaquın Sevilla, "Optical fiber relative-humidity sensor with polyvinyl alcohol film", Appl. Opt. **43**, 4127-4132 (2004)

169. Francisco J. Arregui, Zuri Ciaurriz, Maria Oneca, Ignacio R. Matıas, "An experimental study about hydrogels for the fabrication of optical fiber humidity sensors", Sens. Actuators, B **96**, 165–172 (2003)

170. Jinesh Mathew, Yuliya Semenova,Ginu Rajan,Pengfei Wang and Gerald Farrell, "Improving the sensitivity of a humidity sensor based on fiber bend coated with a hygroscopic coating", Opt. Laser Technol. **43**, 1301–1305 (2011)

171. Anu Vijayan , Madhavi Fuke , Ranjit Hawaldar, Milind Kulkarni , D. Amalnerkar , R.C. Aiyer, "Optical fiber based humidity sensor using Co-polyaniline clad", Sens. Actuators, B **129**, 106–112 (2008)

172. Wenqing Cao, Yixiang Duan, "Optical fiber-based evanescent ammonia sensor", Sens. Actuators, B **110**, 252–259 (2005)

173. Mark A. Arnold and Tiffany J. Ostler, "Fiber Optic Ammonia Gas Sensing Probe", Anal. Chem. **58**, 1137-1140 (1986)

174. Otto S. Wolfbeis, Leonie J. Weis, Marc J. P. Leiner and Werner E. Ziegler "Fiber-optic Fluorosensor for Oxygen and Carbon Dioxide", Anal. Chem. **60**, 2028-2030 (1988).

175. Mahesh Uttamlal and David R. Wal, "A Fiber-Optic Carbon Dioxide Sensor for Fermentation Monitoring", Nat. Biotechnol. **13**, 597 - 601 (1995)

176. Otto S. Wolfbeis, Barna Kovdcs, Kisholoy Goswami and Stanley M. Klainer, "Fiber-Optic Fluorescence Carbon Dioxide Sensor for Environmental Monitoring", Mikrochim. Acta **129**, 181-188 (1998)

177. Christjanem Unkholm, David R. Walt and Fred P. Milanovich, "A Fiber-Optic Sensor for CO_2 Measurement", Talanta **35**, 109-112 (1988).

178. S. Sekimoto, H. Nakagawa , S. Okazaki, K. Fukuda, S. Asakura, T Shigemori and S. Takahashi, "A fiber-optic evanescent-wave hydrogen gas sensor using palladium-supported tungsten oxide", Sens. Actuators, B **66**, 142–145 (2000).

179. Susan L. R. Barker, Raoul Kopelman, Terrance E. Meyer and Michael A. Cusanovich, "Fiber-Optic Nitric Oxide-Selective Biosensors and Nanosensors", Anal. Chem. **70**, 971-976 (1998).

180. Sheila A. Grant, Joe H. Satcher Jr. and Kerry Bettencourt, "Development of sol–gel-based fiber optic nitrogen dioxide gas sensors", Sens. Actuators, B **69**, 132–137 (2000).

181. Shelly John Mechery and Jagdish P. Singh, "Fiber optic based gas sensor with nanoporous structure for the selective detection of NO_2 in air samples", Anal. Chim. Acta. **557**, 123–129 (2006)

Fiber optic sensor for determining the quality of alcohol-water mixtures

2.1 Introduction

Water is an almost universal solvent and aqueous solutions of alcohols have found widespread use in several sectors such as beverage industries, personal care products, pharmaceutical and chemical industry, chromatography solvents to food additives, supercritical water technology etc [1]. They have also found use in bio science as solvents assisting protein denaturation due to the promotion of the R-helix structure of peptides and proteins [1]. Hence in-situ detection and quantification of alcohol with high sensitivity and selectivity is a critical factor in many industrial as well as biotechnical applications. Moreover accurate measurement of ethanol is unavoidable in clinical and forensic analysis in order to analyze human body fluids like blood, serum, urine and breath. In order to manage fermentation process and thus to control the quality of products, detection of ethanol is important in food [2,3] and beverage industries [4,5].

This wide application range is due to the fact that a lot of physical and chemical properties of alcohol-water mixtures exhibit nonlinear dependence on solvent composition and shows peaks at certain critical concentrations depending on the nature of alcohol [6-9]. With increasing chain length, the solubility of alcohols in water decreases and among monohydroxyl alcohols that are miscible with water in any proportion, tert-butyl alcohol (TBA) possesses the biggest alkyl group. The TBA-water mixture is characterized by anomalies like a sharp minimum of the Excess molal volume and a maximum of the molal heat capacity at TBA molar fraction 0.04 [10]. Sato et al. have shown in a series of publications that the thermodynamics of mixing of short alcohols such as ethanol [11], methanol [12], 1-propanol [13] and 2-propanol [14] with water are complex functions of the liquid composition.

While much is known about the macroscopic chemical behavior of these solutions, the solvation structure is poorly understood for many

aqueous alcohols. Since alcohol molecules possess alkyl and hydroxyl groups, the way of dissolution in water is highly complicated due to the hydrophilic and hydrophobic interactions of alcohol and water molecules in solution, which in turn cause the anomalies [15]. Binary mixtures of alcohol and water were studied extensively using various techniques like X-ray absorption and X-ray emission(XA and XE) [16], ultrafast spectroscopy [17], Infrared (IR) absorption spectroscopy [18], neutron diffraction[19,20,21], Small-angle X-ray Scattering (SAXS) [22,23], light scattering [24-26], microwave analysis [27], time resolved spectroscopy [28], computer simulations[29-34] etc., in the light of hydrogen-bond network, aggregation, hydrophobic interaction, 'clathrate' formation, and 'hydrophobic hydration' for several years to correlate solution structure with the observed anomalies. Even after being investigated for decades, the structure and topology of the hydrogen-bonded network in aqueous solutions of alcohols is an area where open questions still remain and the conclusions drawn from experimental studies are conflicting [16,19]. The observed anomalies with alcohol-water mixtures were first attributed to the ice-like or clathrate-like structures created in surrounding water due to the hydrophobic head groups present in alcohol [21,25,26,35-38]. The results shown by neutron diffraction experiments [19] and x-ray emission spectroscopy [16] clearly challenge the "iceberg" model and suggest that rather than being enhanced or depleted, the structure of water in the mixture is close to that of the pure liquid. However, there are obvious inconsistencies between these experimental studies. The small fraction (~0.13) of water molecules predicted by Dixit et al. [19] to exist singly with no hydrogen-bonds to other water molecules is suggested to be incompatible with the simulated XE spectra of Guo et al.[16]. According to theoretical studies based on the RISM (Reference Interaction Site Model) approach, alcohol molecule resides in the cavity of the H-bonding network created by the surrounding water molecules which, in turn, lowers the compressibility of the medium [34]. However, with further addition of alcohol, the tetrahedral network structure gradually converts to the zigzag chain structure of alcohol increasing the compressibility of the water–alcohol mixtures [34]. Recently Naiping *et.al.* have reported the influence of structure formation with ethanol and water on the taste or brand preference of the otherwise colorless and tasteless water-ethanol solution called vodka [39].

37

Thus understanding the structure of molecules in alcohol-water solutions and the evaluation of alcohol concentration in alcohol-water mixture is currently a considerable challenge. During the last decades many analytical methods have been developed for the measurement of ethanol and other alcohols [40,41] and can be classified into three major categories namely chromatographic[42-44], resistive[45-60], capacitive [61] and optical[62,63]. Among these techniques, the chromatographic method is the most accurate and sensitive with a lower limit of ethanol detection on the order of 0.005% v/v reported by Zimbo et.al. [44]. Drawbacks of this method include high cost, as well as the necessity for sample pretreatment and long operation times. Somewhat less precise but more rapid measurements are achieved by the use of resistive methods where enzymes [46- 49], metal oxides [50-53] nanoparticles [54-59] and polymers [60] are used as sensing materials. Enzyme based ethanol concentration detection is based on either of two enzymes, alcohol oxidase or alcohol dehydrogenase, by monitoring O_2 consumption or H_2O_2 formation [46-48]. The specificity of the enzyme binding sites provides highly selective and accurate sensors. The disadvantage of the sensors lies in their instability due to protein denaturing when exposed to high temperature, pressure, or pH extremes. Regarding nanoparticle based detection, Hsueh et.al. reported a highly sensitive ethanol vapor sensor based on ZnO nanowire [54]. A zinc oxide based ceramic semi-conductor ethanol gas sensor was reported by Bhooloka Rao [55] while Tan et.al. [56,58,59] presented different sensors based on nano-sized α -Fe_2O_3 with SnO_2, ZrO_2, TiO_2 solid solutions. A polymer based sensor was designed by Lee et.al [60] while Dubas et.al [64] developed an absorbance based ethanol sensor using dye–Chitosan polyelectrolyte multilayers.

Among various sensing techniques, the simplest approach in the determination of alcohols is an optical sensor based method. Optical sensors generally have the advantages of low-cost manufacturability, safety, and miniaturization and are intended for use in real-time, in situ monitoring. Several authors have reported optical ethanol sensors based on fluorescence [65-72], Raman spectroscopy [73], Fabry Perot cavity [74] and optical fibers [75-80].

Due to their inherent advantages, fiber optic sensors are an ideal choice and have been implemented for the detection of ethanol [81-83]. Passive

nonselective fiber-optic sensors based on determination of refractive index changes as a function of the alcohol content using surface plasmon resonance [84] have been reported by Matsubara et. al. Recently fiber optic sensors incorporating an active sensitive terminal have been developed for monitoring lower alcohols in gas or liquid mixtures. An optical fiber long-period grating with solgel derived SnO_2 coating was successfully implemented by Gu et.al. [85,86] while Penza et.al. [87,88] have reported the sensitivity of Langmuir–Blodgett (LB) films with single-walled carbon nanotubes (SWCNTs) for ethanol vapour detection.

This chapter describes the fabrication of an extrinsic fiber optic sensor probe by using etched plastic clad silica (PCS) fiber. Also we discuss the theory and principle of operation of the designed fiber optic probe and the successful utilization of the probe for quantifying alcohol concentration in their binary mixtures with water. The designed sensor works on the principle of hydrophilic adhesion of molecules on to the silica fiber and can be effectively utilized for determining the concentration of ethanol, methanol and 2-propanol in their binary mixtures with water.

2.2 Fabrication of fiber probe

The designed sensor probe consists of two fibers, one of which transmits light into the medium to be investigated and the second fiber directs the modulated light back into the photo detector. We have used plastic clad, step index silica fiber with a core diameter of 400 μm (Newport F-MBC, 0.37 NA) having a length of 50 cm for the probe preparation. After removing the sheath from the tip of both the fibers (around 1mm), the tip is dipped in acetone for removing the cladding. The prepared tip of each of the fiber is then dipped in hydro fluoric acid (48%) for about 30 minutes for etching. Etching produces a tapered region with a core of reduced diameter and both the fibers are then aligned parallel and glued together at one end as shown in figure 2.1 to form the sensor probe.
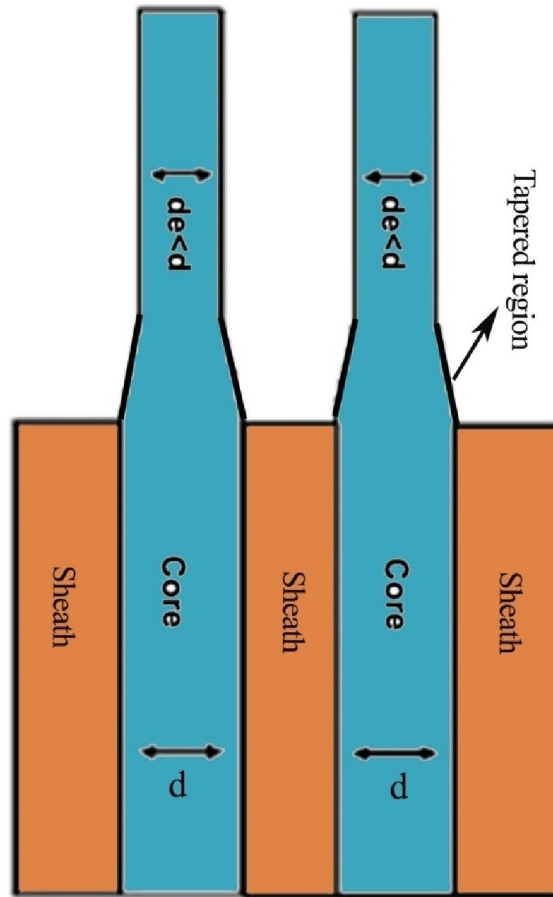
Figure 2.1 Structure of fiber probe

2.3 Theory

The principle underlying the working of the sensor probe is explained by Kumar et.al [89]. Consider the fiber structure shown in figure 2.2. Light from a multimode fiber of core diameter d, is coupled into the decladded fiber region of smaller diameter d_e through an intermediate taper which is also decladded. The core refractive indices of all these three regions are same (n_i)
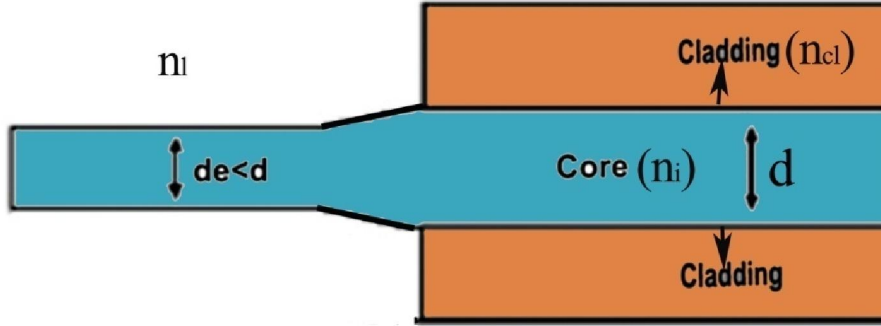
Figure 2.2 Fiber structure

When light propagates from a fiber of diameter d to a region of diameter d_e through a tapered region, the fraction of optical power coupled is given by Kumar et al. [89] as

$$P = P_0 \left[\frac{n_i^2 - n_l^2}{R^2 \left(n_i^2 - n_{cl}^2 \right)} \right] \qquad (2.1)$$

where P_0 is the input power, n_i is the core refractive index, n_{cl} the cladding refractive index and n_l the refractive index of the medium surrounding the taper and R=d/ d_e. From (1) it is clear that the coupled power P decreases with the increase in n_l^2. Thus power lost to the surrounding medium through the tapered region P_0-P is proportional to the refractive index of the surrounding medium, n_l.

2.4 Simulation studies

In order to study the working of the sensor probe a planar structure with parameters similar to that of the fiber is simulated using BeamPROP software package of RSoft.
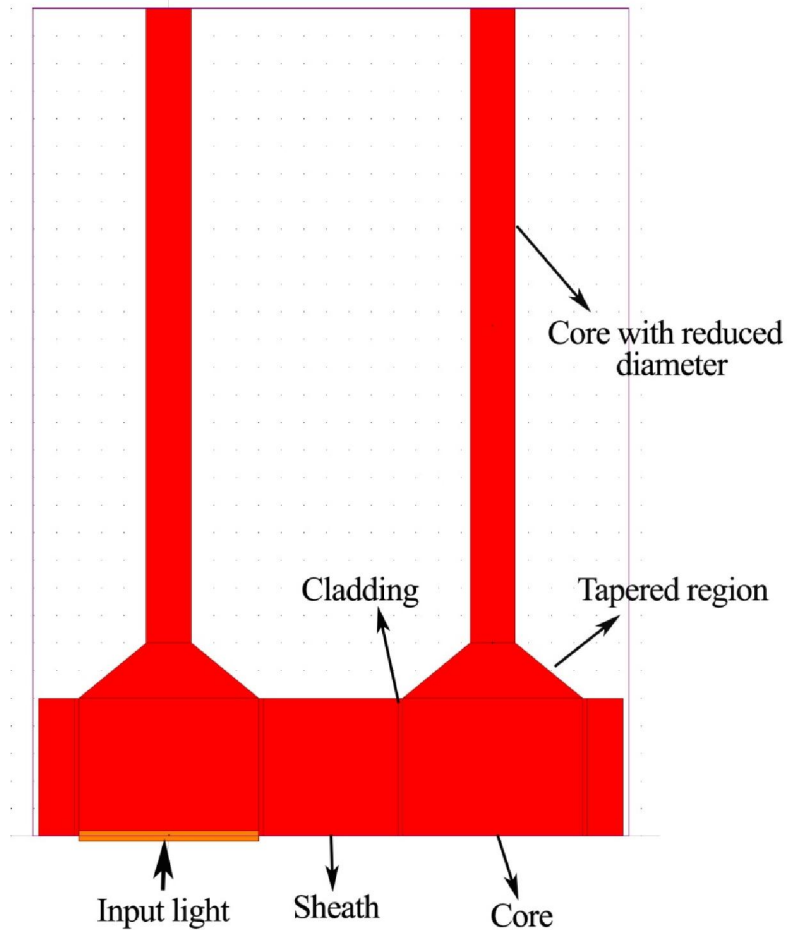
Figure 2.3 Structure of the fiber probe for simulation

A structure as shown in figure 2.3 is simulated where there is a core at the center having a width of 400 μm and refractive index 1.45. Laterally, the core extends to cladding of thickness 10 μm on either side with a refractive index of 1.4. Then on either side there is a layer analogous to sheath with a thickness of 105 μm making the total lateral width 630 μm. Axially, the core extends to a tapered region without the cladding and sheath layer. Then there is a layer corresponding to etched layer having width less than 400 μm . Two such structures are aligned exactly parallel like the fiber probe. Light of wavelength 532nm is coupled to one of the fibers and light propagation was simulated using the software.   The field patterns thus

obtained for structures with different parameters are shown in figure 2.4a, 2.4b, 2.4c, 2.4d, 2.4e, 2.4f, 2.4g, 2.4h, 2.4i and 2.4j. The simulation result of an un-etched fiber
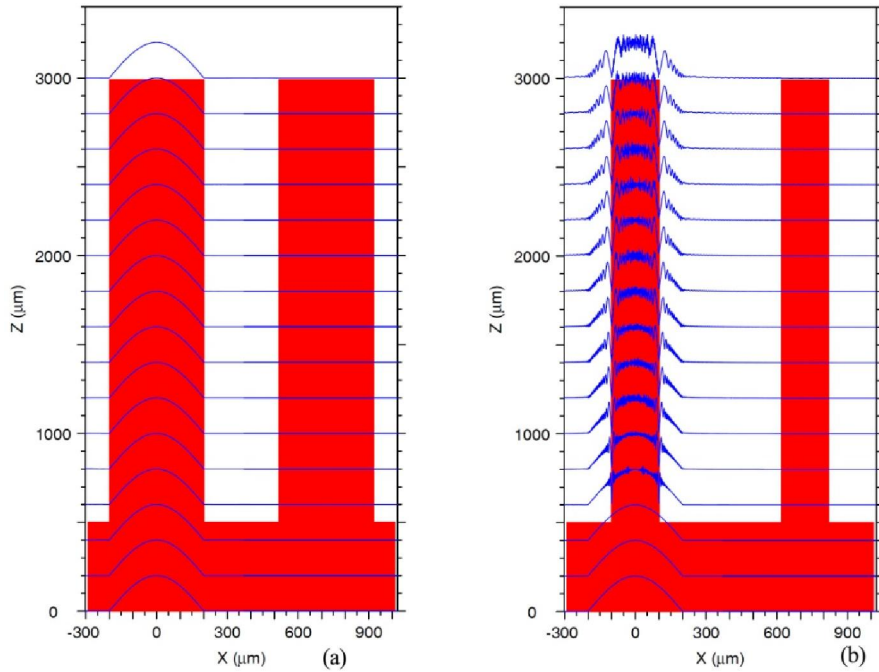
Figure 2.4 a) Fibers (400μm dia) b) Fibers (400μm dia)
etched to 200μm dia tip

probe is presented in figure 2.4a, where there is neither tapered region nor diameter reduction. In this case the unaltered fiber core of the two fibers extends out without cladding. From the simulation result it is obvious that the coupled light pass through the fiber and field coupling between the two fibers does not exist. Figure 2.4b shows the results where the fibers are reduced to a diameter of 200 μm but without a tapered region. In this case also there is no evidence for field coupling.
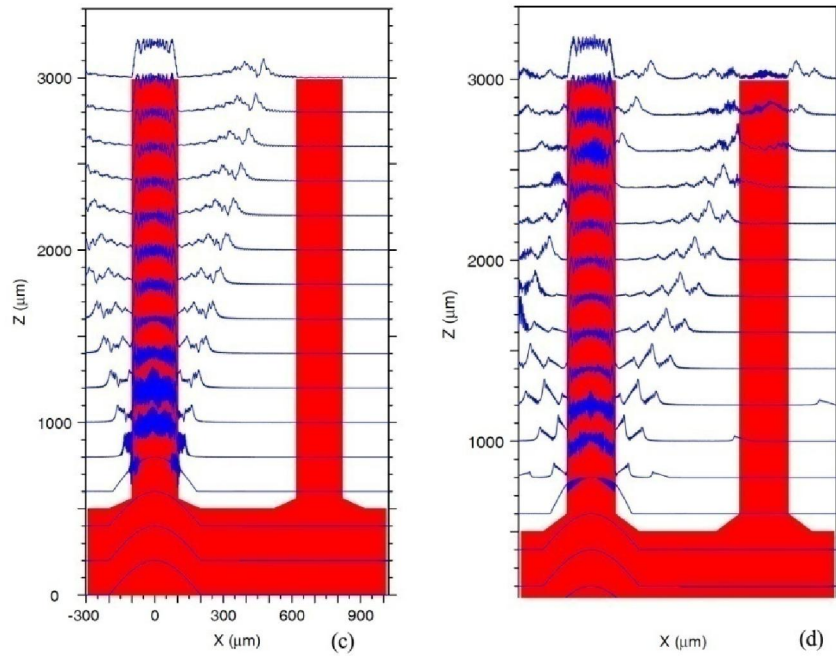
Figure 2.4 Fibers etched to 200µm dia with c) 60 µm taper
d) 100 µm taper
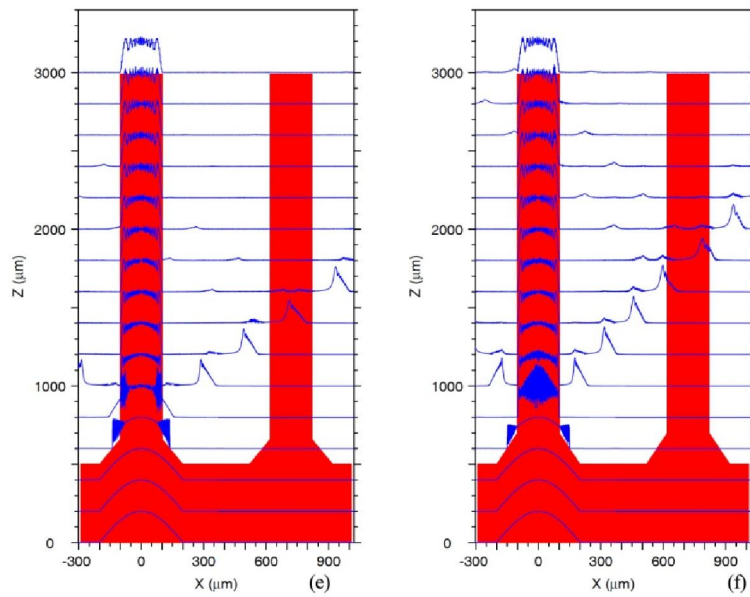
Figure 2.4 Fibers etched to 200µm dia with e) 160 µm taper
f) 200 µm taper
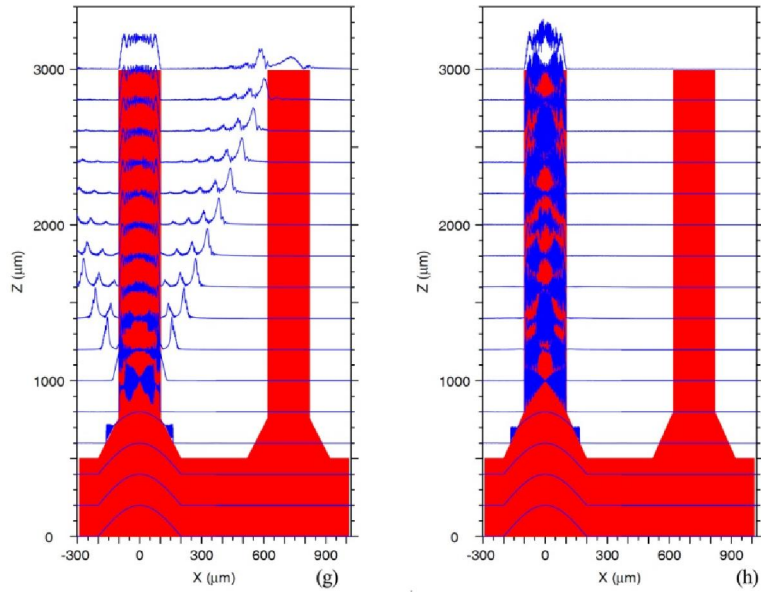
Figure 2.4 Fibers etched to 200µm dia with g) 260 µm taper
h) 300 µm taper
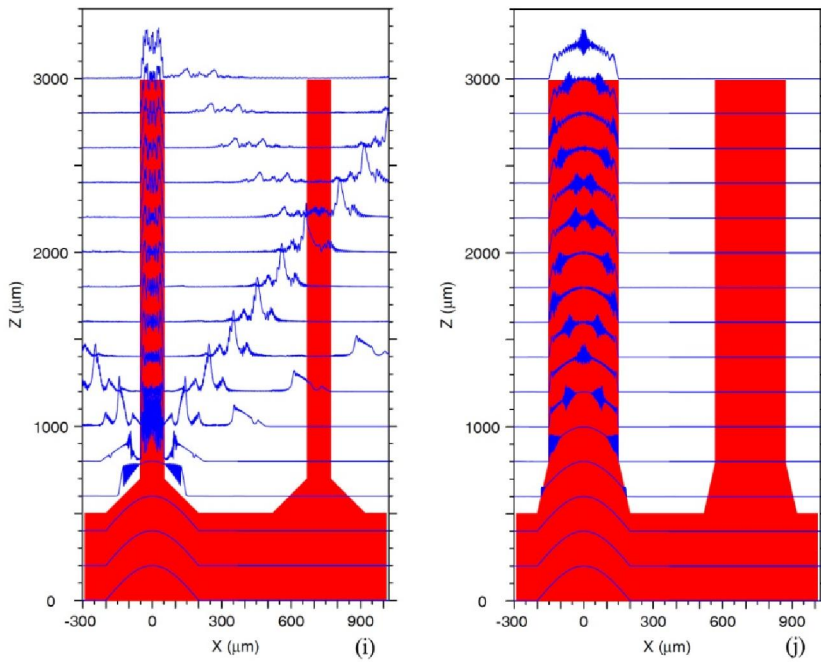
Figure 2.4 i)Fiber etched to 100µm dia with 200 µm taper j) Fiber etched
to 300µm dia with 300 µm taper

Figures 2.4c, 2.4d, 2.4e, 2.4f, 2.4g and 2.4h shows the results for probes with tapered regions of different lengths and a narrowed core of width 200 μm. The height of the tapered region is 60 μm in the case of figure 2.4c while it is 100 μm , 160 μm , 200 μm , 260 μm and 300 μm respectively for figures 2.4d, 2.4e, 2.4f, 2.4g and 2.4h. Figure 2.4i shows the result for the probe where the tapered region has a height of 200 μm and the etched core has a width of 100 μm. From the graphs it is evident that there exists field coupling from the input fiber to the other and its strength varies with the dimension of the tapered region.

2.5 Experimental

The experimental setup used for the study is presented in figure 2.5.The emission from a 20mW diode pumped solid state laser source (λ=532 nm) is launched into one of the fiber arms of the sensor. The modulated optical signal is collected by the second arm, which is coupled to the detector head (Newport 818-SL) of a power meter (Newport 1815-C). To move the fiber probe in and out of liquid, the liquid carrying beaker is kept on a translation stage which can be moved with a resolution of 10μm.
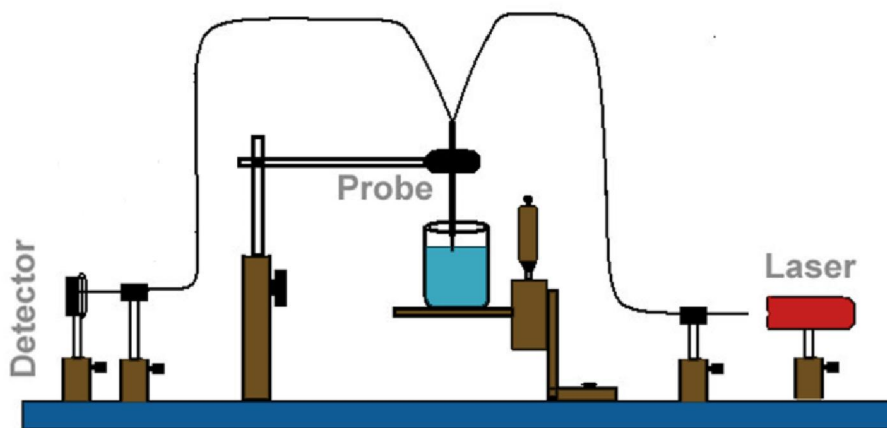
Figure 2.5 Schematic diagram of the experimental setup
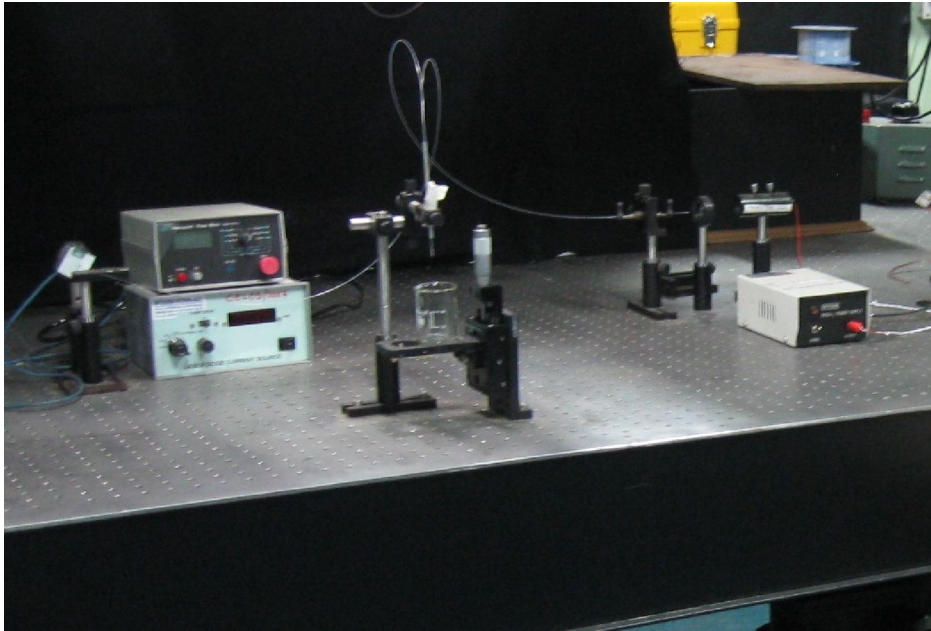
Figure 2.6 Photograph of the experimental setup for sensing

2.6 Results and Discussions

We used pure water as the test medium to investigate the response of the fiber probe to liquid medium. Water was taken in the beaker and the probe was immersed in and then pulled out from water using the translation stage. The output power is plotted as a function of the liquid level displacement from the tip of the fiber probe and is shown in figure 2.7. The curve ABCD is the response obtained while moving the probe into water from air and DEFG represents the response obtained for the probe displacement in the opposite direction. The point 'A' represents the output power when the probe was in air while 'B' indicates the point where the tip touched water surface. The point 'C' represents the intersection point of water surface and the tapered region. When the fiber probe is in air, a part of light intensity leaks through the etched region of the input fiber and gets coupled into the output fiber as shown in the simulation results. The coupled light then reflects back from the tip of the second fiber and is collected back

at the receiver. This power remains constant, and can be termed as the reference value. The detector output reduces from the reference value when the probe is immersed in water. A sharp increase in output is obtained when the probe tip is pulled out of water surface as shown by the curve FG in figure 2.7. The marking 'F' corresponds to the point where the probe tip is just out of water surface. The marking 'B' corresponds to the point at which the probe tip touch water surface while moving in and 'F' the point at which the tip leaves the water surface while moving out. A separation of around 750μm is observed between 'B' and 'F' and this is due to the surface tension effect of water.
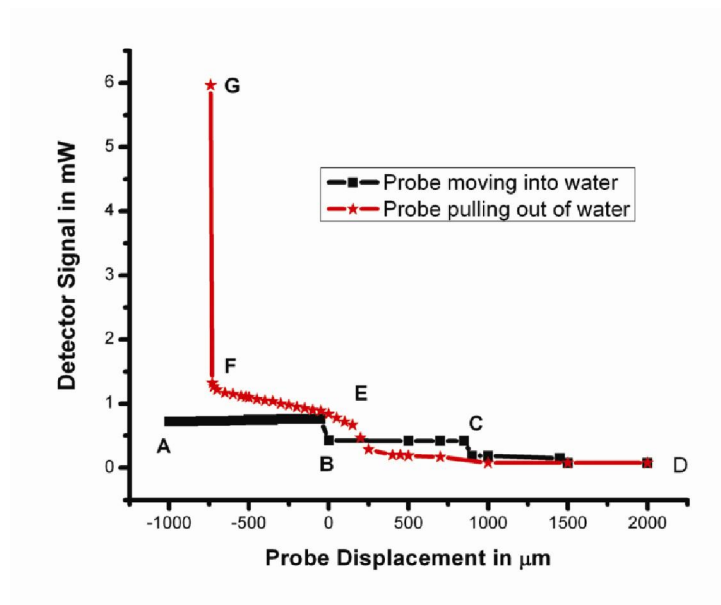
Figure 2.7 Response of the probe when dipped and pulled out of water

To explain this phenomenon of sharp increase in output, another experiment was conducted. Light was allowed to pass through a silica fiber which has a decladded region and the output was recorded. Then a medium of higher refractive index was added around the decladded region and the varying intensity as a function of time was recorded. The experiment was

48

done with liquids like ethanol (RI 1.36), 2-propanol (RI 1.375) and water (RI 1.33). Another medium with a higher refractive index was made by mixing ethyleneglycol and water having a measures refractive index 1.43. The experiment was repeated for this liquid too. The result thus obtained is shown in figure 2.8. From the basic theories of decladded optical fiber, it is clear that the output should decrease when a medium with refractive index higher than 1 is added around the decladded region. From the result it is observed that for water the output increases while for all other liquids it decreases. Silica is hydrophilic in nature and hence water molecules adsorb on to the fiber [90]. This enhances back reflection of light into the core at the core medium interface and hence causes the increase in output. Adsorption does not happen in the case of alcohols and the medium with refractive index 1.43. An entirely opposite response was obtained when the silica fiber was replaced with a polymer optical fiber and the result is shown in figure 2.9. In this case the output power reduced when water was the ambient medium while it increased when ethanol was introduced.
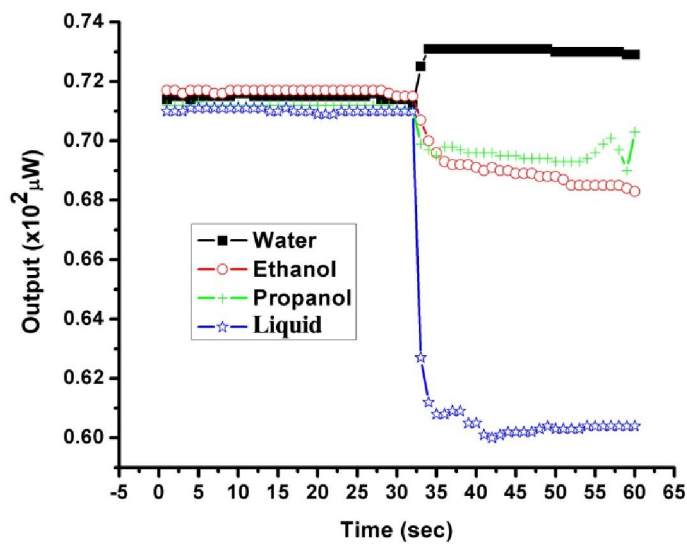
Figure 2.8 Response of decladded PCS fiber towards various ambient liquids

49
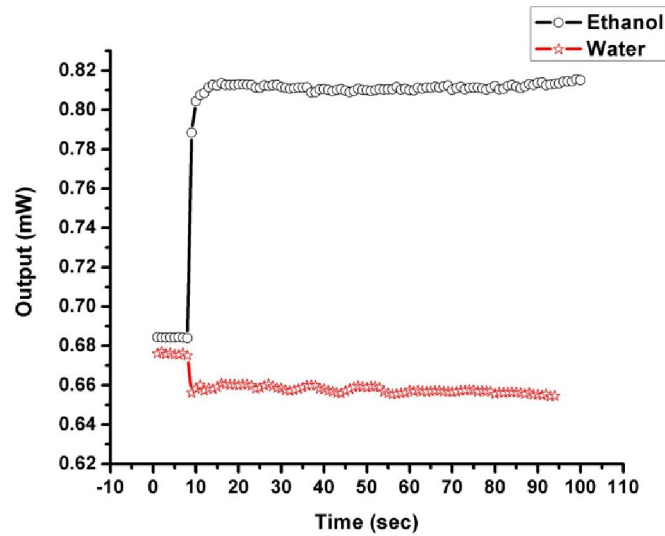
Figure 2.9 Response of decladded polymer fiber towards various ambient liquids

As per equation 2.1, the optical power leaking through the tapered region is proportional to the refractive index around the tapered region. From the simulation studies as well it is clear that the input light leaks through the tapered region and couples to the second fiber. A fraction of light reflects back from the tip of the second fiber and is collected back at the detector and this represents the intensity at the point 'A' in figure 2.7. When the tip touches water surface back reflection reduces due to absorption by water. This causes the reduction in output at the point 'B'. As the tapered region intersects with water, though more power leaks out, the increase in absorption cause the further reduction of output power at point 'C'. Since silica is hydrophilic water molecules adsorb on to it and once the fiber comes out of water they act as scattering centers. This increases the field coupling and causes the drastic increase in output marked by FG in the response curve.

As time progresses the output intensity drops to reference value due to evaporation of the adsorbed molecules and is shown in figure 2.10. This response of the probe can be utilized as a liquid level sensor.

50
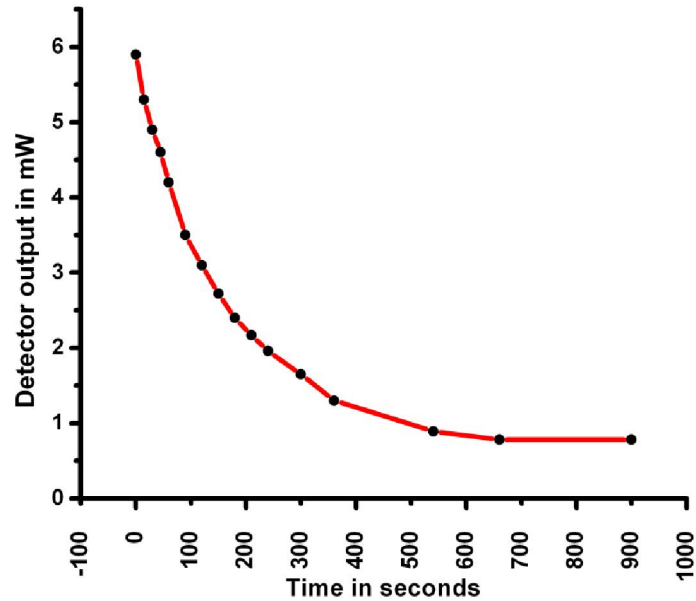
Figure 2.10 Detector output decreasing with time

To further verify these conclusions, the experiment was repeated using ethanol water mixtures. Ethanol was mixed with de ionized water at various volumetric ratios using ultrasonicator to prepare the test solutions at required concentrations. Efforts were taken to conduct experiments at constant temperature of 25^0C. The beaker filled with the test solution was kept on the translational stage (figure 2.5) and after immersing in it, the probe was pulled out. The initial intensity maximum and the time taken by the intensity to drop to the reference value were recorded for each ethanol concentration. The evaporation rate of ethanol is higher than that of water and it is obvious that in this mixture with water the evaporation rate increase with the increase in ethanol concentration. The time taken by the response to reach reference as a function of ethanol volumetric concentration is given in figure 2.11. From the response given in figure 2.11, it is evident that the output drops to reference value at a faster rate when the ethanol

51

concentration is higher. As the ethanol concentration in the solution became high (more than 80%) the sudden rise in the intensity was not observed. This proves the assumption of molecular adsorption on to the fiber. These adsorbed molecules cause the sudden increase in output and eventually on evaporation the output drops to reference value. Since ethanol does not have hydrophilic head groups adsorption does not occur.
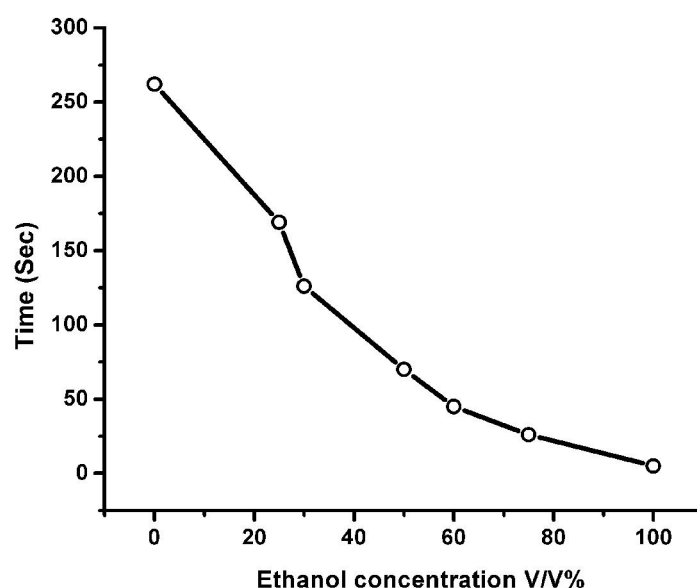
Figure 2.11 Time required for the intensity to drop to reference value

Another interesting observation from the experiment with ethanol water solution is that the initial intensity maximum varies with ethanol concentration. The plot in figure 2.12 gives the output intensity as a function of ethanol concentration where the X axis gives the volumetric percentage of ethanol in the solution and Y axis gives the ratio of the maximum output to that of the reference value. Even though the maximum output and the ratio of maximum output to the reference value gives the same trend, the method of taking the ratio helps in reducing noise due to the ambient light. We repeated

52

the experiment several times by varying the input power, wavelength of the laser etc but the curve peaks around 60% V/V concentration and when converted to mole fraction of ethanol it is around 0.3.

The experiment was repeated with aqueous mixtures of methanol and 2-propanol and the results obtained are shown in figure 2.13 and figure 2.14 respectively.
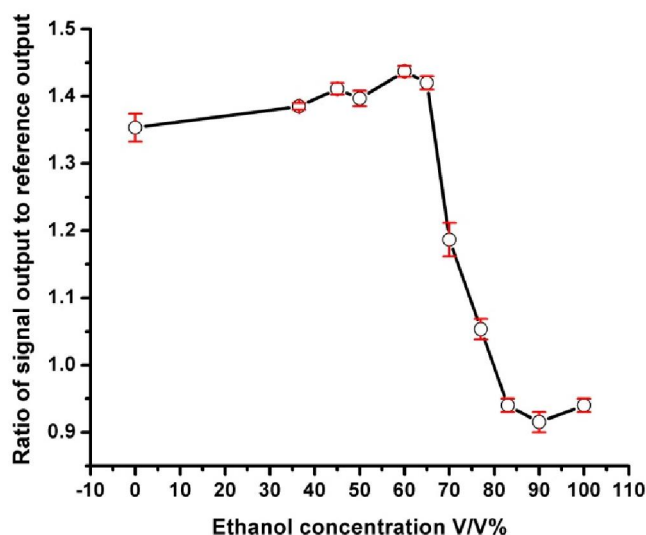
Figure 2.12 Sensor output as a function of ethanol concentration

From the results obtained using the probe for ethanol, methanol and 2-propanol it is obvious that the probe can be used as a sensor for determining the volumetric concentration of alcohol-water binary mixture. In the case of ethanol it is evident from figure 2.12 that the response is almost linear in the ethanol volumetric concentration range 0% to 60% and 60% to 90%. In the case of methanol the response is linear (figure 2.13) in the volumetric concentration range 50% to100% while for 2-propanol (figure 2.14) the linear range for volumetric concentration is in between 0% to 40% and 40% to 100%.
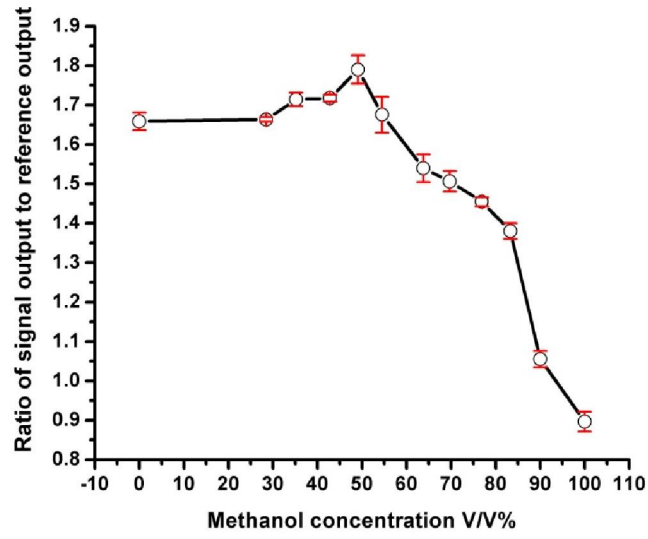
Figure 2.13 Sensor output as a function of methanol concentration
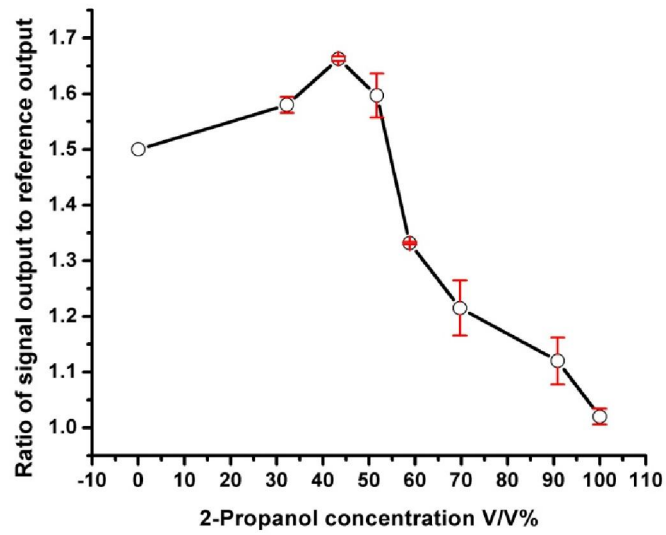
Figure 2.14 Sensor output as a function of 2-propanol concentration

The results reveal that the phenomenon is related to molecular level and hence rather than volumetric ratio mole fraction gives a better insight. In order to compare the results the sensor parameter was normalized and plotted as a function of alcohol mole fraction. The results thus obtained for methanol, ethanol and 2-propanol are shown in figure 2.15 while that for tert-butanol is shown in figure 2.16. The plots give the variation of the sensor parameter as a function of alcohol mole fraction. The X axis gives the mole fraction of alcohol in the solution while the Y axis gives the normalized ratio of the initial maximum output (detector output just after pulling out the probe from liquid) to that of the reference value (detector output just before immersing the probe into the liquid).
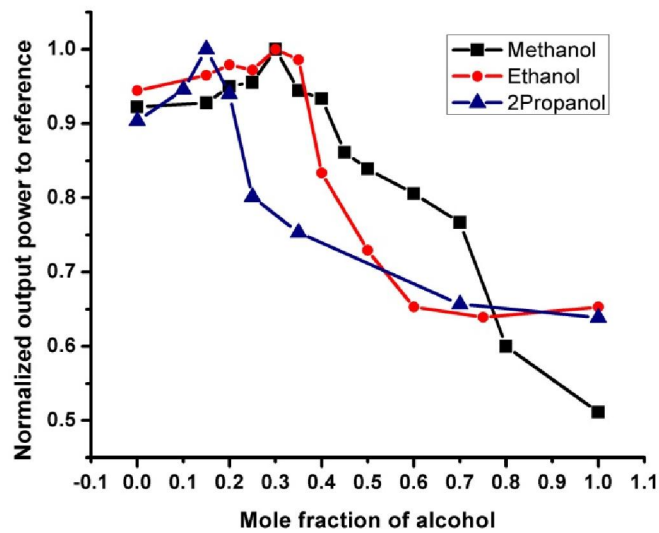
Figure 2.15 Normalized sensor parameter as a function of alcohol mole fraction.

55
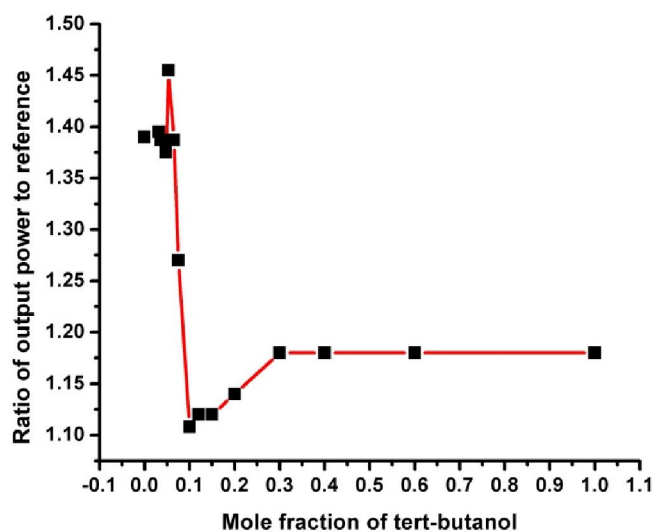
Figure 2.16 Sensor parameter as a function of tert-butanol mole
fraction.

It is evident from figure 2.15 that methanol and ethanol shows maximum output intensity at the alcohol mole fraction of 0.3 and 2-propanol at 0.15. Tert-butanol shows a different type of response in which the output intensity starts to decrease at the mole fraction of 0.05 and shows a dip at 0.1(figure 2.16). These critical mole fractions obtained using the fiber probe is similar to the values available in the literature and hence the response can be explained only in terms of cluster formation in the alcohol water mixture. Butanol and higher alcohols are more hydrophobic in nature and the alcohol molecules take part directly in the micellization process and become unique components of the micelle aggregate whereas the less hydrophobic alcohols, methanol to propanol, are mainly soluble in aqueous solution [91].

In its pure form water molecules form cluster of around 30 molecules and on addition of alcohol molecules these clusters start to break due to hydrophobic interaction between water and alcohol molecules [91]. In the case of methanol, ethanol and 2-propanol, the large structure of water break down completely at the critical concentration causing a drastic reduction in the cluster size of water. This reduction in size of the water cluster eventually

reduces scattering which in turn causes a decrease in light coupling. Further addition of alcohol reduces the hydrophilic head groups per unit volume and hence the output power reduces continuously.

In the case of tert-butanol, the decrease in intensity after first critical point at 0.05 can be attributed to the breakdown of water structure. Unlike in the case of other alcohols, micellization occurs in tert-butanol-water mixtures. The tert-btanol molecules encapsulate water molecules and this causes a drought in hydrophilic head groups in the solution. This can be the cause of the sharp dip at mole fraction of 0.1.

Conclusions

In this chapter we discussed the design and fabrication of an intensity modulated extrinsic optical fiber sensor probe. The probe was fabricated by chemically etching a plastic clad silica fiber using hydro fluoric acid. The theory of working was explained and the simulation results using RSoft was presented. The effective use of the probe as a water level detector was explained. The probe was used for the measurement of critical concentration of binary mixtures of alcohol and water. The critical mole fractions obtained using the robust and inexpensive probe are 0.3 for methanol and ethanol, 0.15 for 2-propanol and 0.05 and 0.1 for tert-butanol, which agrees well with the values found using methods like neutron diffraction studies and microwave analysis. The results also give an evidence for micellization in tert-butanol water mixtures. The probe can be effectively used for quality evaluation of alcohol-water mixtures which has applications in food and beverage industries.

References

1. F Franks, Water Science Reviews, vol. 1, (Cambridge University Press, Cambridge, UK, 1985)
2. Stanislav Miertu, Jaroslav Katrlik, Andrea Pizzariello , Miroslav Stredansky, Juraj S vitel , Jozef S Vorc, "Amperometric biosensors based on solid binding matrices applied in food quality monitoring". Biosens. Bioelectron. **13**,911–923 (1998)
3. M. Boujtita, M. Chapleau, N. El. Murr, "Biosensors for analysis of ethanol in food: effect of the pasting liquid". Anal. Chim. Acta **319**,91-96 (1996)
4. Mohammed Boujtita , John P. Hart , Robin Pittson, "Development of a disposable ethanol biosensor based on a chemically modified screen-printed electrode coated with alcohol oxidase for the analysis of beer", Biosens. Bioelectron. **15**,257–263 (2000)

5. Mihaela Niculescu, Thomas Erichsen , Valentin Sukharev, Zoltan Kerenyi , Elisabeth Csöregi, and Wolfgang Schuhmann, "Quinohemoprotein alcohol dehydrogenase-based reagentless amperometric biosensor for ethanol monitoring during wine fermentation", Anal. Chim. Acta **463**,39–51 (2002)

6. William D . T. Dale, Peter A Flavelle and Peeter Kruus, "Concentration fluctuations in water-methanol mixtures as studied by ultrasonic absorption", Can. J. Chem. **54**, 355-366 (1976)

7. Y. Nagasawa, Y. Nakagawa, A. Nagafuji, T. Okada and H. Miyasaka, "The microscopic viscosity of water–alcohol binary solvents studied by ultrafast spectroscopy utilizing diffusive phenyl ring rotation of malachite green as a probe", J. Mol. Struct. **217**, 735-736 (2005).

8. Shaoxian Song and Changsheng Peng, "Viscosities of Binary and Ternary Mixtures of Water, Alcohol, Acetone and Hexane", J. Dispersion Sci. Technol. **29**, 1367-1372 (2008).

9. Y. Tanaka, Y. Matsuda, H. Fujiwara, H. Kubota, and T. Makita, "Viscosity of (Water + Alcohol) Mixtures Under High Pressure", Int. J. Thermophys. **8**, 147-163 (1987).

10. Cees De Visser, Gerald Perron. and Jacques E. Desnoyes, "The heat capacities, vslumes, and expansibilities of tert-butyl alcohol - water mixtures from 6 to 65 ^{0}C", Can. J. Chem. **55**, 856-862 (1977)

11. T. Sato, A. Chiba, and R. Nozaki, "Dynamical aspects of mixing schemes in ethanol–water mixtures in terms of the excess partial molar activation free energy, enthalpy, and entropy of the dielectric relaxation process", J. Chem. Phys. **110**, 2508-2521 (1999)

12. T. Sato, A. Chiba, and R. Nozaki, "Hydrophobic hydration and molecular association in methanol–water mixtures studied by microwave dielectric analysis", J. Chem. Phys. **112**, 2924-2932 (2000).

13. T. Sato, A. Chiba, and R. Nozaki, "Composition-dependent dynamical structures of 1-propanol–water mixtures determined by dynamical dielectric properties", J. Chem. Phys. **113**, 9748-9758 (2000)

14. T Sato and R Buchner, "Dielectric relaxation spectroscopy of 2-propanol–water mixtures", J. Chem. Phys. **118**, 4606-4613 (2003).

15. G. Onori and A. Santucci, "Dynamical and structural properties of water/alcohol mixtures", J. Mol. Liq, **69,** 161-181 (1996).

16. J.-H. Guo, Y. Luo, A. Augustsson, S. Kashtanov, J.-E. Rubensson, D. K. Shuh, H. Agren and J. Nordgren, "Molecular Structure of Alcohol-Water Mixtures", Phys. Rev. Lett. **91**, 157401(1-4) (2003).

17. Y. Nagasawa, Y. Nakagawa, A. Nagafuji, T. Okada and H. Miyasaka, "The microscopic viscosity of water–alcohol binary solvents studied by ultrafast spectroscopy utilizing diffusive phenyl ring rotation of malachite green as a probe", J. Mol. Struct. **735-736**, 217-223 (2005).

18. N. Nishi, S. Takahashi, M. Matsumoto, A. Tanaka, K. Muraya, T. Takamuku and T. Yamaguchi, "Hydrogen Bonding Cluster Formation and Hydrophobic Solute Association in Aqueous Solution of Ethanol", J. Phys. Chem. **99**, 462-468 (1995).

19. S. Dixit, J. Crain, W. C. K. Poon, J. L. Finney and A. K. Soper, "Molecular segregation observed in a concentrated alcohol–water solution", Nature **416**, 829-832(2002).

20.   D. T. Bowron and J. L. Finney, "Association and Dissociation of an Aqueous Amphiphile at Elevated Temperatures", J. Phys. Chem. B, **111**, 9838-9852 (2007).

21. A.K.Soper and J. L. Finney " Hydration of Methanol in Aqueous Solution", Phys.Rev.Lett. 71, 4346-4349 (1993)
22. K. Nishikawa, Y. Kodera, and T. Iijima, "Fluctuations in the Particle Number and Concentration and the Kirkwood-Buff Parameters of *tert* -Butyl Alcohol and Water Mixtures Studied by Small-Angle X-ray Scattering", J. Phys. Chem., **91**, 3694-3699 (1987).
23. Y. Koga, "A saxs study of concentration fluctuations in t-butanol—water system", Chem.Phys.Lett **111**, 176–180 (1984)
24. G.W.Euliss and C.M.Sorensen, "Dynamic light scattering studies of concentration fluctuations in aqueous *t*-butyl alchohol solutions", J.Chem.Phys., **80**, 4767-4773 (1984).
25. K Iwasaki and T Fujiyama, "Light-Scattering Study of Clathrate Hydrate Formation in Binary Mixtures of tert-Butyl Alcohol and Water", J. Phys. Chem. **81,** 1908-1912 (1977)
26. K Iwasaki and T Fujiyama, "Light-Scattering Study of Clathrate Hydrate Formation in Binary Mixtures of tert-Butyl Alcohol and Water. 2. Temperature Effect", J. Phys. Chem. **83,** 463-468 (1979)
27. T.Sato, A.Chiba and R.Nozaki, "Hydrophobic hydration and molecular association in methanol–water mixtures studied by microwave dielectric analysis", J.Chem.Phys.,**112**, 2924-2932 (2000).
28. Tuhin Pradhan, Piue Ghoshal and Ranjit Biswas, "Structural transition in alcohol–water binary mixtures: A spectroscopic study", J. Chem. Sci., **120**, 275–287 (2008)
29. S. K. Allison, J. P. Fox, R. Hargreaves, and S. P. Bates, "Clustering and microimmiscibility in alcohol-water mixtures: Evidence from molecular-dynamics simulations", Phys. Rev.B, **71**, 024201(1-5) (2005).
30. K Yoshida, T Yamaguchi, A Kovalenko and F Hirata, "Structure of tert-Butyl Alcohol-Water Mixtures Studied by the RISM Theory", J. Phys. Chem. B, **106**, 5042-5049 (2002)
31. A. Laaksonen, P. G. Kusalik and I. M. Svishchev, "Three-Dimensional Structure in Water-Methanol Mixtures", J. Phys. Chem. A **101**, 5910-5918 (1997)
32. P G Kusalik, A P Lyubertsev, D L Bergman and A Laaksonen, "Computer Simulation Study of tert-Butyl Alcohol. 2. Structure in Aqueous Solution", J. Phys. Chem. B**104** ,9533-9539 (2000)
33. K Nakanishi, K Ikari, S Okazaki and H Touhara, "Computer experiments on aqueous solutions. III. Monte Carlo calculation on the hydration of tertiary butyl alcohol in an infinitely dilute aqueous solution with a new water–butanol pair potential", J. Chem. Phys. **80**, 1656-1670 (1984)
34. I Omelyan, A Kovalenko and F Hirata, "Compressibility of tert-Butyl Alcohol-Water Mixtures: The Rism Theory" J. Theor.Comput. Chem. **2 ,**193-203 (2003)
35. Frank, H. S. and Evans, M. W," Free volume and entropy in condensed systems. III. Entropy in binary liquid mixtures; partial molal entropy in dilute solutions; structure and thermodynamics in aqueous electrolytes", J. Chem. Phys. **13**, 507–532 (1945).
36. Tsai, J., Gerstein, M. and Levitt, M. "Keeping the shape but changing the charges: A simulation study of urea and its iso-steric analogs", J. Chem. Phys. **104**, 9417–9430 (1996).
37. Dixit, S., Poon, W. C. K. and Crain, J. "Hydration of methanol in aqueous solutions: a Raman spectroscopic study", J. Phys. Condens. Matter **12**, L323–L328 (1999).

38. Wakisaka, A., Komatsu, S. and Usui, Y. "Solute–solvent and solvent–solvent interactions evaluated through clusters isolated from solutions: preferential solvation in water–alcohol mixtures". J. Mol. Liq. **90**, 175–184 (2001).
39. Naiping Hu, Dan Wu, Kelly Cross, Sergey Burikov, Tatiana Dolenko, Svetlana Patsaeva, and Dale W. Schaefer, "Structurability: A Collective Measure of the Structural Differences in Vodkas", J. Agric. Food Chem., **58**, 7394-7401 (2010).
40. D. N. Simon, R. Czolk, and H. J. Ache, "Doped sol-gel films for the development of optochemical ethanol sensors", Thin Solid Films **260**,107-110 (1995)
41. Yuan Gee Lee and Tse-Chuan Chou, "Ionic liquid ethanol sensor". Biosens. Bioelectron. **20**,33–40 (2004)
42. T Buttler, K.A.J.Johansson, L.G.O.Gorton, and G.A. Marko-Varga, "On-line fermentation process monitoring of carbohydrates and ethanol using tangentialflow filtration and column liquid chromatography". Anal. Chem. **65**, 2628–2636 (1993)
43. K.Johansson, G. Jonsson-Petterson, L. Gorton, G. Marko-Varga, and E. Csoregi, "A reagentless amperometric biosensor for alcohol detection in column liquid chromatography based on co-immobilized peroxidase and alcohol oxidase in carbon paste" J. Biotech. **31**, 301–316 (1993)
44. M Zinbo, "Determination of one carbon to three-carbon alcohols and water in gasoline/alcohol blends by liquid chromatography", Anal. Chem., 56, 244–247 (1994)
45. Henriette Jensenius, Jacob Thaysen, Anette A. Rasmussen, Lars H. Veje, Ole Hansen, and Anja Boisen, "A microcantilever-based alcohol vapor sensor-application and response model", Appl.Phy.Lett. **76** , 2615-2617 (2000)
46. A.M Azevedo, D.M.F.Prazeres, J.M.S.Cabral, and L.P. Fonseca, "Ethanol biosensors based on alcohol oxidase" Biosens. Bioelectron. **21**, 235–247 (2005)
47. M Boujitita, J.P. Hart, and R. Pittson, "Development of a disposable ethanol biosensor based on a chemically modified screen-printed electrode coated with alcohol oxidase for the analysis of beer". Biosens. Bioelectron., **15**, 257–263 (2000)
48. M. Boujtita, M. Chapleau and N. El Murr, "Biosensors for analysis of ethanol in food: effect of the pasting liquid", Anal. Chim. Acta **319**, 91-96 (1996)
49. Mihaela Niculescu, Thomas Erichsen , Valentin Sukharev , Zoltan Kerenyi , Elisabeth Csöregi , Wolfgang Schuhmann, "Quinohemoprotein alcohol dehydrogenase-based reagentless amperometric biosensor for ethanol monitoring during wine fermentation", Anal. Chim. Acta **463**, 39–51 (2002)
50. K K Makhija, Arabinda Ray, R M Patel, U B Trivedi and H N Kapse, "Indium oxide thin film based ammonia gas and ethanol vapour sensor", Bull. Mater. Sci. **28** , 9–17 (2005)
51. G. Sberveglieri, E. Comini, G. Faglia, M.Z. Atashbar and W. Wlodarski, "Titanium dioxide thin films prepared for alcohol microsensor applications", Sens. Actuators, B **66**, 139–141 (2000)
52. Mohammed Mabrook and Peter Hawkins, "A rapidly-responding sensor for benzene, methanol and ethanol vapours based on films of titanium dioxide dispersed in a polymer operating at room temperature", Sens. Actuators, B **75**,197-202 (2001)
53. C. G. Dighavkar, A. V. Patil, S. J. Patil and R. Y. Borse, "Effect on Ethanol Gas Sensing Performance of Cu Addition to TiO2 Thick Films", Sensors & Transducers Journal **116** , 28-37 (2010)

54. Ting-Jen Hsueh, Shoou-Jinn Chang, Cheng-Liang Hsu, Yan-Ru Lin and I.-Cherng Chen, "Highly sensitive ZnO nanowire ethanol sensor with Pd adsorption", Appl.Phs.Lett . **91**, 053111(1-3) (2007)

55. B. Bhooloka Rao, "Zinc oxide ceramic semi-conductor gas sensor for ethanol vapour", Mater. Chem. Phys. **64**, 62–65 (2000)

56. O.K. Tan, W. Cao and W. Zhu, "Alcohol sensor based on a non-equilibrium nanostructured χ ZrO2 – (1- χ)α –Fe2O3 solid solution system", Sens. Actuators, B **63**, 129–134 (2000)

57. Chaikarn Liewhiran and Sukon Phanichphant, "Influence of Thickness on Ethanol Sensing Characteristics of Doctor-bladed Thick Film from Flame-made ZnO Nanoparticles", Sensors **7**, 185-201(2007)

58. O.K. Tan, W. Cao, W. Zhu, J.W. Chai, J.S. Pan, "Ethanol sensors based on nano-sized α -Fe2O3 with SnO2, ZrO2, TiO2 solid solutions", Sens. Actuators, B **93**, 396–401(2003)

59. O.K. Tan, W. Zhu, Q. Yan, L.B. Kong," Size effect and gas sensing characteristics of nanocrystalline xSnO2 -(1-x) α –Fe2O3 ethanol sensors" Sens. Actuators, B **65**, 361–365 (2000)

60. Y G Lee and Tse-Chuan Chou, "Ionic liquid ethanol sensor", Biosens. Bioelectron. **20**, 33–40 (2004)

61. Seong-Jeen Kim, Byung-Hyun Jeon, Kyu-Seong Choi and Nam-Ki Min, "Capacitive porous silicon sensors for measurement of low alcohol gas concentration at room temperature", J Solid State Electrochem. **4**, 363-366 (2000)

62. Silviya Petrova, Yordan Kostov, Kim Jeffris, and Govind Rao, "Optical Ratiometric Sensor for Alcohol Measurements", Anal. Lett. **40**, 715–727 (2007)

63. R. Nagarajan, A. Gupta, R. Mehrotra, andM.M. Bajaj, "Quantitative Analysis of Alcohol, Sugar, and Tartaric Acid in Alcoholic Beverages Using Attenuated Total Reflectance Spectroscopy", J. Autom. Methods Manage. Chem. **2006**, 1-5 (2006)

64. Stephan T. Dubas, Chularat Iamsamai and Pranut Potiyaraj, "Optical alcohol sensor based on dye–Chitosan polyelectrolyte multilayers" Sens. Actuators, B **113** ,370–375 (2006)

65. Q. Chang, J.R. Lakowicz, and G. Rao, "Fluorescence lifetime-based sensing of methanol", Analyst **122**, 173–177 (1997)

66. G. J.Mohr, F. Lehmann, U. W.Grummt, and U. E. Spichiger-Keller, "Fluorescent ligands for optical sensing of alcohols: Synthesis and characterization of p-N,N-dialkylamino- trifluoroacetylstilbenes". Anal. Chim. Acta **344**, 215–225 (1997)

67. G. J. Mohr, and U. E. Spichiger-Keller, "Novel fluorescent sensor membranes for alcohol based on p-N,N-dioctylamino-4'-trifluoroacetylstilben". Anal. Chim. Acta **351**, 189–196 (1997)

68. P. Blum, G. J. Mohr, K. Matern, J. Reichert, and U. E. Spichiger-Keller, "Optical alcohol sensor using lipophilic Reichardt's dyes in polymer membranes" Anal. Chim. Acta **432**, 269–275 (2001)

69. G. Orellana, A. M. Gomez-Carneros, C. de Dios, A.A. Garcia-Mertinez, and M. C. Moreno- Bondi, "Reversible fiber-optic fluorescing of lower alcohols" Anal. Chem. **67**, 2231–2238 (1995)

70. Silviya Petrova, Yordan Kostov, Kim Jeffris, and Govind Rao, "Optical Ratiometric Sensor for Alcohol Measurements", Anal. Lett. **40**, 715–727 (2007)

71. D. N. Simon, R. Czolk, H. J. Ache, "Doped sol-gel films for the development of optochemical ethanol sensors" , Thin Solid Films **260**, 107 -110 (1995)

72. Huarong Tang , Yaming Li, Chengbin Zheng, Jun Ye, Xiandeng Houa and Yi Lv, "An ethanol sensor based on cataluminescence on ZnO nanoparticles", Talanta **72**, 1593–1597 (2007)

73. Danielle Cleveland, Matthew Carlson, Evan D. Hudspeth, Lauren E. Quattrochi, Kathleen L. Batchler, Shrimati A. Balram, Seongun Hong, Robert G. Michel "Raman Spectroscopy for the Undergraduate Teaching Laboratory: Quantification of Ethanol Concentration in Consumer Alcoholic Beverages and Qualitative Identification of Marine Diesels Using a Miniature Raman Spectrometer", Spectrosc. Lett. **40**, 903–924, 2007

74. Jun Gao, Ting Gao, and Michael J. Sailor, "Porous-silicon vapor sensor based on laser interferometry", Appl. Phys. Lett. **77**, 901-903 (2000)

75. Yoshiaki Kurauchi , Takayuki Yanai, Naoyoshi Egashira and Kazuya Ohga, "Fiber-Optic Sensor with a Chitosan/Poly(Vinyl Alcohol Cladding) for the Determination of Ethanol in Alcoholic Beverages", Anal. Sci. **10**, 213-217 (1994)

76. M. Penza, G. Cassano, P. Aversa, F. Antolini, A. Cusano A. Cutolo, M. Giordano L. Nicolais, "Alcohol detection using carbon nanotubes acoustic and optical sensors", Appl. Phys. Lett. **85**, 2379-2381 (2004)

77. M Penza, G Cassano, PAversa, A Cusano, A Cutolo, MGiordano and L Nicolais, "Carbon nanotube acoustic and optical sensors for volatile organic compound detection", Nanotechnology **16**, 2536–2547 (2005)

78. Zhengtian Gu and Yanping Xu, "Design optimization of a long-period fiber grating with sol–gel coating for a gas sensor" Meas. Sci. Technol. **18**, 3530–3536 (2007)

79. Zhengtian Gu, Yanping Xu and Kan Gao , "Optical fiber long-period grating with solgel coating for gas sensor", Opt. Lett. **31**(16) 2405-2407 2006

80. Guillenno Orellana, Ana M. Gomez Cameros, Cesar de Dios, Ana A. Garcia-Martinez, and Maria C. MorenoBondi, "Reversible Fiber-optic Fluorosensing of Lower Alcohols", Anal. Chem. **67**,2231 -2238 (1995)

81. Yoshiaki Kurauchi, Takayuki Yanai, Naoyoshi Egashira and Kazuya Ohga, "Fiber-Optic Sensor with a Chitosan /Poly(vinyl alcohol) Cladding for the Determination of Ethanol in Alcoholic Beverages", Anal. Sci. **10**,213-217 (1994)

82. G R C Possetti, L C Cocco, C I Yamamoto, L V R de Arruda, R Falate, M Muller and J L Fabris, "Application of a long-period fiber grating-based transducer in the fuel industry" Meas. Sci. Technol. **20**, 034012(1-9) (2009.)

83. Cesar Elosuaa, Candido Bariaina, Ignacio R. Matiasa, Francisco J. Arreguia, Elena Vergarab and Mariano Lagunab, "Optical fiber sensing devices based on organic vapor indicators towards sensor array implementation", Sens. Act. B **137** ,139–146 (2009)

84. Y G Lee and Tse-Chuan Chou, "Ionic liquid ethanol sensor", Biosens. Bioelectron. **20**, 33–40 (2004)

85. Zhengtian Gu and Yanping Xu, "Design optimization of a long-period fiber grating with sol–gel coating for a gas sensor" Meas. Sci. Technol. **18**, 3530–3536 (2007)

86. Zhengtian Gu, Yanping Xu and Kan Gao , "Optical fiber long-period grating with solgel coating for gas sensor", Opt. Lett. **31**, 2405-2407 (2006)

87. M. Penza, G. Cassano, P. Aversa, F. Antolini, A. Cusano A. Cutolo, M. Giordano L. Nicolais, "Alcohol detection using carbon nanotubes acoustic and optical sensors", Appl. Phys. Lett. **85,** 2379-2381 (2004)

88. M Penza, G Cassano, PAversa, A Cusano, A Cutolo, MGiordano and L Nicolais, "Carbon nanotube acoustic and optical sensors for volatile organic compound detection", Nanotechnology **16**, 2536–2547 (2005)

89. A. Kumar, T. V. B. Subrahmanyam, A. D. Sharma, K. Thyagarajan, B. P. Pal and I. C. Goyal, "Novel refractometer using a tapered optical fiber", Electron. Lett. **20**, 534-535(1984)

90. M. Ogita, Y. Nagai, M.A. Mehta and T. Fujinami, "Application of the adsorption effect of optical fibers for the determination of critical micelle concentration", Sens. Actuators, B , 64,147–151 (2000)

91. S. S. N. Murthy, "Detailed Study of Ice Clathrate Relaxation:Evidence for the Existence of Clathrate Structures in Some Water-Alcohol mixtures", J. Phys. Chem. A **103**, 7927-7937 (1999).

Fabrication of asymmetric LPFGs using electrical arc and CO_2 laser

3.1 Introduction

A long period fiber grating (LPFG) is a periodic modulation of the optical characteristics of an optical fiber, obtained by either inducing a physical deformation in the fiber material or by modifying the refractive index of the core of the fiber [1,2], where the period is greater than 100 μm. Long Period Fiber Gratings or LPFG's are classically realized by exposing the photo sensitive optical fiber to ultra-violet light (either through an amplitude mask or by using point by point technique) [2]. But with the advancement of technology over two decades since the first report[1], LPFGs have been virtually written in all kind of fibers, namely, in standard singlemode telecommunications fibers [1], in two-mode (or few-mode) fibers [3,4], polarization maintaining fibers [5], D-fibers [6], non-photosensitive fibers [7,8,9] and multimode fibers [10]. LPFGs were also fabricated in specially designed fibers like dispersion shifted [1], dispersion compensating [11], depressed inner cladding [12], dual core [13], twin core [14] and progressive three layered [15] with specific properties for optical communications and sensing. Abramov et.al. [16] reported LPFG in hybrid fibers containing silica and polymers [] while LPFG in a metal coated fiber was reported by Costantini et.al. [17]. LPFG were also fabricated in microstructured polymer fiber [18] and in photonic crystal fibers [19-22].

Regarding writing techniques, Vengsarkar et.al [1] exposed hydrogen loaded germanosilicate fibers to a 248 nm KrF laser through an amplitude mask made of chrome-plated silica. Ultra violet radiation from a frequency-doubled argon-ion continuous-wave laser (λ=244 nm) was used by Vikram Bhatia et.al [23] for fabricating the LPFG. Gratings inscription was also achieved through the radiation delivered by CW Ar ion laser [24-26]. Nanosecond pulses from an ArF excimer laser (193 nm) was used to inscribe gratings in a hydrogen loaded boron co doped germanosilicate fiber using point by point technique [27,28] . Frequency quadrupled Nd:YAG laser (266 nm) was used by several authors [29-31] of which Shu et.al. [30]

employed amplitude mask on non hydrogenated B–Ge codoped fiber while Visneck Costa et.al.[31] adopted point-by-point technique on hydrogen-loaded photosensitive fibers. Gratings were written in hydrogenated photosensitive fiber with the tripled output of high repetition-rate diode pumped Q-switched Nd:YAG laser (355nm) by Blows et.al.[32]. Femtosecond laser radiation at several wavelengths like 211 nm [33], 264 nm [34] 352 nm [35,36] and 400 nm [37,38] were also used for inscribing long period fiber gratings. Broadband UV sources were also used for fabrication of LPFGs in hydrogenated photo sensitive fibers [39-41]. Though different laser intensities and wavelengths were used, in all cases gratings were written in photosensitive fibers and/or in hydrogenated ones.

Although the UV-based fabrication method is a well-established technology, it has problems. It requires complex and time-consuming processes, including hydrogen loading, UV writing, and annealing. Furthermore, UV-induced gratings decay and, in general, cannot stand high temperatures. Moreover it requires photosensitive fibers and the lasers used for fabrication are costly.

There are, however, several alternative techniques for grating fabrication that does not require the fiber to be photosensitive. Such methods include physical deformation of the fiber [42], core-index variation produced by thermal effects using 800 nm femtosecond laser radiation [43], 10.6 μm CO_2 lasers [44-53] or electric arcs [7-9,54-64], periodic corrugation of the silica cladding of fiber through chemical etching [65-67] etc. LPFGs were reported to be written in hydrogenated Corning SMF-28 fiber using nanosecond pulses from a 157 nm F2 laser [68,69]. Among other techniques, LPFGs were fabricated by heating a heavily twisted standard fiber at high temperatures [52,70]. Gratings can also be produced by exposure of a fiber, through an amplitude mask, to a beam of He ions [71]. This method requires that the fiber cladding be reduced to ~53 μm by etching. Later, the etching process was overcome by exposure of the fiber to a focused beam of protons, which have a longer stopping distance [72]. It is known that gamma radiation can lead to considerable changes in the refractive index of optical fibers [73] and, therefore, it may be an alternative to produce long-period gratings.

LPFGs produced through exposure to CO_2 laser radiation and to arc discharges share most of their properties and have been catching an increasing attention from the fiber gratings community. Comparatively, the

major disadvantage of the electric arc technique is the limitation in the minimum period that can be written due to the dimensions of the arc [74]. On the other hand, it is simpler, harmless and one of the most cost effective techniques.

3.2 Mechanism of LPFG formation

3.2.1 UV LPFG

The basis of this type of grating inscription is connected with the induction of permanent refractive index changes in fiber core by UV irradiation. The radiation has wavelength coinciding with the 5.12 eV absorption band of germanium oxygen-deficient centers which has a maximum at 242 nm. Currently there are two models which describe the mechanism for fiber photosensitivity namely the *colour-centre model* [75] and *the densification model* [76].

The *colour-centre model*, considers that the UV exposure of the 5.12 eV band brings about the release of photoelectrons, which become trapped in neighbouring sites, thus creating new colour centres. The following modification of the UV absorption spectrum of the germanosilicate glass leads to refractive index modification at longer wavelengths. However this model failed in the correct estimation of the induced index changes and the search for another model paved way for the *densification model*. In 1995 Fonjallaz et.al [77] noticed a strong increase in tension in a germanosilicate fiber core by UV laser light, which was linearly proportional to the refractive index modulation. Although it is known that an increase in tension lowers the refractive index through the photoelastic effect, an overall positive index change was only observed in the experiment. The *densification model* considers structural changes to more compact configurations as an important component of fiber photosensitivity. The UV-induced increase of the refractive index in fiber core, due to both *colour-centre* and *compaction* effects, is believed to exceed the decrease caused by the photoelastic effect. The amount of each contribution might vary strongly as a function of fiber content, pre-irradiation treatment and irradiation wavelength.

66

3.2.2 Thermal induced Gratings

Unlike in the case of UV induced LPFGs, the mechanism of grating formation is still not well understood in the case of thermal induced long period fiber gratings. Depending on the types of the employed fibers and on the fabrication techniques, possible mechanisms suggested for refractive index modulation in the thermal-induced LPFGs are residual stress relaxation [78-81], glass densification [82-84], physical deformation [9,42,85] and dopant diffusion [86].

3.2.2.1 Residual stress relaxation

A standard single mode fiber consists typically of a germanium-doped silica core and a pure silica cladding. As a result of the doping, the properties of the core, in particular, its thermal expansion coefficient increases and its viscosity decreases compared to the properties of the cladding. The elastic stress associated with the difference in thermal expansion coefficient is known as thermal stress and is present in the fiber preform itself. Another type of stress is known as draw induced, which occurs during drawing and is associated with the different viscosities of core and cladding materials. During fiber drawing the higher viscosity material, in this case the cladding, cools more rapidly than the core and bears the brunt of the drawing tension. The melted core, in turn, is surrounded by the solid cladding and cannot expand being under compressive stress during cooling. Simultaneously, due to a higher thermal expansion coefficient, the core also exerts a hydrostatic pressure on the cladding. Thus residual stress is formed in optical fibers during the drawing process, resulting mainly from a superposition of thermal stress caused by a difference in thermal expansion coefficients between core and cladding and mechanical stress caused by a difference in the viscoelastic properties of the two regions [80,81, 87]. Such residual stress can change refractive index in the fibers through the stress-optic effect and thus affect the optical properties of the fibers. Residual stresses can be released during fiber annealing, that is, the fiber is heated to a high temperature (>1000 ºC) and is held for some time, followed by slow cooling to room temperature.

Residual stress relaxation usually results in a decrease in refractive index in the fibers. The efficiency of refractive-index decrease depends strongly on the types of fiber and can be enhanced linearly with the drawing

67

force during the drawing process of the fiber. In a Ge–B-codoped fiber the refractive-index change due to residual stress relaxation was measured as $-2.1X10^{-4}$ [80] while in a Corning SMF-28 fiber it was $-7.2X10^{-4}$ [81]. It has been proposed that the periodic stress relaxation caused by arc discharges or CO_2 laser radiation is an important mechanism of gratings formation [88,89]. In addition to residual elastic stresses and strains, conventional silica optical fibers can also exhibit inelastic, or even "stress-free," strains. Relaxation of inelastic stress is also a possible mechanism for LPFGs formation [88].

3.2.2.2 Glass structure changes

Densification arises from modifications of ring structures in the silica network and is the mechanism proposed to explain the changes observed in fibers having moderate and high germanium content in the core upon exposure to UV-laser radiation [90-92].

If glass is maintained at constant temperature, the volume changes with time due to structural relaxation until it reaches certain equilibrium glass structure. The temperature that corresponds to the equilibrium glass structure is called the fictive temperature or the structural temperature. Thus the fictive temperature of a glass is defined as the temperature at which the glass is formed after melting and the glass structure at this temperature and at room temperature is the same [93]. The fictive temperature of glass depends on the cooling rate and it increases with the increase in cooling rate. Therefore, different cooling rates lead to fibers with different fictive temperatures which, in turn, results in fibers with different intrinsic properties such as viscosity, thermal expansion coefficient and refractive index [93,94].

In the case of slow cooling, the glass can follow changes in temperature. As the temperature decreases, the viscosity of the glass increases, and it takes a longer time for the glass structure to reach an equilibrium state. Thus the density of the glass cooled slowly becomes larger than that of the glass cooled quickly. The refractive index is given by the Lorentz–Lorenz formula given by

$$\frac{(n^2-1)}{(n^2+2)} = \frac{N_A \propto}{3M} \rho_m \qquad 3.1$$

where ρ_m is the mass density, α is the mean molecular polarizability, N_A the Avogadro number and M is the molecular weight

Thus refractive index increases with the density and hence the rapidly cooled glass has a lower refractive index than the slow cooled one.

In the case of arc discharges and CO_2 laser irradiation, the fiber is rapidly heated to a temperature which is more than that employed during the drawing process and is cooled rapidly and frozen. Because of the faster cooling rate, the fictive temperature of the quickly resoldified glass becomes higher. The viscosity and density of the molten glass thus decreases and these contribute to the reduction in the refractive index.

The change of glass structure is found to be the dominant mechanisms in the thermal-induced LPFGs written in a commercial boron-doped single-mode fiber [82-84]. Residual stress relaxation in the fiber core, which is the dominant mechanism in a conventional Ge-doped or Ge–B-codoped fiber, plays only a minor role in the boron-doped fiber that has a core with a small residual stress and a low fictive temperature. For the CO2-laser-induced LPFGs in the Ge-doped or Ge–B-codoped fibers, e.g., Corning SMF-28 fiber, with large residual stress, the resonance wavelength shifts toward the shorter wavelength with the increase in the laser exposure dose due to the negative index modulation resulting from residual stress relaxation[78-80,95]. For the CO2-laser-induced LPFGs in the boron-doped fibers with small residual stress, on the contrary, the resonance wavelength shifts toward the longer wavelength with the increase in the laser exposure dose due to the positive index modulation resulting from glass densification.[81-84]

3.2.2.3 Physical deformation

In the case of thermal induced LPFGs two types of geometric deformations can occur in a fiber namely microbending [42] and tapering [9,85]. The former, occurs when the fiber is submitted intentionally to lateral strain during heating while the latter occurs when the fiber is submitted to axial strain. The extent of the change in the fiber cross-section depends not only on the pulling tension but also on the temperature established on the fiber. During CO_2 laser irradiation, the fiber usually elongates or tapers based on the so-called "self-regulating" mechanism,[87] resulting from constant axial tension and the CO_2-laser-induced local high temperature in the fiber. Thus the fiber diameter decreases and eventually reaches a critical point at which

the fiber elongation stops because no sufficient energy is absorbed to keep the softening temperature. Moreover, the CO_2-laser-induced high temperature in the fiber causes, not only the fiber elongation and the diameter decrease but also the ablation of glass on the fiber surface. Such physical deformation induces a change in effective refractive index in the fiber, and thus LPFGs are created in the periodically tapered optical fibers [49,96-98].

3.2.2.4 Dopant diffusion

One of the first mechanisms proposed for the formation of arc-induced LPFGs was the diffusion of core dopants [86,99].This is a phenomenon in which the core dopant diffuses to cladding due to heating and Dianov etal [99] have fabricated LPFG in nitrogen doped fiber by utilizing this phenomenon. As the electric arc heats the fiber, owing to its small atomic weight, nitrogen diffuses to cladding and hence the core refractive index reduces. However for Ge-doped fibers, the desired modifications caused by dopant diffusions were achieved by keeping the fibers at temperatures above 1200 ºC for few hours. But during LPFGs fabrication the duration of the arc discharge is only a few seconds and, therefore, the diffusion coefficients of the dopants must be high in order to have a significant influence of diffusion on the grating formation.

3.3 Theory of long period fiber gratings

Consider an optical fiber, as depicted in Figure 3.1, having a core radius r_1, cladding radius r_2 and different refractive indices in each layer: n_1, n_2 and n_3.
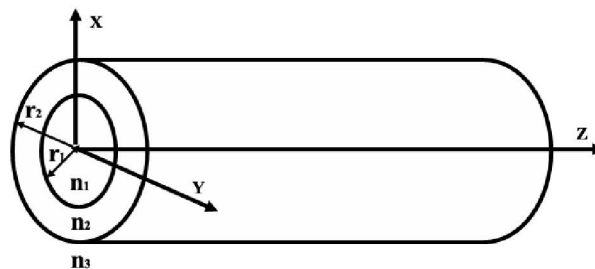
Figure 3.1. The structure of optical fiber

Generally the cylindrical waveguide supports many modes of propagation and by adjusting the core radius and the refractive index difference between the core and the cladding (Δn) the fiber can be made to support only one mode (single mode fiber). In the case of a single mode fiber most of the energy is guided by the core, but a certain amount is also guided by the cladding. The core mode thus "sees" an effective refractive index that lies between the core and the cladding refractive indices. The other modes available in an optical fiber may be classified, according to the value of the third layer, as: cladding modes, radiation modes and leaky modes. The first occurs when the refractive index of the third layer is lower than that of the cladding, such as the case of a stripped fiber ($n_3 = 1$ air). In this case, several discrete cladding modes are guided by total internal reflection at the cladding-air interface. The effective refractive indices of those modes range between n_2 and n_3. If the cladding is infinite, ie $n_2 = n_3$, total internal reflection is not possible and, therefore, light is lost through a continuum of radiation modes. When $n_2 < n_3$, light can propagate a certain distance due to hollow waveguide and these discrete modes are called leaky-modes.

The field equations of the core and cladding modes are solutions of the wave equation that satisfy continuity conditions at the boundary. In general, the modes are TE, TM and hybrid HE/EH modes. If Δn is small, the weakly guide approximation can be used and the modes can be treated as linearly polarized, LP. The LP modes are a superposition of TE, TM and hybrid modes. For a single mode fiber, the core mode is HE_{11} or LP_{01} and the field equation can be obtained considering two layers: core and cladding. For the cladding modes, a three layer geometry is required, even when Δn is small. As far as LPFGs are concerned, the type of modes of interest depends on the symmetry of the perturbation that enables coupling from the core mode to the cladding modes. If the perturbation is axis symmetric the coupling is made to LP_{0j} (or HE_{1j}) cladding modes (j>1). On the other hand,

71

if the perturbation is asymmetric coupling is made to LP_{1j} (or HE_{2j} + TE_{0j} + TM_{0j}) cladding modes (j>0) [100-103].

An LPFG can be represented by a sinusoidal Z dependent periodic index variation given by $\Delta n^2(z) = \Delta n^2 \sin(Kz)$, where $K = 2\pi/\Lambda$ and Λ is the grating period. The LPFG couples incident light guided by the core to the forward-propagating cladding modes of the optical fiber, which decay rapidly through radiation. The fiber supports many cladding modes and thus the LPFG induces a corresponding series of attenuation bands in the transmission spectrum of the fiber.

The light coupling from the fundamental core mode to the mth order cladding modes occurs at wavelengths that satisfy the phase-matching condition [100]

$$\beta_{core} - \beta_{cl}^{m} = \frac{2\pi}{\Lambda} \tag{3.2}$$

where β_{core} is the propagation constant of the LP_{01} fundamental core mode, β_{cl}^{m}, is the propagation constant of the mth order cladding mode and Λ is the grating period.

The effective refractive index of a medium is defined as $n_{eff} = \beta/k$, where k is the wave number in vacuum. Since $k = 2\pi/\lambda$, the propogation constants β_{co} and $\beta cl,m$ can be written as [100]

$$\beta_{core} = \frac{2\pi n_{eff,core}}{\lambda_m} \tag{3.3}$$

and

$$\beta_{cl}^{m} = \frac{2\pi n_{eff,cl}^{m}}{\lambda_m} \tag{3.4}$$

where $n_{eff,core}$ is the effective refractive index of the fundamental core mode (LP_{01}) and $n_{eff,cl}^{m}$ is the effective refractive indexes of the phase matched cladding mode (LP_{0m}).

If λ_m is the wavelength at which phase matching occurs with the mth forward propagating cladding mode, then an attenuation band is created in the

72

transmission spectrum centred at the wavelength λ_m. Thus from 3.2, 3.3 and 3.4, λ_m can be deduced as

$$\lambda_m = \left[n_{eff,core}(\lambda, \varepsilon, T, n_i) - n^m_{eff,cl}(\lambda, \varepsilon, T, n_i, n_s) \right] \Lambda \qquad (3.5)$$

Both indices ($n_{eff,core}$ and $n_{eff,cl}{}^m$) depend on the indices of the various fiber layers, n_i, the wavelength λ, the temperature T, and the strain experienced by the fiber ε. Also, $n_{eff,cl}{}^m$ is a function of the refractive index of the surrounding medium, n_s.

For each individual resonance, its transmission loss can be calculated by[100]

$$T = 10 \log \left\{ 1 - \frac{\sin^2 \left[k_g L \sqrt{1 + \left(\dfrac{\partial}{k_g} \right)^2} \right]}{1 + \left(\dfrac{\partial}{k_g} \right)^2} \right\} \qquad (3.6)$$

where δ is the detuning parameter

$$\partial = \pi \left\{ \frac{n_{eff,core} - n^m_{eff,cl}}{\lambda_m} - \frac{1}{\Lambda} \right\} \qquad (3.7)$$

k_g is the grating coupling constant and L is the grating length.

Figure 3.2 shows the sample transmission spectrum of an LPFG illustrating the attenuation bands corresponds to various LP_{0m} cladding modes to which the fundamental guided mode couples. Since these attenuation bands are functions of applied strain, ambient temperature and refractive index, long period fiber gratings can be used as sensors, where the shift in resonance band gives the measure of ambient change.

73
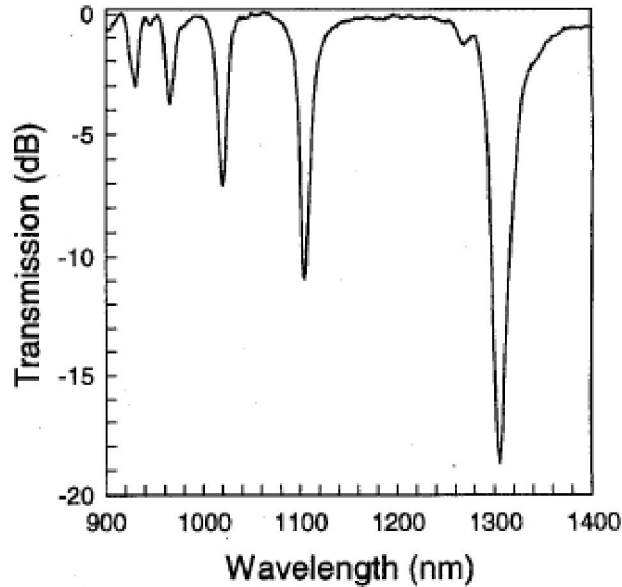
Figure 3.2 Transmission spectrum of an LPFG (reproduced from [1])

3.4 Fabrication of Periodically tapered LPFG using fusion splicer

Long period fiber gratings were fabricated in commercially available standard telecommunication fiber (SMF-28) received from Newport using point-by-point technique. As shown in figure 3.3, a bare single mode fiber (Newport SMF-28) without its protective coating was placed between the electrodes of a fusion splice machine (Fujikura FSM-50S), while its ends were fixed on two fiber holders. The fiber holder was fixed on a computer-controlled translation stage (Newport) with a resolution of 100nm. An arc discharge with a current of 5 mA was then applied for 200 ms, which raises the temperature of the fiber section positioned in between the electrodes to its softening point. The fusion splicer was programmed to taper the fiber by a length of 50μm during each arc. The fiber was then moved by the translation stage through a distance equal to the grating period and another arc discharge along with tapering was applied. Care was taken to provide sufficient time

74

between arcs to allow the fiber to get cooled. The periodic tapering was continued and the optical transmission of the fiber was monitored during the LPFG fabrication process in order to obtain the desired spectral attenuation notches. The setup employed for the experiments consists of a white light source (Yokogawa AQ4305) coupled to one end of the fiber, while the other end was connected to an optical spectrum analyzer, OSA (Yokogawa AQ6319), set to a resolution of 0.05 nm. All the three writing parameters, namely discharge current, discharge time and tapering length were found out by trial and error method so that the fiber should retain its mechanical strength during the formation of grating.
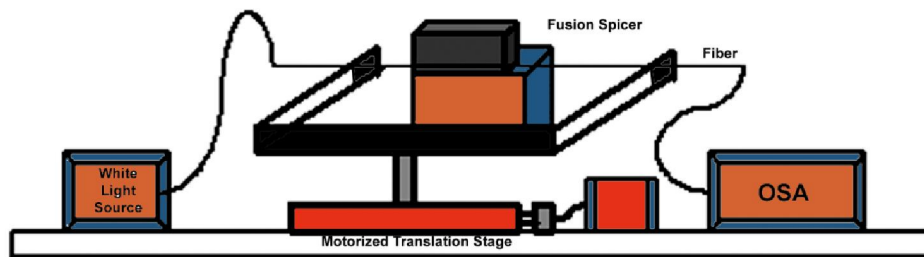
Figure 3.3 LPFG fabrication setup using arc fusion splicer

The transmission spectrum was acquired and processed by a computer to determine the LPFG central dip wavelength and transmittance. The size of the arc limited the minimum grating period Λ, and we got a peak attenuation of 14 dB at 1318 nm after 34 engravings with a grating period of 500μm. The spectral evolution of the LPFG is shown in figure 3.4, illustrating the transmission spectra with various grating period numbers of 10, 21, 30 and 34. When fabrication was repeated without the tapering option, gratings were not formed eventhough arc current and duration were the same.

75
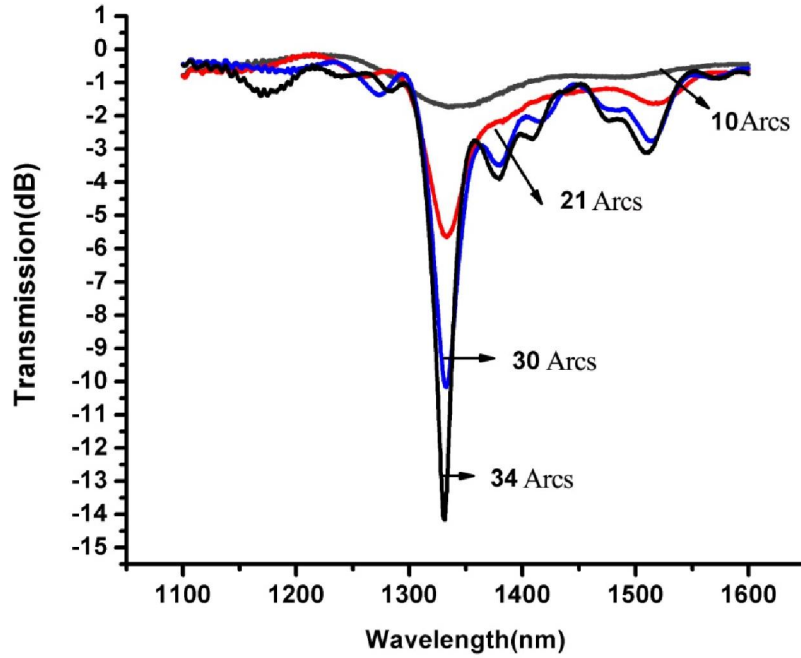
Figure 3.4 Evolution of resonance peaks for the arc induced LPFG

As discussed in section 3.2 the different mechanisms involved in the formation of arc induced gratings are modulation of core diameter due to fiber tapering, stress relaxation, glass structure changes and dopant diffusion. But it has been shown that the change of glass structure play the dominant role in LPFGs written in boron-doped single-mode fiber [82-84] while residual stress relaxation in the fiber core, is the dominant mechanism in a conventional Ge-doped or Ge–B-codoped fiber like SMF 28. Since we have used SMF 28 for LPFG fabrication, the effect of glass structure change on refractive index modulation can thus be omitted. Also since the temperature generated during arc cannot induce Ge diffusion to the cladding, the effective refractive index variation in the periodically tapered LPFG can be expressed as [104]

$$\Delta n = \Delta n_{residue} + \Delta n_{taper} \tag{3.8}$$

76

where $\Delta n_{residue}$ is the initial refractive index change induced by the residual stress relaxation as a result of the high local temperature and the constant strain during the tapering process. Δn_{taper} is the refractive index perturbation caused by the periodic tapering of the fiber.

3.4.1 Origin of Asymmetry

Rego et.al.[61] did extensive studies on the asymmetric mode coupling of arc induced LPFGs. They studied the temperature distribution in the arc that is applied to the fiber. Since the current in the arc is direct (dc), the arc is directional and it is found that the center between the electrodes is not the center of symmetry of arc glow (figure 3.5).
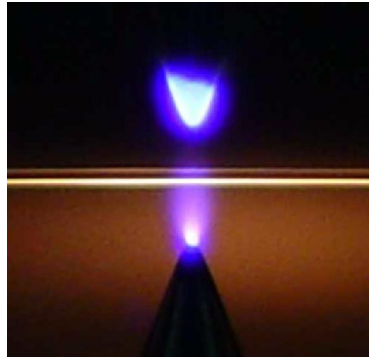
Figure 3.5 Photograph of arc glow (reproduced from Rego etal [61])

The electrode at the bottom (cathode) glows only at its tip, while the electrode at the top (anode) glows over a much larger area. The arc is brighter near the lower electrode. This causes a gradient of temperature with respect to the line joining the electrodes and hence along the diameter of the fiber.

As discussed in section 3.2 glass structure change is reported to be the dominant mechanism involved in grating formation in Boron doped fibers while it has little effect in the case of normal SMF 28 fibers. It has been shown that the mode coupling is symmetric in the case of LPFGs fabricated using fusion splicer in Boron doped fibers while asymmetric in SMF 28[60]. Thus it is evident that the temperature gradient has little or no effect on glass structure changes. The origin of asymmetry in this case (SMF

28) can thus be attributed to stress relaxation and physical deformation. Two types of geometric deformation of the fiber occur in an arc discharge namely tapering and microbending. Tapering is a symmetric diameter reduction and an elongation of the fiber and it cannot induce coupling to the asymmetric cladding modes. Rego et al [61] has also shown the asymmetric geometrical microbending induced in the fiber core by the electric arc. Hence the microbending and temperature gradient can be assumed to be the possible cause for asymmetric mode coupling.

This periodic asymmetric refractive index modulation causes the LPFG to couple light guided by the core mode (LP_{01}) to the forward propagating asymmetric cladding modes (LP_{1m}^{Clad}) of the optical fiber, which decay rapidly through radiation. Since the fiber supports many cladding modes, the LPFG induces a corresponding series of attenuation bands in the transmission spectrum of the fiber. The centre wavelength λ_m of the attenuation bands depends on the grating period Λ, external temperature, strain experienced by the fiber and the refractive index of the medium surrounding the fiber.

3.5 Fabrication of LPFG using CO_2 laser

The LPFGs were fabricated in commercially available standard telecommunications fiber (SMF-28) received from Newport using the point-by-point technique. As shown in figure 3.6, a motorized translation stage with a resolution of 10nm (Newport) was used to shift the fiber. A 12 W continuous wave CO_2 laser (LASY-12, 10.6μm, 12W) was used for fabrication. The optical transmission of the fiber was monitored during the LPFG fabrication process in order to obtain the desired spectral attenuation notches. The setup employed for the experiments consists of a white light source (Yokogawa AQ4305) coupled to one end of the fiber, while the other end was connected to an optical spectrum analyzer, OSA (Yokogawa AQ6319), set to a resolution of 0.05 nm. The fiber was exposed to CO_2 laser radiation using a shutter for a fraction of a second and then translated by the required grating period. During the experiments the fiber was kept under constant longitudinal tension. The beam diameter of the CO_2 laser limited the minimum grating period Λ. For a grating period of 600μm, we got an attenuation of 14 dB at 1520nm after 76 periods producing a grating length

of 4.5cm. The spectral evolution of the LPFG is shown in figure 3.7 and the photograph of the LPFG in figure 3.8.
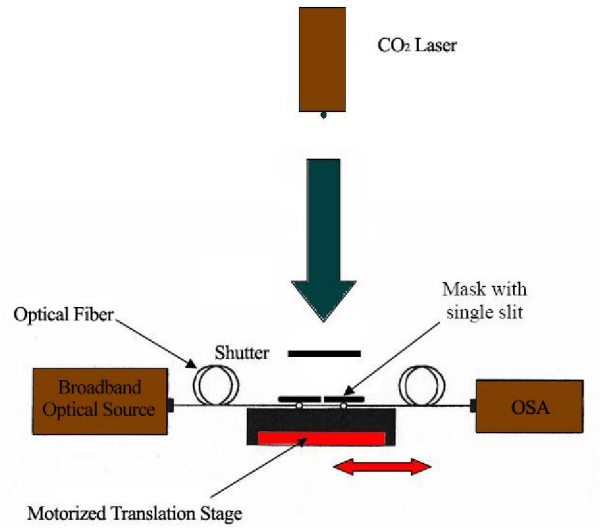
Figure 3.6 Experimental setup for LPFG fabrication using CO_2 laser
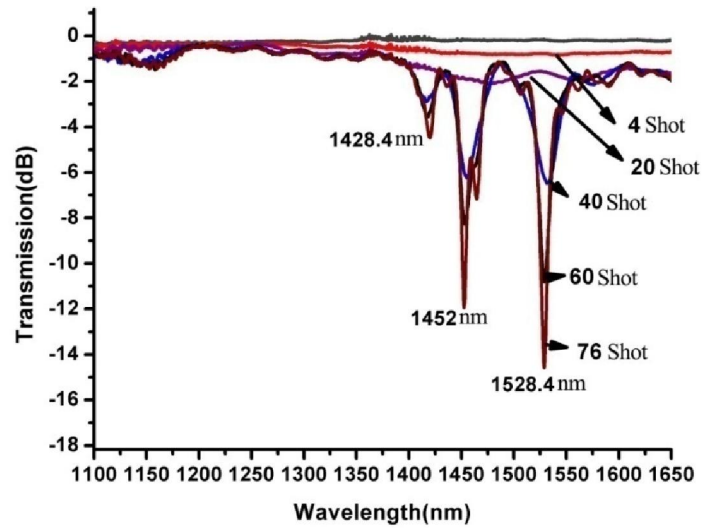
Figure 3.7 Evolution of resonance peaks for CO_2 inscribed LPFG
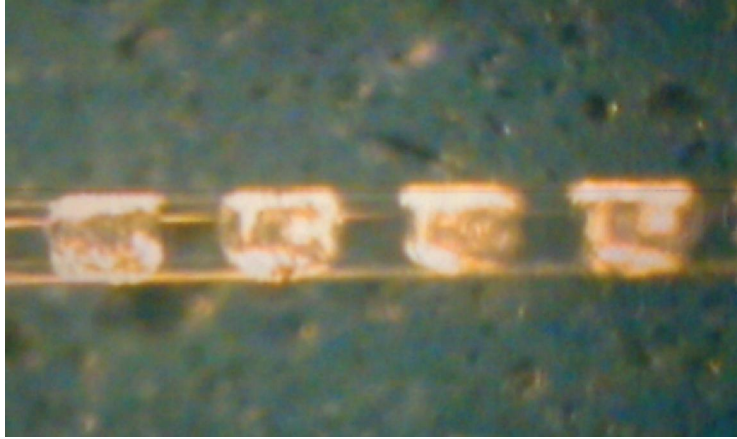
Figure 3.8 Photograph of CO_2 inscribed LPFG

The focused CO_2 laser beam creates a local high temperature in the fiber, which led to the vapourization of SiO_2 from the surface of the fiber. As a result, periodic grooves are carved on the fiber as shown in Figure 3.9. Such grooves induce periodic refractive index modulation along the fiber axis due to the photo elastic effect, thus creating an LPFG.
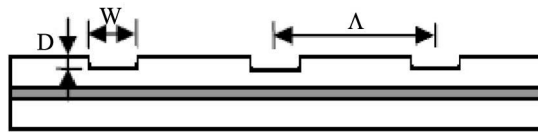
Figure 3.9 structure of CO_2 inscribed LPFG

Since the LPFG is fabricated in SMF 28, the dominant mechanism involved in the refractive index modulation is stress relaxation. Thus the refractive index modulation in the CO2 laser carved LPFG can be expressed as

$$\Delta n = \Delta n_{residual} + \Delta n_{groove} \tag{3.9}$$

where $\Delta n_{residual}$ is the refractive index perturbation induced by the residual stress relaxation resulting from the heating and Δn_{groove} is the initial refractive index perturbation induced by the periodic grooves on the fiber.

3.5.1 Origin of Asymmetry

In the case of CO_2 fabrication the laser energy is strongly absorbed on the incident side of the fiber and the non uniform absorption results in asymmetrical refractive index profile within the cross-section of the LPFGs. Thus, a larger refractive index change is induced on the incident side of the fiber compared to the opposite side which in turn causes asymmetrical mode coupling.

3.6 Temperature sensitivity of LPFG

The sensitivity of LPFGs to temperature is influenced by the period of the LPFG governed by the order of the cladding mode to which coupling takes place (105) and by the composition of the optical fiber (106). The origin of the temperature sensitivity may be understood by differentiating equation (3.5) (107)

$$\frac{d\lambda_m}{dT} = \Lambda\left(\frac{dn_{eff,core}}{dT} - \frac{dn_{eff,cl}^m}{dT}\right) + \left(n_{eff,core} - n_{eff,cl}^m\right)\frac{d\Lambda}{dT} \qquad (3.10)$$

where λ_m is the central wavelength of the attenuation band, T is the temperature, $n_{eff,core}$ is the effective refractive index of the core mode, $n_{eff,cl}{}^m$ is the effective refractive index of the mth cladding mode and Λ is the period of the LPFG.

In general, the effective refractive indices of the core and the cladding at a particular temperature T can be written as

$$n_{eff,core}(T) = n_{eff,core}(T_0) + \xi_{core}\Delta T \qquad (3.11)$$

and

$$n_{eff,cl}^m(T) = n_{eff,cl}^m(T_o) + \xi_{cl}^m\Delta T \qquad (3.12)$$

where T_0 is a reference temperature, $\Delta T = T - T_0$, and ξ_{core} and ξ_{cl} are the thermo-optic coefficients of the core and the cladding, respectively.

The first term on the right-hand side of equation 3.10 i.e., $\Lambda\left(\frac{dn_{eff,core}}{dT} - \frac{dn_{eff,cl}^m}{dT}\right)$ [105] is the material contribution, and is related to

the change in the differential refractive index of the core and cladding arising from the thermo-optic effect. This contribution depends upon the composition of the fiber and also on the order of the cladding mode. The second term i.e., $\left(n_{eff,core} - n_{eff,cl}^{m}\right)\dfrac{d\Lambda}{dT}$ is the waveguide contribution as it results from changes in the LPFG's period with respect to the changing temperature. Since the thermal expansion coefficient of silica is very small $\sim 0.5 \times 10^{-6}/^{0}C$ [107], the waveguide contribution due to $d\Lambda/dT$ can be neglected for lower temperatures. However, at high temperatures, due to a much stronger dependence on temperature [107] the role of the thermal expansion coefficient becomes as important as that of the refractive index. Therefore, at low temperatures, it is the temperature dependence of the effective indices that determines mainly the temperature sensitivity of the resonance wavelength. From equation 3.10,3.11 and 3.12 it is evident that the temperature sensitivity of the resonance wavelength can be positive or negative, depending on whether the thermo-optic coefficient of the core is larger or smaller than that of the cladding.

In order to study the temperature characteristics of the fabricated LPFGs , they are kept in a setup as shown in figure 3.10. An IR lamp is used to heat the chamber and is connected through an auto transformer. The temperature is varied by changing the voltage applied to the IR lamp and measurements were taken after stabilizing the temperature. For temperature readouts, we used an electronic thermometer placed next to the probe. As usual an OSA –white light source arrangement was used to measure the spectral shift and the grating was kept at constant tension during all the investigations.
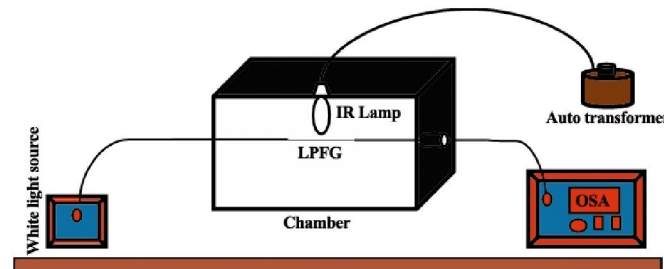
Figure 3.10 Experimental setup to find temperature sensitivity

82

The temperature response of a UV fabricated LPFG was studied first. The grating with a period of 435 μm was fabricated in Boron doped single mode fiber which had a length of 10mm. Figure 3.11 below shows the transmission spectrum of the LPFG which has attenuation peaks at 1418nm, 1473nm and 1570 nm.
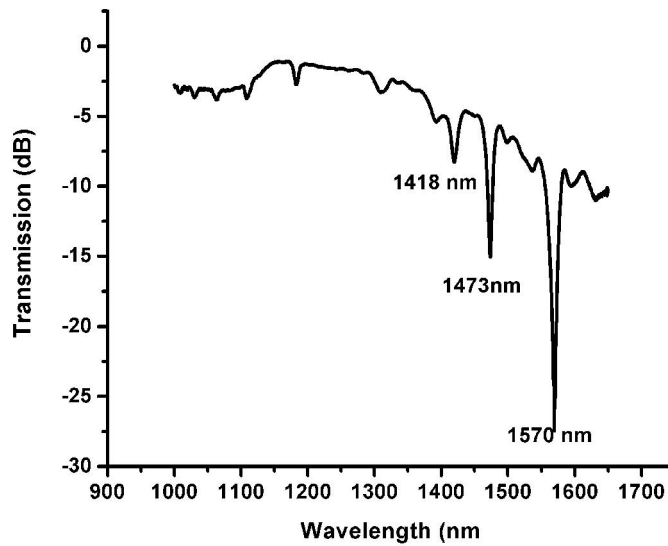
Figure 3.11 Transmission Spectrum of UV LPFG

The transmission spectrum of the LPFG was recorded by varying the temperature and the figure 3.12 shows the shift in 1418nm and 1473 nm attenuation peaks as the temperature changed from 25^0C to 75^0C. It is evident that the resonance peak shifts to lower wavelengths as the temperature increases and the measured temperature dependence of the peak wavelengths (1418nm, 1473nm and 1570 nm) is shown in figure 3.13. The points represent the average shifts calculated while the temperature increase and decrease. A total shift of -1.3nm and -1.9nm occurs for the 1418 nm and 1473nm peaks respectively for the change in temperature from 25^0C to 75^0C while 1570 band shows a shift of -1.6nm for the same temperature change. Also dλ/dT is found decreasing for the 1570 nm attenuation peak.
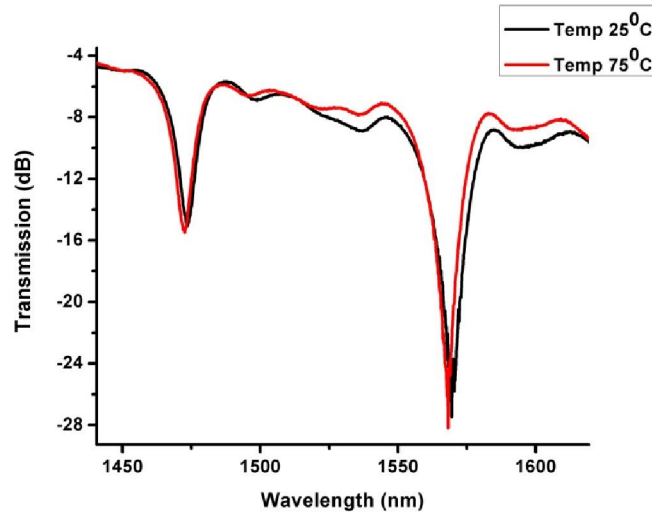
Figure 3.12 UV-LPFG spectrum at temperature 25^0C and 75^0C
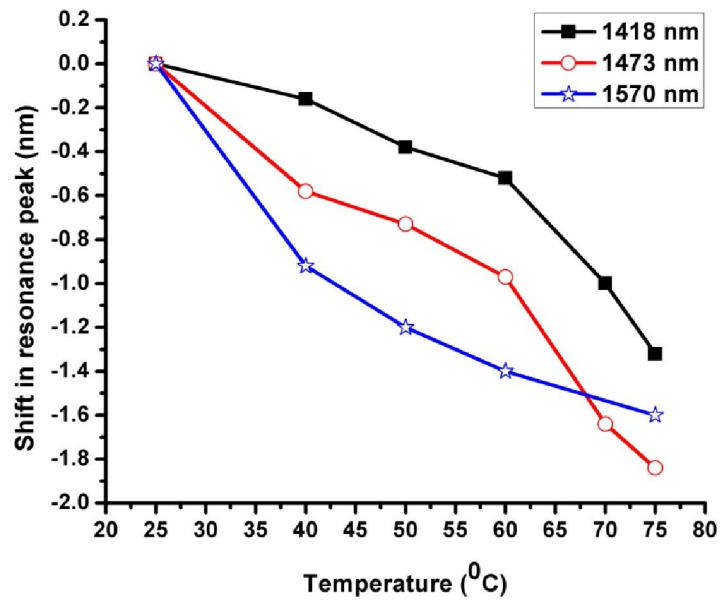
Figure 3.13 Shift in resonance peak of UV- LPFG as a function of temperature

The temperature sensitivity of the arc induced LPFG was then evaluated and the LPFG transmission spectra thus obtained for an ambient temperature of 25^0C and 80^0C are shown in figure 3.14. It is evident from the graph that the LPFG is insensitive to temperature in the range of measurements. The transmission spectrum of the CO_2 inscribed LPFG obtained for temperatures 25^0C and 80^0C is shown in figure 3.15. Even though small, a red shift in resonance peak with increasing temperature is observed. The shift in resonance peak with respect to rise in temperature is shown in figure 3.16.
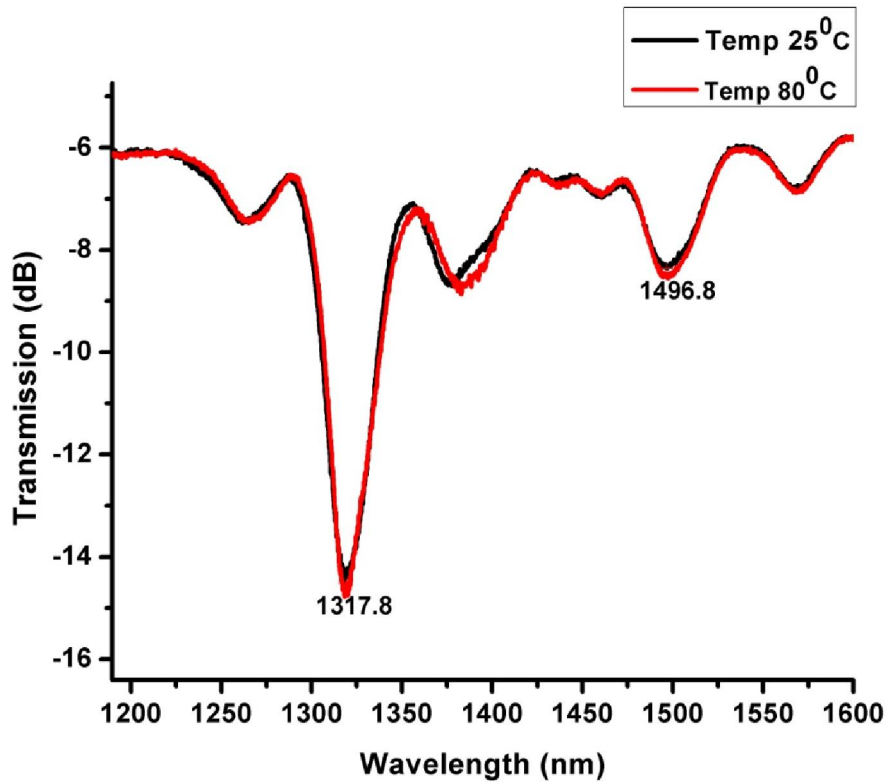
Figure 3.14 Spectrum of arc induced LPFG at temperatures 25^0C and 80^0C

85
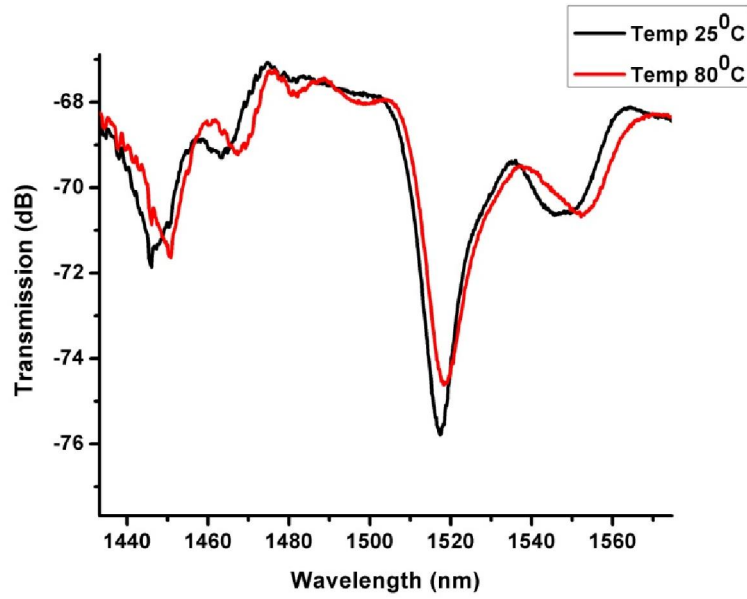
Figure 3.15 Spectrum of CO_2 induced LPFG at temperatures 25^0C and 80^0C
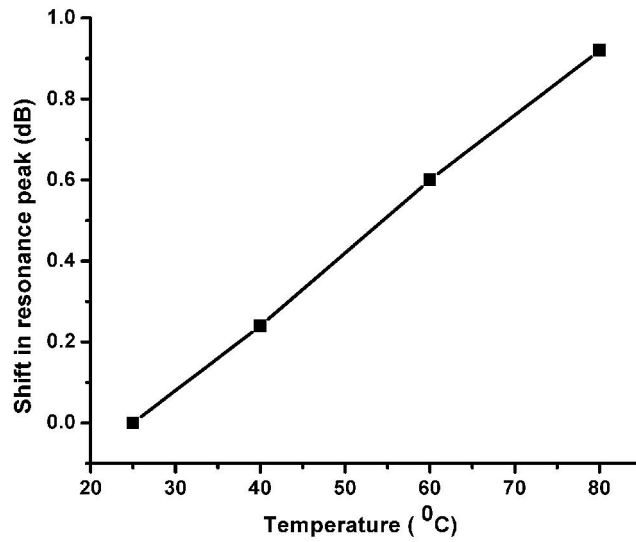
Figure 3.16 Shift in resonance peak of CO_2 induced LPFG as a function of temperature

86

The temperature response of all the LPFGs and an FBG are combined in one graph and is shown in figure 3.17. While the arc induced LPFG shows no sensitivity, the CO_2 inscribed LPFG has a temperature sensitivity of 11 pm/^{0}C and UV LPFG has -24 pm/^{0}C. Hence the following conclusions can be deducted. Even though the LPFG are formed by thermal method in similar SMF 28 fiber, the arc induced LPFG was found insensitive to temperature while the 1417 nm peak of CO_2 inscribed LPFG shows a red shift of 1 nm for a temperature change from 25 ^{0}C to 80 ^{0}C. The UV fabricated LPFG in Ge doped fiber shows a blue shift for temperature rise and has shown a maximum sensitivity of -24 pm/^{0}C.
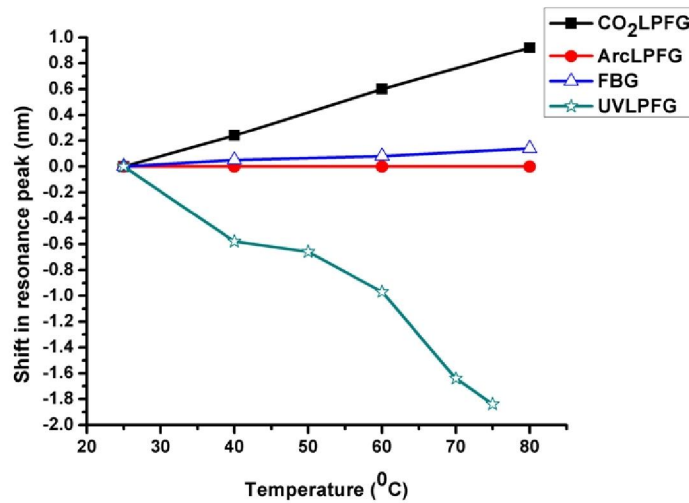
Figure 3.17 Temperature response of different LPFGs and FBG

The difference in temperature sensitivity between the SMF-28 and Boron doped silica fibers ie. red shift and blue shift, can be explained on the basis of the thermo-optic coefficients of the core and the cladding materials [107,108]. As per equation 3.10, 3.11 and 3.12, if the thermo optic coefficient of core is higher than that of cladding, the peak shift will be positive. Since the addition of boron to the core brings down the thermo optic coefficient of core below that of the cladding, blue shift occurs for the

attenuation peak with respect to increasing temperature. Thus the presence of Boron alters the temperature dependence of the effective refractive index [56] and hence the UV fabricated LPFG has a negative wavelength shift with increasing temperature. In the case of SMF-28, thermo optic coefficient of core is higher than that of cladding and hence the CO_2 inscribed LPFG in SMF 28 has a positive shift.

There are contradictory reports comparing the temperature sensitivity of LPFGs written by the arc and that with UV technology. Humbert *et al* [55] fabricated LPFG with a period of 600μm in SMF 28 fiber using electric arc and got temperature sensitivities around70 pm/^{0}C. Almost similar sensitivity was reported by Hwang et al [42] for the LPFG based on arc induced microbends in standard single mode telecommunication fiber with 620 μm period. Temperature sensitivity as high as 154pm/^{0}C in single mode fibers fabricated using UV were reported [109]. Allsop *et al* have found arc inscription a better method to achieve high temperature sensitivity [110]. In contrast Smietana et al [109] have observed that the thermal sensitivity of LPFGs fabricated in boron co-doped fiber is independent of the writing method.

Since LPFG fabricated in SMF 28 using CO_2 laser irradiation has shown sensitivity to temperature, the temperature insensitivity of the periodically tapered arc induced LPFGs in similar fiber can thus be attributed to the fabrication method. It has been shown by Rego et al [54] that the thermal sensitivity of arc induced LPFGs depends on the arc current and pulling tension. Hence it can be concluded that the fabrication method makes the arc induced LPFG temperature insensitive.

Conclusions

In this chapter the basic theory related to long-period fiber gratings is presented. Afterwards, the different mechanisms proposed in the literature for the formation of thermal induced gratings are discussed. The fabrication process of asymmetric LPFGs in SMF 28 using fusion splicer and CO_2 laser is also elaborated. Compared with the UV laser exposure technique, the fabrication methods discussed in the chapter based on electric arc and CO_2 laser are much more flexible and cost effective because neither photosensitivity nor any other pretreated processess are required to induce a grating in the glass fibers. Moreover, the writing process can be controlled to

generate complicated grating profiles via point-by-point technique without any expensive masks. Possible mechanisms of refractive index modulations in the fabricated asymmetric LPFGs are due to residual stress relaxation and physical deformation. The periodically tapered LPFG fabricated using electric arc from fusion splicer is found to be insensitive to temperature in the temperature range 25^0C to 80^0C. For telecommunication and sensing applications spectral stability is of prime importance, and an LPFG with temperature insensitive attenuation band is an attractive feature. The fabricated LPFGs have been employed for sensor development and are discussed in the next chapter.

References

1. A N Vengsarkar, P J Lemaire, J B Judkins, V Bhatia, T Erdogan and J E Sipe, "Long-period fiber gratings as band-rejection filters" J. Lightwave Technol. **14**, 58-65 (1996).

2. S W James and R P Tatam, "Optical fiber long-period grating sensors: characteristics and applications", Meas. Sci. Technol. **14**, R49-R61 (2003).

3. C.D. Poole, H.M. Presby and J.P. Meester. "2-Mode Fiber Spatial-Mode Converter Using Periodic Core Deformation*", Electron. Lett. **30**, 1437-1438 (1994.).

4. S. Ramachandran, M. Das, Z. Wang, J. Fleming and M. Yan, "High extinction, broadband polarisers using long-period fiber gratings in few-mode fibers", Electron. Lett. **38**, 1327- 1328 (2002.).

5. K.J. Han, Y.W. Lee, J. Kwon, S. Roh, J. Jung and B. Lee, "Simultaneous measurement of strain and temperature incorporating a long-period fiber grating inscribed on a polarization maintaining fiber", IEEE Photonics Technol. Lett.**16,** 2114-2116 (2004.)

6. X. Chen, K. Zhou, L. Zhang and I. Bennion, "Optical chemsensors utilizing long-period fiber gratings UV-Inscribed in D-Fiber with enhanced sensitivity through cladding etching IEEE Photonics Technol. Lett**. 16**, 1352-1354 (2004).

7. G. Rego, R. Falate, J.L. Santos, H.M. Salgado, J.L. Fabris, S.L. Semjonov and E.M. Dianov, "Arc-induced long-period gratings in aluminosilicate glass fibers", Opt. Lett. **30**, 2065- 2067 (2005).

8. G. Rego, A.F. Fernandez, A. Gusarov, B. Brichard, F. Berghmans, J.L. Santos and H.M. Salgado, "Effect of ionizing radiation on the properties of arc-induced long-period fiber gratings", Appl. Opt. **44**, 6258-6263 (2005).

9. G. Rego, O. Okhotnikov, E. Dianov and V. Sulimov, "High-temperature stability of long-period fiber gratings produced using an electric arc", J. Lightwave Technol. **19**, 1574- 1579 (2001).

10. S. Lee, R. Kumar, P. Kumar, P. Radhakrishnan, C. Vallabhan and V. Nampoori, "Long period gratings in multimode optical fibers: application in chemical sensing", Opt. Commun. **224**, 237-241 (2003).

11. T.J. Eom, S.J. Kim, T.Y. Kim, C.S. Park and B.H. Lee, "Optical pulse multiplication and temporal coding using true time delay achieved by long-period fiber gratings in dispersion compensating fiber", Opt. Express **12**, 6410-6420 (2004)

12. L. Dong, L. Reekie and J. Cruz, "Long period gratings formed in depressed cladding fibers", Electron. Lett. **33**, 1897-1898 (1997)

13. G. Humbert, A. Malki, S. Fevrier, P. Roy, J.L. Auguste and J.M. Blondy, "Long period grating filters fabricated with electric arc in dual concentric core fibers", Opt. Commun. **225**, 47-53 (2003)

14. H.L. An, B. Ashton and S. Fleming, "Long-period-grating-assisted optical add-drop filter based on mismatched twin-core photosensitive-cladding fiber", Opt. Lett. **29**, 343-345 (2004)

15. T. Allsop, D. Webb and I. Bennion, "Investigations of the spectral sensitivity of long period gratings fabricated in three-layered optical fiber", J. Lightwave Technol. **21**, 264- 268 (2003)

16. A.A. Abramov, B.J. Eggleton, J.A. Rogers, R.P. Espindola, A. Hale, R.S. Windeler and T.A. Strasser, "Electrically tunable efficient broad-band fiber filter", IEEE Photonics Technol. Lett. **11**, 445-447 (1999).

17. D.M. Costantini, C.A.P. Muller, S.A. Vasiliev, H.G. Limberger and R.P. Salathe, "Tunable loss filter based on metal-coated long-period fiber grating", IEEE Photonics Technol. Lett. **11**, 1458-1460 (1999).

18. M. van Eijkelenborg, W. Padden and J. Besley, "Mechanically induced long-period gratings in microstructured polymer fiber", Opt. Commun. **236**(1-3), 75-78 (2004).

19. G. Kakarantzas, T. Birks and P. Russell, "Structural long-period gratings in photonic crystal fibers", Opt. Lett. **27**, 1013-1015 (2002).

20. G. Humbert, A. Malki, S. Fevrier, P. Roy and D. Pagnoux, "Electric arc-induced long-period gratings in Ge-free air-silica microstructure fibers", Electron. Lett. **39**, 349-350 (2003).

21. K. Morishita and Y. Miyake, "Fabrication and resonance wavelengths of long-period gratings written in a pure-silica photonic crystal fiber by the glass structure change", J. Lightwave Technol. **22**(2), 625-630 (2004).

22. B.J. Eggleton, P.S. Westbrook, R.S. Windeler, S. Spalter and T.A. Strasser, "Grating resonances in air-silica microstructured optical fibers", Opt. Lett. **24**(21), 1460-1462 (1999).

23. V. Bhatia, D. Campbell, R.O. Claus and A.M. Vengsarkar, "Simultaneous strain and temperature measurement with long-period gratings", Opt. Lett. **22**, 648-650 (1997).

24. V. Grubsky and J. Feinberg, "Long-period fiber gratings with variable coupling for real-time sensing applications", Opt. Lett. **25**, 203-205 (2000)

25. D.S. Starodubov, V. Grubsky and J. Feinberg, "All-fiber bandpass filter with adjustable transmission using cladding-mode coupling", IEEE Photonics Technol. Lett. **10**, 1590- 1592 (1998)

26. E.M. Dianov, D.S. Stardubov, S.A. Vasiliev, A.A. Frolov and O.I. Medvedkov, "Refractiveindex gratings written by near-ultraviolet radiation", Opt. Lett. **22**, 221-223 (1997)

27. B. Ortega, L. Dong, W. Liu, J. deSandro, L. Reekie, S. Tsypina, V. Bagratashvili and R. Laming, "High-performance optical fiber polarizers based on long-period gratings in birefringent optical fibers", IEEE Photonics Technol. Lett. **9**, 1370-1372 (1997).

28. B. Guan, H. Tam, S. Ho, S. Liu and X. Dong, "Growth of long-period gratings in H-2-loaded fiber after 193-nm UV inscription", IEEE Photonics Technol. Lett. **12**, 642-644 (2000).

29. C. Ye, S. James and R. Tatam, "Simultaneous temperature and bend sensing with long-period fiber gratings", Opt. Lett. **25**, 1007-1009 (2000).

30. Xuewen Shu, Tom Allsop, Bashir Gwandu, Lin Zhang and Ian Bennion, "High-Temperature Sensitivity of Long-Period Gratings in B–Ge Codoped Fiber", IEEE Photonics Technol. Lett. **13**, 818-820 (2001.

31. Rita Zanlorensi Visneck Costa, Ricardo Canute Kamikawachi, Marcia Muller and Jose Luis Fabris, "Thermal characteristics of long-period gratings 266 nm UV-point-by-point induced", Opt. Commun. **282**, 816–823 (2009)

32. J. Blows and D.Y. Tang, "Gratings written with tripled output of Q-switched Nd: YAG laser", Electron. Lett. **36**, 1837-1839 (2000).

33. A.I. Kalachev, D.N. Nikogosyan and G. Brambilla, "Long-period fiber grating fabrication by high-intensity femtosecond pulses at 211 nm", J. Lightwave Technol. **23**(8), 2568-2578 (2005).

34. A. Dragomir, D.N. Nikogosyan, A.A. Ruth, K.A. Zagorul'ko and P.G. Kryukov, "Long-period fiber grating formation with 264 nm femtosecond radiation", Electron. Lett. **38**, 269-271 (2002).

35. S.A. Slattery and D.N. Nikogosyan, "Long-period fiber grating inscription under high-intensity 352 nm femtosecond irradiation: Three-photon absorption and energy deposition in cladding", Opt. Commun. **255**, 81-90 (2005)

36. Mykhaylo Dubov, Ian Bennion Stephen, A. Slattery and David N. Nikogosyan, "Strong long-period fiber gratings recorded at 352 nm", Opt. Lett. **30**, 2533-2535 (2005)

37. K.A. Zagorul'ko, P.G. Kryukov, Y.V. Larionov, A.A. Rybaltovskii, E.M. Dianov, N.S. Vorob'ev, A.V. Smirnov, M.Y. Shchelev and A.M. Prokhorov, "Fabrication of a long-period grating in a fiber by second-harmonic radiation from a femtosecond Ti: sapphire laser", Quantum Electron. **31**, 999-1002 (2001)

38. P.G. Kryukov, Y.V. Larionov, A.A. Rybaltovskii, K.A. Zagorul'ko, A. Dragomir, D.N. Nikogosyan and A.A. Ruth, "Long-period fiber grating fabrication with femtosecond pulse radiation at different wavelengths", Microelectron. Eng. **69**, 248-255, 2003.

39. Yi Jiang, Caijie Tang and Jingjing Xu, "Fabrication of long-period gratings with a mercury-arc lamp", Opt. Commun. 283, 1311–1315 (2010)

40. Toru Mizunami, Yutaku Sho, Kouitirou Yamamoto, Yoshihito Ishida, "Long-period fiber-gratings produced by exposure with a low-pressure mercury lamp and their sensing characteristics", Opt. Commun. **282**, 4699–4705 (2009)

41. X. Li, C. Yue, L. Xia, X. Chen and S. Xie. "Novel technique for long period gratings fabrication using broad spectrum ultraviolet source", Microwave Opt. Technol. Lett **33**, 368-370 (2002).

42. In Kag Hwang, Seok Hyun Yun and Byoung Yoon Kim, "Long-period fiber gratings based on periodic microbends", Opt. Lett. **24** , 1263 -1265 (1999)

43. Yuki Kondo, Kentaro Nouchi, Tsuneo Mitsuyu, Masaru Watanabe, Peter G. Kazansky and Kazuyuki Hirao, "Fabrication of long-period fiber gratings by focused irradiation of infrared femtosecond laser pulses", Opt. Lett. **24**, 646-648 (1999)

44. D. D. Davis, T. K. Gaylord, E. N. Glytsis, S. G. Kosinski, S. C. Mettler and A. M. Vengsarkar, "Long-period fiber grating fabrication with focused CO_2 laser pulses", Electron. Lett. **34**, 302-303 (1998).

45. D. D. Davis, T. K. Gaylord, E. N. Glytsis and S. C. Mettler, "CO_2 laser-induced long-period fiber gratings: spectral characteristics, cladding modes and polarisation independence," Electron. Lett. **34**, 1416-1417 (1998).

46. M. I. Braiwish, B. L. Bachim and T. K. Gaylord, "Prototype CO_2 Laser-induced Long-period Fiber Grating Variable Optical Attenuators and Optical Tunable Filters", Appl. Opt. **43**, 1789-1793 (2004).

47. Yi-Ping Wang, D. N. Wang, ei Jin, Yun-Jiang RaO andng-Ding Peng, "Asymmetric long period fiber gratings fabricated by use of CO_2 laser to carve periodic grooves on the optical fiber", Appl. Phys. Lett. **89**, 151105 (2006)

48. Victor Grubsky and Jack Feinberg, "Fabrication of Axially Symmetric Long-Period Gratings with a Carbon Dioxide Laser", IEEE Photonics Technol. Lett. **18** , 2296-2298 (2006)

49. Lei Su, Kin Seng Chiang and Chao Lu, "CO_2-Laser-Induced Long-Period Gratings in Graded-Index Multimode Fibers for Sensor Applications", IEEE Photonics Technol. Lett. **18**, 190-192 (2006)

50. Petr Cısarovsky, Jırı Dunovsky, Ladislav Kolarık, Filip Todorov , Ivan Kaxık and Vlastimil Matejec, "Recording of long-period gratings in special single-mode fibers by a CO_2 laser", Mater. Sci. Eng., C **26**, 448 – 452 (2006)

51. Radan Slavık, "Coupling to circularly asymmetric modes via long-period gratings made in a standard straight fiber", Opt. Commun. **275**, 90–93 (2007)

52. Seungtae Oh, Kyung Rok Lee, Un-Chul Paek and Youngjoo Chung, "Fabrication of helical long-period fiber gratings by use of a CO_2 laser", Opt. Lett. **29**, 1464-1466 (2004)

53. Yi-Ping Wang, Limin Xiao, D. N. Wang and Wei Jin, "Highly sensitive long-period fiber-grating strain sensor with low temperature sensitivity", Opt. Lett. **31**, 3414-3416 (2006)

54. Gaspar Rego, Rosane Falate, Oleg Ivanov and José Luís Santos, "Simultaneous temperature and strain measurements performed by a step-changed arc-induced long-period fiber grating", Appl. Opt. **46**, 1392-1396 (2007).

55. Georges Humbert and Abdelrafik Malki, "Electric-arc-induced gratings in non-hydrogenated fibers: fabrication and high-temperature characterizations", J. Opt. A: Pure Appl. Opt. **4**, 194–198 (2002)

56. G. Rego, P. V. S. Marques, J. L. Santos and H. M. Salgado, "Arc-Induced Long-Period Gratings", Fiber Integr. Opt. **24**, 245 -259 (2005)

57. Gaspar Rego, "Long-Period Gratings Arcinduced In B/Ge Codoped Fibers: Thermal Behavior And Uniform Exposure To Uv-Radiation", Microwave Opt. Technol. Lett. **50**, 68-70 (2008)

58. P. Palai, M.N. Satyanarayan, Mini Das, K. Thyagarajan and B.P. Pal, "Characterization and simulation of long period gratings fabricated using electric discharge", Opt. Commun. **193**, 181-185 (2001)

59. Sung Hyun Nam, Chun Zhan, Jon Lee, Corey Hahn, Karl Reichard, Paul Ruffin, Kung-Li Deng and Shizhuo Yin, "Bend-insensitive ultra short long-period gratings by the electric arc method and their applications to harsh environment sensing and communication", Opt. Express **13**, 731-737 (2005)

60. Gaspar Rego, Oleg V. Ivanov, and P.V.S. Marques, "Demonstration of coupling to symmetric and antisymmetric cladding modes in arc-induced long-period fiber gratings", Opt. Express **14**, 9594- 9599 (2006)

61. O. V. Ivanov and G. Rego, "Origin of coupling to antisymmetric modes in arc-induced long-period fiber gratings", Opt. Express **15**, 13936- 13941 (2007)

62. Gaspar Rego and Oleg V. Ivanov, "Two types of resonances in long-period gratings induced by arc discharges in boron/ germanium co-doped fibers", Opt. Lett. **32**, 2984-2986 (2007)

63. Paulo Caldas, Gaspar Rego, Oleg V. Ivanov and Jose L. Santos, "Characterization of the response of a dual resonance of an arc-induced long-period grating to various physical parameters", Appl. Opt. **49**, 2994-2996 (2010)

64. G. Rego, F. Durr, P.V.S. Marques and H.G. Limberger, "Strong asymmetric stresses arc-induced in pre-annealed nitrogen-doped fibers", Electron. Lett. **42**, 334-335 (2006)

65. C.Y. Lin and L.A. Wang, "Loss-tunable long period fiber grating made from etched corrugationstructure", Electron. Lett. **35**, 1872-1873 (1999).

66. C. Y. Lin and Lon A. Wang, "A Wavelength- and Loss-Tunable Band-Rejection Filter Based on Corrugated Long-Period Fiber Grating", IEEE Photonics Technol. Lett.**13**, 332-334 (2001)

67. Chunn-Yenn Lin, Lon A. Wang, and Gia-Wei Chern "Corrugated Long-Period Fiber Gratings as Strain, Torsion, and Bending Sensors", J. Lightwave Technol. **19**, 1159-1168 (2001)

68. K. P. Chen, P. R. Herman, R. Tam and J. Zhang, "Rapid long-period grating formation in hydrogen-loaded fiber with 157 nm F2-laser radiation", Electron. Lett. **36**, 2000–2001 (2000).

69. K. P. Chen, P. R. Herman, J. Zhang, and R. Tam, "Fabrication of strong long-period gratings in hydrogen-free fibers with 157-nm F2-laser radiation," Opt. Lett. **26**, 771–773 (2001).

70. O.V. Ivanov, "Fabrication of long-period fiber gratings by twisting of a standard single-modefiber", Opt. Lett. **30**, 3290-3292 (2005)

71. M. Fujimaki, Y. Ohki, J.L. Brebner and S. Roorda, "Fabrication of long-period optical fibergratings by use of ion implantation", Opt. Lett. **25**, 88-89 (2000).

72. M. von Bibra, A. Roberts and J. Canning, "Fabrication of long-period fiber gratings by use of focused ion-beam irradiation", Opt. Lett. **26**, 765-767 (2001).

73. A.F. Fernandez, B. Brichard and F. Berghmans, "In situ measurement of refractive index changes induced by gamma radiation in germanosilicate fibers", IEEE Photonics Technol. Lett. **15**, 1428-1430 (2003).

74. X. Shu, L. Zhang and I. Bennion, "Sensitivity characteristics near the dispersion turning points of long-period fiber gratings in B/Ge codoped fiber", Opt. Lett. **26**, 1755-1757 (2001).

75. Hand D P and Russell P S J," Photoinduced refractive index changes in germanosilicate fibers", Opt. Lett. **15**, 144–146 (1990)

76. Limberger H G, Fonjallaz P Y, Salathe R P and Cochet F, "Compaction- and photoelastic-induced index changes in fiber Bragg gratings", Appl. Phys. Lett. **68**, 3069–3071 (1996)

77. Fonjallaz P Y, Limberger H G, Salathe R P, Cochet F and Leuenberger B, "Tension increase correlated to refractive-index change in fibers containing UV-written Bragg gratings", Opt. Lett. **20**, 1346–1348 (1995).

78. C. S. Kim, Y. Han, B. H. Lee, W. T. Han, U. C. Paek, and Y. Chung, "Induction of the refractive index change in B-doped optical fibers through relaxation of the mechanical stress," Opt. Commun. **185**, 337-342 (2000).

79. B. H. Kim, Y. Park, T. J. Ahn, D. Y. Kim, B. H. Lee, Y. Chung, U. C. Paek, and W. T. Han, "Residual stress relaxation in the core of optical fiber by CO2 laser irradiation," Opt. Lett. **26**, 1657-1659 (2001).

80. B. H. Kim, T.-J. Ahn, D. Y. Kim, B. H. Lee, Y. Chung, U.-C. Paek, and W.-T. Han, "Effect of CO2 Laser Irradiation on the Refractive-Index Change in Optical Fibers," Appl. Opt. **41**, 3809-3815 (2002).

81. Y. Li, T. Wei, J. A. Montoya, S. V. Saini, X. Lan, X. Tang, J. Dong and H. Xiao, "Measurement of CO_2-laser-irradiation-induced refractive index modulation in single-mode fiber toward long-period fiber grating design and fabrication," Appl. Opt. **47**, 5296-5304 (2008).

82. K. Morishita and A. Kaino, "Adjusting resonance wavelengths of long-period fiber gratings by the glass-structure change," Appl. Opt. **44**, 5018-5023 (2005).

83. V. Grubsky and J. Feinberg, "Rewritable densification gratings in boron-doped fibers," Opt. Lett. **30**, 1279-1281 (2005).

84. Y. Liu, H. W. Lee, K. S. Chiang, T. Zhu and Y. J. Rao, "Glass Structure Changes in CO2-Laser Writing of Long-Period Fiber Gratings in Boron-Doped Single-Mode Fibers," J. Lightwave Technol. **27**, 857-863 (2009).

85. M. Kim, D. Lee, B. Hong and H. Chung, "Performance characteristics of long-period fibergratings made from periodic tapers induced by electric-arc discharge", J. Korean Phys. Soc. **40**, 369-373 (2002)

86. S.G. Kosinski and A.M. Vengsarkar, "Splice-based long-period fiber gratings" (Optical Fiber Communications Conference 1998, 278-279)

87. U. C. Paek and C. R. Kurkjian, "Calculation of cooling rate and induced stresses in drawing of optical fibers," J. Am. Ceram. Soc. **58**, 330-335 (1975).

88. A.D. Yablon, "Optical and mechanical effects of frozen-in stresses and strains in optical fibers", IEEE Journal of Selected Topics in Quantum Electronics **10**, 300-311 (2004).

89. B.H. Kim, Y. Park, T.J. Ahn, D.Y. Kim, B.H. Lee, Y. Chung, U.C. Paek, and W.T. Han, "Residual stress relaxation in the core of optical fiber by CO_2 laser irradiation", Opt. Lett. **26**, 1657-1659 (2001).

90. H.G. Limberger, P.Y. Fonjallaz, R.P. Salathe and F. Cochet, "Compaction- and photoelastic- induced index changes in fiber Bragg gratings", Appl. Phys. Lett. **68**, 3069-3071 (1996)

91. E.M. Dianov, V.G. Plotnichenko, V.V. Koltashev, Y.N. Pyrkov, N.H. Ky, H.G. Limberger and R.P. Salathe, "UV-irradiation-induced structural transformation of germanosilicate glass fiber", Opt. Lett. **22**, 1754-1756 (1997.)

92. M. Douay, W.X. Xie, T. Taunay, P. Bernage, P. Niay, P. Cordier, B. Poumellec, L. Dong, J.F. Bayon, H. Poignant and E. Delevaque, "Densification involved in

the UV-based photosensitivity of silica glasses and optical fibers", J. Lightwave Technol. **15**, 1329-1342 (1997).

93. R. Bruckner, "Properties and Structures of Vitreous Silica. I", J. Non-Cryst. Solids **5**, 123-175 (1970).

94. R. Bruckner, "Properties and Structures of Vitreous Silica. II.", J. Non-Cryst. Solids **5**, 177-216 (1971).

95. L. Jin, Z. Wang, Q. Fang, Y. Liu, B. Liu, G. Kai and X. Dong, "Spectral characteristics and bend response of Bragg gratings inscribed in all-solid bandgap fibers", Opt. Express **15**, 15555-15565 (2007).

96. G. Kakarantzas, T. E. Dimmick, T. A. Birks, R. Le Roux and P. S. J. Russell, "Miniature all-fiber devices based on CO2 laser microstructuring of tapered fibers", Opt. Lett. **26**, 1137-1139 (2001).

97. H. Xuan, W. Jin and M. Zhang, "CO_2 laser induced long period gratings in optical microfibers", Opt.Express **17**, 21882-21890 (2009).

98. Y. Zhu, P. Shum, X. Chen, C.-H. Tan and C. Lu, "Resonance-temperature-insensitive phase-shifted long-period fiber gratings induced by surface deformation with anomalous strain characteristics", Opt.Lett. **30**, 1788-1790 (2005).

99. E.M. Dianov, V.I. Karpov, M.V. Grekov, K.M. Golant, S.A. Vasiliev, O.I. Medvedkov, and R.R. Khrapko, "Thermo-induced long-period fiber gratings", (23rd European Conference on Optical Communications1997, 53-56)

100. A M. Vengsarkar, P J. Lemaire, J B. Judkins, V Bhatia, T Erdogan, and J E. Sipe, "Long-Period Giber Gratings as Band-Rejection Filters", J. Lightwave Technol. **14**, 58-65 (1996).

101. Turan Erdogan, "Fiber Grating Spectra", J. Lightwave Technol. **15**, 1277-1294 (1997).

102. Turan Erdogan, "Cladding-mode resonances in short- and long period fiber grating filters", J. Opt. Soc. Am. A **14**, 1760-1773 (1997).

103. O V Ivanov, S A Nikitov and Yu V Gulyaev, "Cladding modes of optical fibers: properties and applications", Phys. Usp. **49**, 167 -191 (2006)

104. Li-Yang Shao, Jian Zhao, Xinyong Dong, H. Y. Tam, C. Lu and Sailing He, "Long-period prating fabricated by periodically tapering standard single-mode fiber", Appl. Opt. **47**, 1549-1552 (2008).

105. Vikram Bhatia, "Applications of long-period gratings to single and multi-parameter sensing", Opt. Express **4** , 457-466 (1999).

106. K. Shima, K. Himeno, T. Sakai, S. Okude, A. Wada, R.Yamauchi, "A novel temperature-insensitive long-period fiber grating using a boron-codoped-germanosilicate-core fiber" (Optical Fiber Communications Conference (OFC'97), 1997)

107. Mei Nar Ng and Kin Seng Chiang, "Thermal effects on the transmission spectra of long-period fiber gratings", Opt. Commun. **208**, 321–327 (2002)

108. Shu X, Allsop T, Gwandu B, Zhang L and Bennion I, "Room-temperature operation of widely tunable loss filter", Electron. Lett. **37,** 216-218 (2001)

109. M Smietana, W J Bock and P Mikulic, "Comparative study of long-period gratings written in a boron co-doped fiber by an electric arc and UV irradiation", Meas. Sci. Technol. **21**, 025309(1-8) (2010)

110. Allsop T, Dubov M, Dobb H, Main A, Martinez A, Kalli K, Webb D J and Bennion I A, "comparison of the spectral properties of high temperature annealed long period gratings inscribed by fs laser, UV and fusion-arc", Proc. SPIE **6193,** 61930M(1-9) (2006)

Fiber optic sensor for the quality evaluation of ethanol blended petrol

4.1 Introduction

Fossil fuels are complex mixtures of liquid hydrocarbons, volatile and flammable, with physical and chemical properties that accounts for its high applicability as a source of energy for motor vehicles. The chemical structure of these fuels contains a variable number of carbon atoms associated with the formation of paraffins, iso-paraffins, naphthenes, olefins or aromatic compounds. However, the exact composition of a particular type of fuel depends on the characteristics of the raw material, their production process, its use as a final product and the specifications imposed by regulatory agencies [1].

Fuel additives are compounds added to fuel in order to improve its efficiency and its performance [2-5]. Several organic compounds have been used as fuel additives, such as methanol, ethanol, tertiary butyl alcohol and methyl tertiary butyl ether. Ethanol was the first fuel among the alcohols to be used to power vehicles in the 1880s and 1890s and is a prospective material for use in automobiles as an alternative to petroleum based fuels. At present instead of pure ethanol, a blend of ethanol and petrol is used as a more attractive fuel with good anti-knock characteristics and the exact volumetric concentration of ethanol in the fuel is specified by the respective governments. The main reason for advocating ethanol is that it can be manufactured from natural products or waste materials while fossil fuels are produced from non-renewable natural resources. Ethanol is mainly produced from sugarcane and its use can be a boon to farmers. Moreover, combustion of ethanol-petrol blend provides significant reduction in the emission of air pollutants, such as carbon monoxide, carbon dioxide and hydrocarbons thereby reduce the greenhouse effect and tone down global warming [2-5]. Countries are also seeing it as a means to reduce their dependence on oil imports and are taking steps to make mandatory blending of 10 per cent ethanol into petrol.

Since ethanol is cheaper than petrol and can be locally distilled, the fuel may be adulterated by increasing the proportion of ethanol in order to

maximize the profit derived from its sale. Consequently, operating an engine with an ethanol fuel that presents a high water proportion or with a blend that has too high hydrated alcohol content will cause engine damage and poor performance, with possible damage to the environment. One of the most significant factors responsible for rampant practice of adulteration is the non-availability of a standard technique that is followed universally for the in-situ detection of adulteration level. In this context, the development of smart monitoring systems able to assess the fuel conformity and to supply real-time and reliable results assumes a great importance.

Aqueous extraction method is the standard test employed to determine the content of ethanol in the ethanol-petrol blend. Although widespread, this technique presents high response time, low resolution and is not susceptible to real-time monitoring. Besides, this method is subject to errors of parallax and also dependent on a skilled operator to its correct implementation. Therefore, the development of alternate tools to perform the ethanol-petrol blend analysis is of great interest.

The petroleum hydrocarbon detection demands some special characteristics of the sensors to be used. A passive electrical operation is one of the main characteristics because the hydrocarbon environment can be very inflammable, so it is interesting to have a sensor device which does not produce sparks. On addition of ethanol, the refractive index of petrol varies and therefore, it is natural to consider the utilization of optical fiber technology to measure the refractive index because of its unique characteristics such as ease of fabrication, high sensitivity, fast response, compactness, resistant to harsh environments, distributed sensing besides being chemically inert and immune to electromagnetic interference [6-10]. These last two qualities in addition to electricity free operation make optical fiber sensors the safest devices to implement, as hydrocarbon environment is intrinsically hazardous. Also, as the optical fibers are a very low loss communication medium, it makes realization of a distributed sensing network in a hydrocarbon region with signal processing and monitoring from a remote location feasible.

Long period fiber grating (LPFG) has demonstrated its sensitivity to the refractive index value of the surrounding material of the grating and several scientists have exploited this feature of the LPFG to implement

refractive-index sensors based on the change in resonant wavelength [11-35]. The sensitivity to changes in the RI of the surrounding medium enable LPFGs to be used as chemical detectors, that is, to measure the concentration of a particular constituent in liquids, such as, salt solutions [11,12], ethylene glycol [13,14] or hydrocarbon [15-21]. A biosensor based on a LPFG written in a cladding etched fiber was employed to detect the concentration of the haemoglobin protein in a sugar solution [22]. The use of LPFGs as liquid level sensors [23] and as flow sensors [24,25] has also been demonstrated. LPFGs have been used as a biosensor to detect the RI change when an antigen bonds with the antibody [26].

Optical fiber sensors based on long period fiber gratings to determine the ethanol concentration in ethanol blended petrol has already been reported in the literature [15-19]. Falate et al [15] reported the use of an arc LPFG to evaluate the quality of the automotive petrol and got an average sensitivity of 0.15 nm/% for the wavelength shift of the resonance band in the region where the ethanol proportion changes from 20 to 50% in the mixture with petrol. The successful utilization of LPFG for Biodiesel Quality Control was also reported [16]. Possetti et al [17] combined the LPFG with artificial neural networks for smart sensing with high applicability in the petrochemical field. Successful implementation of long period fiber grating based devices for kerosene adulteration in petrol was also reported.

In this chapter, we present the utilization of the fabricated LPFGs (described in chapter 3) for quality evaluation of ethanol blended petrol, which relies on the refractive indexes changes of the grating surrounding media. The refractive index sensitivities of the LPFGs fabricated using electric arc, CO_2 laser beam and UV laser beam are determined using standard liquids. The experiments are carried out with the LPFG immersed in an external medium of petrol blend with ethanol and the periodically tapered LPFG is found to have better refractive index sensitivity than normal arc induced gratings in determining ethanol concentration in ethanol-petrol blend. The obtained results show that long period fiber gratings can be applied for fuel quality control.

4.2 Refractive index sensitivity

LPFGs are sensitive to external index of refraction of the substance surrounding the cladding at the grating location and it arises from the dependence of the phase matching condition upon the effective refractive index of the cladding modes. The effective indices of the cladding modes are dependent upon the difference between the refractive index of the cladding and that of the medium surrounding the cladding. This affects the differential effective mode index and hence the spectral attenuation band corresponding to that cladding mode [13,14,36-39]. In addition to that the evanescent fields of the cladding modes penetrate beyond the cladding-surround interface and this cause interaction of cladding mode with that of the ambient [38,39]. Thus the central wavelengths of the attenuation bands show a dependence on the refractive index of the medium surrounding the cladding, provided that the cladding has the higher refractive index. In the case of an ambient medium with refractive index less than that of cladding, the sensitivity of LPFG to increasing external index of refraction is evident as a shift in central wavelength and a decrease in peak depth of the of the attenuation band [13,34,38]. The decrease in attenuation peak depth is due to the increasing expansion of the cladding mode beyond the cladding boundary with increasing ambient refractive index. As the ambient index increases beyond the cladding index, the cladding modes no longer experience total internal reflection and are referred to as leaky modes. In this case, the peak transmission loss of the resonance band increases as ambient refractive index increases. Also coupling occurs at slightly longer wavelengths than the initial coupling wavelengths when the surrounding material is air (RI=1). As the ambient index increase from that point, the wavelength shift is non-linear, with an initial red shift and then blue shift. In this region the wavelength shift is too small to be calculated or measured [13,33,40,41]. Greater ambient index sensitivity is exhibited in higher order cladding modes because these modes are less bound to the waveguide structure formed by the fiber itself [13,33,40,41].

The influence of variations in the refractive index of medium surrounding the cladding of a LPFG is expressed by [38]

$$\frac{d\lambda_m}{dn_{sur}} = \frac{d\lambda_m}{dn_{eff,cl}^m}\left[\frac{dn_{eff,cl}^m}{dn_{sur}}\right] \tag{4.1}$$

where n_{sur} and $n_{eff,cl}^m$ is the refractive index of the surrounding material and m^{th} effective cladding mode, respectively. The term $dn_{eff,cl}^m \big/ dn_{sur}$ is distinct for each cladding mode, and hence refractive index sensitivity of LPFG depends strongly on the order of the coupled cladding mode. For a given LPFG and cladding mode, the wavelength shift resulted from the refractive index changes may be positive or negative.

Chiang et.al.[42] presented analytical expressions for the shift in resonance wavelength of a LPFG in response to the changes in the refractive index of the external environment. Thus, for external changes in the refractive index from n_{ex0} to n_{ex1}, the wavelength shift $\delta\lambda_m$ is [42]:

$$\delta\lambda_m \cong \frac{u_\infty^2 \lambda_m^3 \Lambda}{8\pi^3 n_{cl}\rho^3}\left[\frac{1}{\left(n_{cl}^2 - n_{ex0}^2\right)^{1/2}} - \frac{1}{\left(n_{cl}^2 - n_{ex1}^2\right)^{1/2}}\right] \tag{4.2}$$

where u_∞ is the mth root of the Bessel function J_0 , λ_m is the resonance wavelength at n_{ex0}, Λ is the grating pitch, and ρ is the cladding radius. It is important to notice that different external media that promotes the same refractive index change from n_{ex0} to n_{ex1} will lead to the same value for $\delta\lambda_m$, and cannot be recognized by the LPFG. The shift in 1473nm and 1570 nm resonance peaks of the LPFG (figure 4.1) plotted using equation 4.2 is shown in figure 4.2.
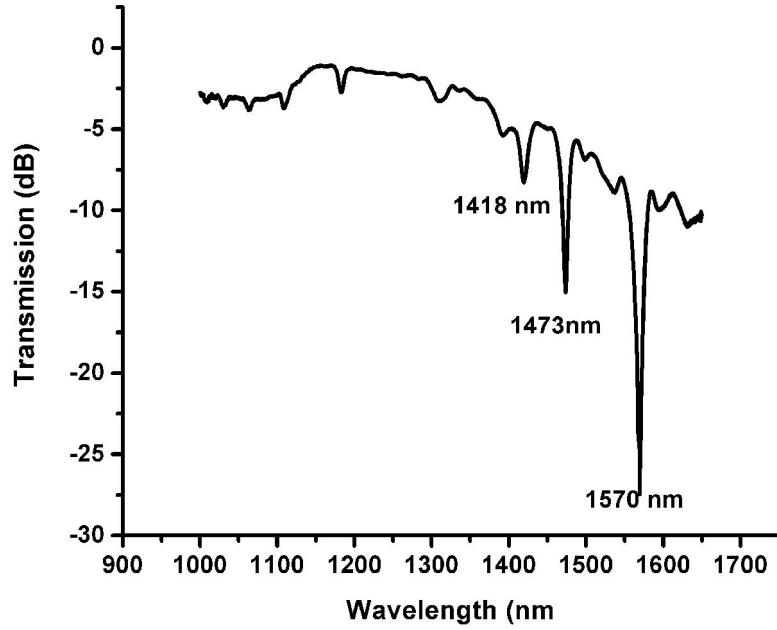
Figure 4.1 LPFG Spectrum
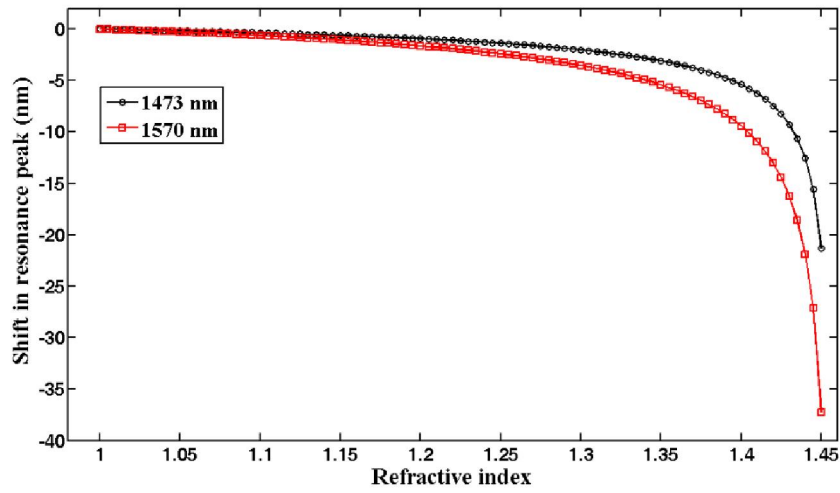
Figure 4.2 Shift in resonance peak for change in ambient refractive index

4.3 Determination of refractive index sensitivity

The experimental setup used to calibrate the LPFGs for ambient refractive index change is shown in figure 4.3. The LPFG was glued tightly inside a glass chamber of volume approximately 20ml. This will ensure that during the experiments the fiber would be under constant tension and this reduces the noise due to the LPFG sensitivity to strain. Also to reduce temperature sensitivity all efforts were made to conduct the experiments at constant temperature of 24^0C. The glass cell has inlet and outlet valves to fill in and drain out liquid samples. To minimize systematic errors and to clean the measurement system, iso-propanol was introduced into the glass cell and cleaned several times after draining out samples from the cell. The LPFG resonance wavelength position relative to iso-propanol was used as the reference for ensuring cleanliness of the LPFG. After draining out iso-propanol, the LPFG was dried before transferring the next sample to the cell.
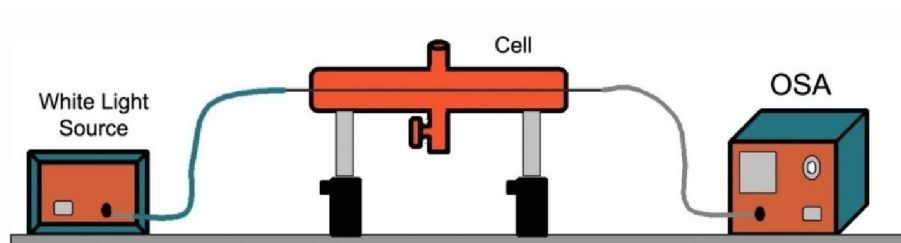
Figure 4.3 Experiment setup for determining refractive index sensitivity

We have calibrated the LPFG for refractive index sensing by determining the shift of the resonant peak for known refractive indices. Water, ethanol, propanol, aqueous solutions of glycerol at various concentrations, coconut oil, paraffin oil and groundnut oil were transferred one after the other into the cell and the LPFG response was recorded. The refractive indices of these solutions were also determined using an Abbe refractometer. The shift in the attenuation peak for the change in ambient refractive index is found to increase with increasing mode order. Thus, for sensor applications, it is desirable to work with the highest-order cladding

mode that falls within the bandwidth of the light source used to interrogate the grating.

The refractive index sensitivity of UV fabricated symmetric LPFG was evaluated and the shift in 1570nm attenuation band with different ambient refractive index is shown in figure 4.4. When external refractive index is less than that of cladding, the LPFG sensitivity to increasing external index of refraction is evident as a blue shift in central wavelength of the attenuation band and a decrease in its peak depth.
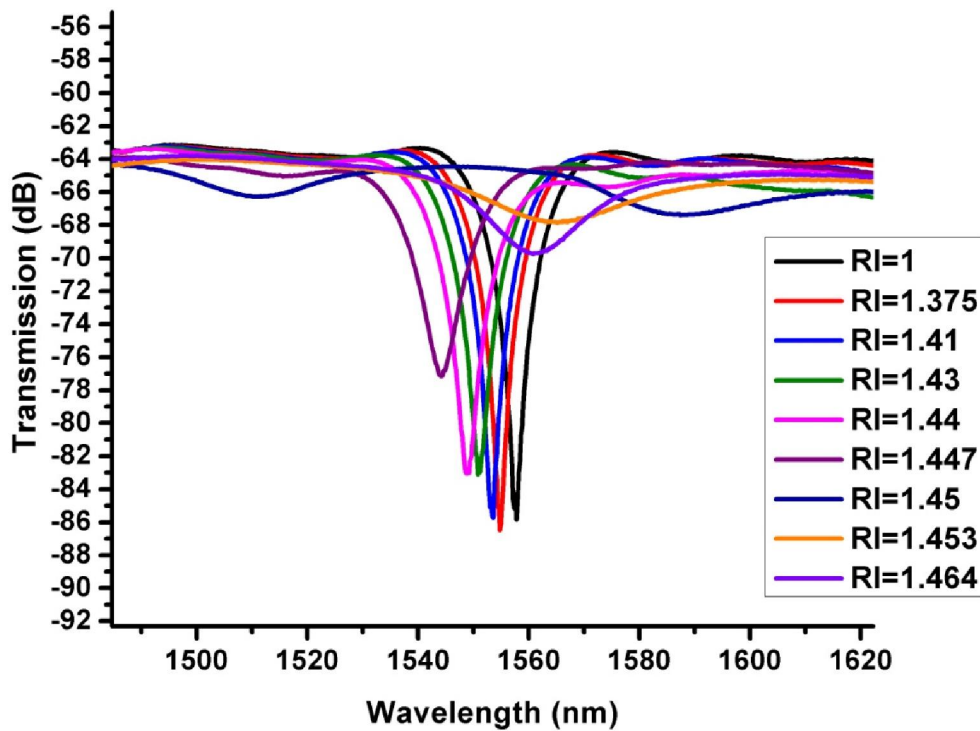
Figure 4.4 LPFG resonance peak for various ambient refractive indices

Once the value of ambient refractive index reaches that of the cladding, discrete cladding modes are no longer guided along the fiber. The absence of distinct attenuation bands in the LPFG transmission spectrum is evident in figure 4.4 at an ambient refractive index around 1.45. . In effect the cladding has an infinitely large radius when $n_{ext} \approx n_{cl}$, such that the cladding modes are converted into radiation modes as a result of the lack of total internal reflection at the cladding boundary. The LPFG is most sensitive

to external refractive index changes in this region where index-matching occurs between the cladding and the surrounding medium. This is obvious in figure 4.5 where the shift in resonance band is plotted as a function of ambient refractive index.
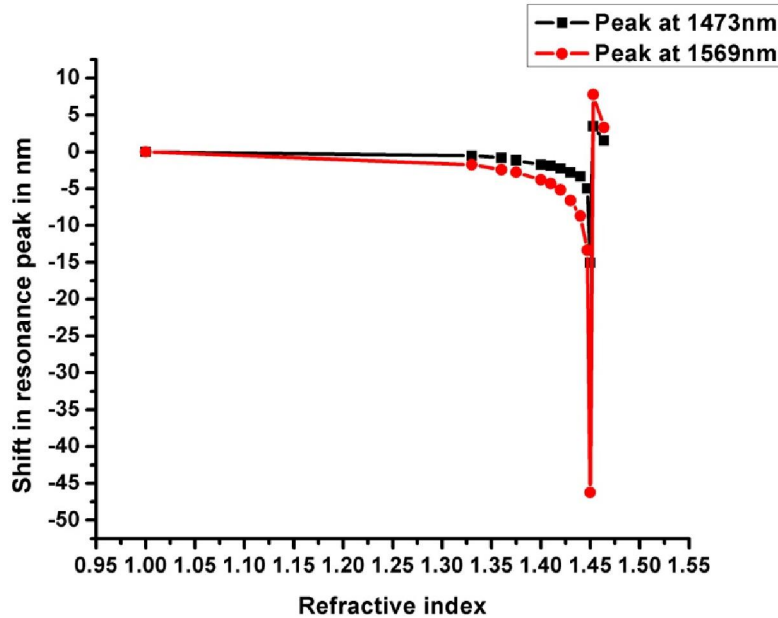
Figure 4.5 Shift in resonance peak for various ambient refractive indices

The change in the 1496nm resonance peak of the transmission spectrum of the arc induced LPFG for different ambient refractive index is shown in figure 4.6. The corresponding wavelength shift for all the three resonance peaks (1318 nm, 1383 nm and 1496nm) as a function of external refractive index is shown in figure 4.7. From figure 4.7 it is evident that the wavelength shift of lower order resonant modes (1318 nm and 1383nm) are negligible for external refractive index change, while measurable blue shift occurs for the higher order (1496 nm) mode. The resonant peak shows a nonlinear shift towards lower wavelength as the refractive index increases from 1 to 1.45, and as the external refractive index goes beyond 1.45 red shift of resonant band occurs.

105
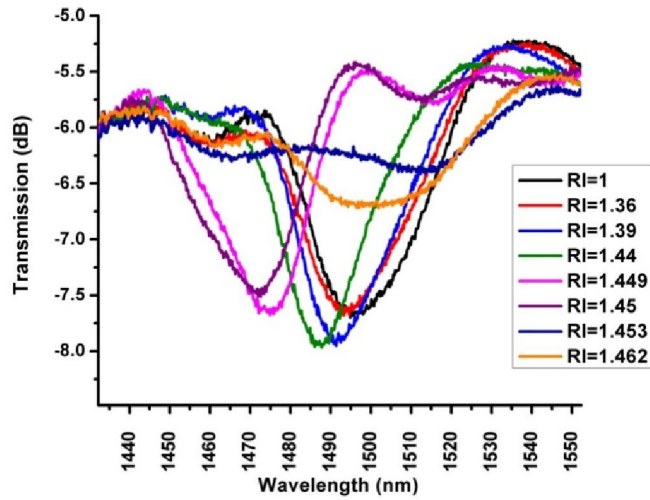
Figure 4.6 Resonance peak of arc induced LPFG for various ambient refractive indices
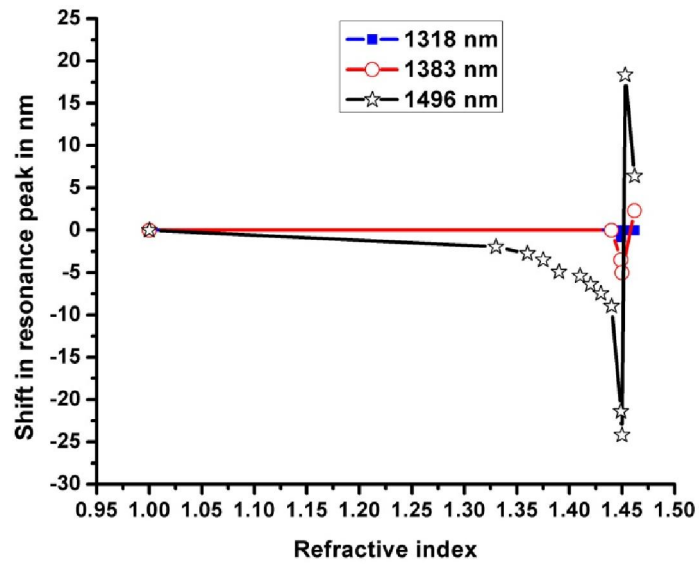
Figure 4.7 Shift in resonance peak for various ambient refractive indices

106
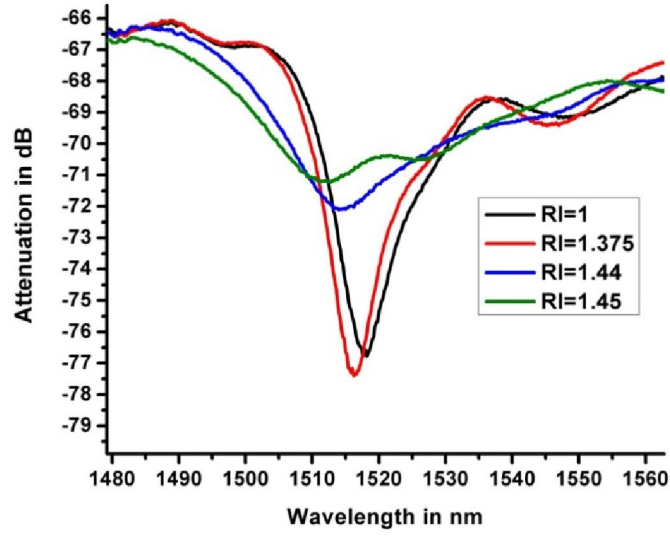
Figure 4.8 Resonance peak of CO_2 LPFG for various ambient refractive indices
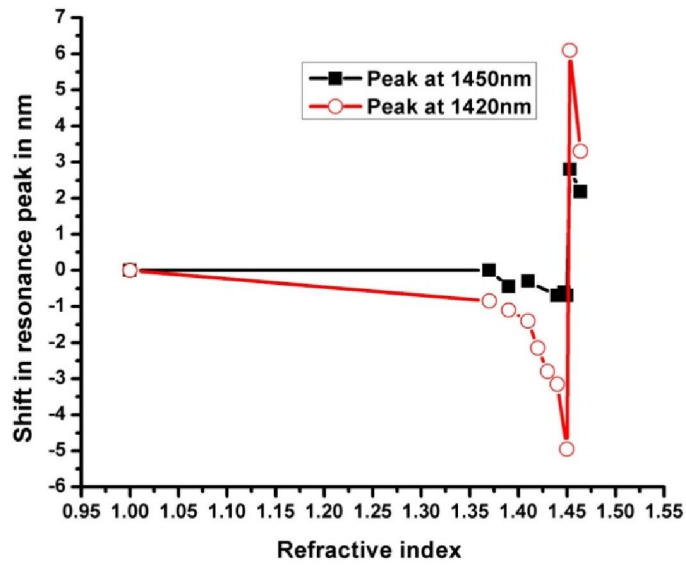
Figure 4.9 Shift in resonance peak for various ambient refractive indices

107

The experiment was repeated for the CO_2 inscribed LPFG and the results obtained are depicted in figure 4.8 and 4.9. While the variation in 1528nm resonance band with various ambient refractive indices is shown in figure 4.8, the shift in resonance bands as a function of ambient refractive index is shown in figure 4.9.

It is known that the higher order modes are highly sensitive to refractive index and the refractive index sensitivities obtained through the derivative of the refractive index response ($d\lambda/dn$) of the three LPFGs are shown in figure 4.10 and 4.11. For the sake of comparison, the sensitivities are considered within two ranges: a low sensitivity range (1 to 1.41), when the sample refractive index is much lower than the cladding refractive index (figure 4.10), and a high sensitivity range (1.43 to 1.45), when the sample refractive index approaches the cladding index (figure 4.11). The calculated sensitivities in these two ranges (total shift in wavelength/ total refractive index change) for all three LPFGs are tabulated in table 4.1. It is obvious that the periodically tapered arc induced LPFG has a slight edge over other LPFGs in the case of refractive index sensitivity in the range 1 to 1.41. In the 1.43 to 1.45 range, the UV fabricated LPFG shows a sensitivity of 1980nm/RIU which is much greater than the other two LPFGs.
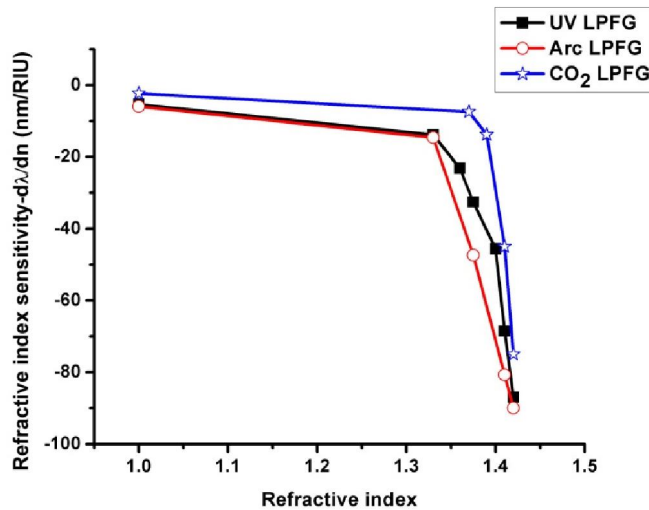
Figure 4.10 Refractive index sensitivities ($d\lambda/dn$) of the LPFGs in the refractive index range 1 to 1.4
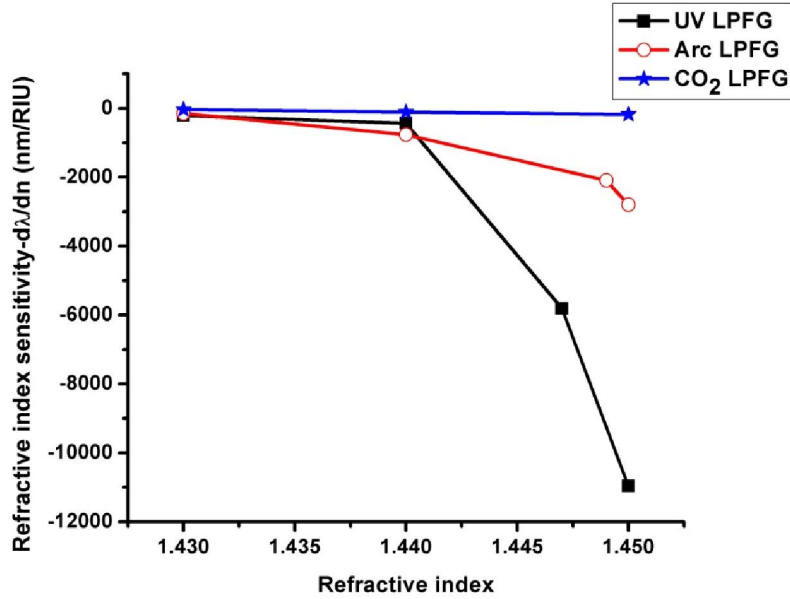
Figure 4.11 Refractive index sensitivities (dλ/dn) of the LPFGs in the
refractive index range 1.43 to 1.45

Table 4.1 Refractive index sensitivities

	1 to 1.41 (nm/RIU)	1.43 to 1.45 (nm/RIU)
UV LPFG	-10.5	-1980
Arc LPFG	-13.4	-837.5
CO_2 LPFG	-3.4	-107.5

4.4 Ethanol concentration in petrol

In order to analyze ethanol blended petrol, samples were prepared
with ethanol percentages of 0, 10, 20, 50, 80 and 100 % in pure petrol.
Experiments were carried out by introducing each set of the samples into the
glass cell (same as the one used for refractive index measurements figure
4.2), in increasing order of ethanol concentration, and performing
consecutive measurements of the LPFG transmission spectrum. After
draining out each sample, the cell was cleaned several times using iso-

propanol. After ensuring the resonance wavelength position of iso-propanol, propanol was drained out and the cell was dried. The refractive index of each sample was measured using an Abbe refractometer just after draining out the sample from the glass cell and in figure 4.12 the refractive indices of the different samples measured with the Abbe refractometer are presented against ethanol concentration.
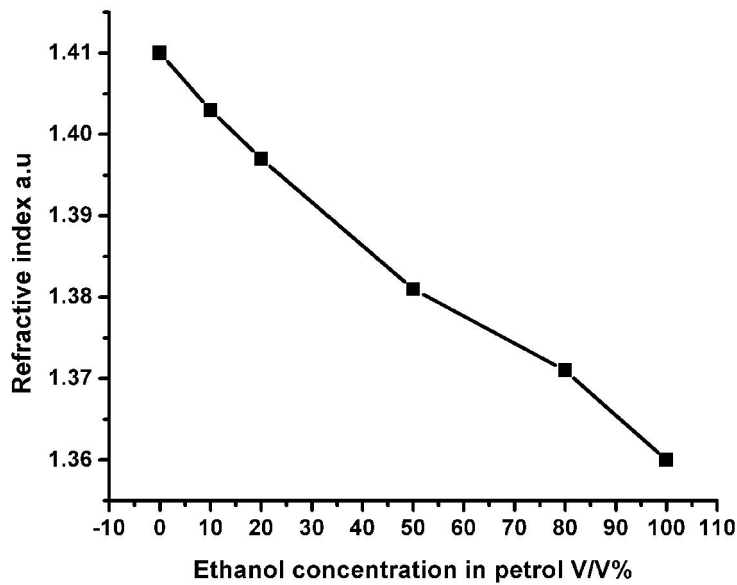
Figure 4.12 Refractive index of ethanol blended petrol as a function of ethanol concentration

The average shift in higher order resonant peak of the LPFGs were determined for each ethanol concentration and is plotted in figure 4.13. From the LPFG response, it is clear that the peak shift is not noticeable up to 10% ethanol concentration in the case of CO_2 and arc induced gratings but appreciable shift in resonance peak is observed as the ethanol concentration varies from 10% to 100% in petrol. Since the mandatory ethanol concentration is in between 10% to 20% the most common adulteration range will be beyond 10% and mixing ethanol beyond 50% is a rare

110

possibility. So if the compulsory ethanol blending is 10%, the most probable adulteration range would be between 10% and 20%, while it will be between 20% and 30% if the blending concentration is 20%. Thus by properly tuning, the fabricated periodically tapered LPFG based transducer system can be effectively used for in-situ monitoring of adulteration in ethanol blended petrol.

Even though the shift in resonance peak is not linear in the entire concentration range of ethanol in petrol, the LPFGs shows measurable shift as the concentration of ethanol is changed from 0% to 100% with good repeatability. The sensitivity of the LPFG sensor for ethanol concentration was calculated by the numerical derivative of the response curve. The calculated sensitivities in the ethanol concentration range 10%-20% and 20% -50% for the three LPFGs are tabulated in table 4.2.
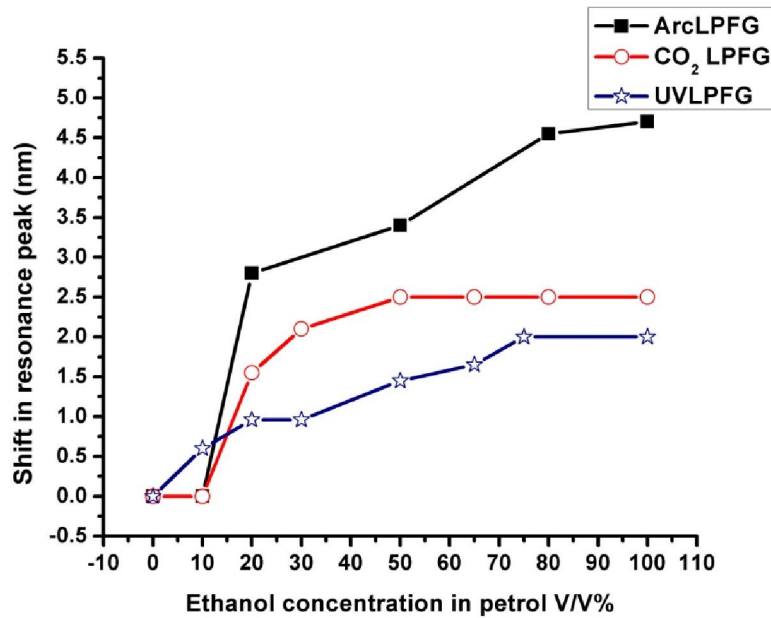
Figure 4.13 Shift in resonance peak as a function of ethanol
concentration in ethanol blended petrol

111

Table 4.2 Sensitivity of LPFGs for ethanol blended petrol

	Sensitivity for ethanol blended petrol in the ethanol volumetric concentration range	
	10%-20%	20%-50%
Arc LPFG	280pm/V%	20pm/V%
CO_2 LPFG	155pm/V%	31pm/V%
UV LPFG	36pm/V%	16pm/V%

From the table it is clear that the periodically tapered arc induced gratings have a better sensitivity in determining ethanol concentration in ethanol blended petrol in the 10% to 20% ethanol range. Possetti et.al.[17] tried the same experiment using normal arc induced LPFG and they got a shift of 1nm for ethanol concentration change from 0% to 40%. The 3nm shift shown by periodically tapered LPFG for the concentration change from 10% -20% is hence better than the normal arc induced grating. Shao et.al [43] have demonstrated the fabrication of periodically tapered long period fiber gratings using resistive filament heating and the method of tapering has proved to increase refractive index sensitivity. Hence the higher sensitivity of periodically tapered arc induced LPFG towards ethanol concentration too can be attributed to tapering.

Conclusions

In this chapter the basic theory related to the refractive index sensitivity of long-period fiber gratings were discussed. Afterwards, the response of the fabricated LPFGs namely UV, electric arc and CO_2 induced long period fiber gratings towards ambient refractive indices were determined. The refractive index sensitivities were evaluated and the LPFGs were successfully utilized for determining the quality of ethanol blended petrol. Besides being insensitive to temperature, the arc induced LPFG have shown better sensitivity among the three LPFGs in determining the purity of ethanol blended petrol. Hence the periodically tapered arc induced LPFG can be successfully utilized as a temperature insensitive transducer for quality evaluation of ethanol blended petrol.

References

1. E. M. Goodger, Hydrocarbon fuels: production, properties and performance of liquids and gases (Wiley, 1975)
2. M. Al-Hasan, "Effect of ethanol–unleaded gasoline blends on engine performance and exhaust emission", Energy Convers. Manag*e., **44**, 1547-1561 (2003)
3. Robert K. Niven, "Ethanol in gasoline: environmental impacts and sustainability review article", Renewable Sustainable Energy Rev. **9**, 535-555 (2005).
4. Wei-Dong Hsieh, Rong-Hong Chen, Tsung-Lin Wu, Ta-Hui Lin, "Engine performance and pollutant emission of an SI engine using ethanol–gasoline blended fuels", Atmos. Environ. **36**, 403–410 (2002)
5. Alan C. Hansen, Qin Zhang and Peter W.L. Lyne, "Ethanol–diesel fuel blends—a review", Bioresour. Technol. **96**, 277–285 (2005)
6. B Culshaw and J Dakin, Optical Fiber Sensors: Systems and Applications, (Artech House, Boston, 1989)
7. D A Krohn, Fiber Optic Sensors: Fundamental and Applications, (Instrument Society of America, Research Triangle Park, North Carolina, 1988).
8. E Udd, Fiber Optic Sensors: An Introduction for Engineers and Scientists, (Wiley, New York, 1991).
9. Francis To So Yu and Shizhuo Yin, Fiber Optic Sensors, (Marcel Dekker, Inc., New York, 2002).
10. B.D.Gupta, Gupta and Banshi Das, Fiber Optic Sensors: Principles and Applications (New India Publishing, New Delhi,2006)
11. G R C Possetti, R C Kamikawachi, C L Prevedello, M Muller and J L Fabris, "Salinity measurement in water environment with a long period grating based interferometer", Meas. Sci. Technol. **20**, 034003(1-6) (2009)
12. Samer K. Abi Kaed Bey , Cathy Chung Chun Lam, Tong Sun and Kenneth T.V. Grattan, "Chloride ion optical sensing using a long period grating pair", Sens. Actuators, A **141**, 390–395 (2008)
13. Patrick H J, Kersey A D and Bucholtz F, "Analysis of the response of long period fiber gratings to external index of refraction ", J. Lightwave Technol. **16,** 1606–1642 (1998)
14. Falciai R, Mignani A G and Vannini, "A Long period gratings as solution concentration sensors", Sens. Actuators, B **74,** 74–77 (2001)
15. R. Falate, R.C. Kamikawachi, M. Muller, H.J. Kalinowski and J.L. Fabris, "Fiber optic sensors for hydrocarbon detection", Sensors and Actuators B, **105,** 430–436 (2005)
16. Rosane Falate, Karen Nike, Pedro Ramos da Costa Neto, Eduardo Cacao Jr., Marcia Muller, Hypolito Jose Kalinowski and Jose Luis Fabris, "Alternative Technique For Biodiesel Quality Control Using An Optical Fiber Longperiod Grating Sensor" , Quim. Nova **30**, 1677-1680 (2007)
17. G R C Possetti, L C Cocco, C I Yamamoto, L V R de Arruda, R Falate, M Muller and J L Fabris, "Application of a long-period fiber grating-based transducer in the fuel industry", Meas. Sci. Technol. **20,** 034012 (1-9) (2009)
18. R. Falate, R. C. Kamikawachi, J. L. Fabris, M. Müller and H. J. Kalinowski, "Fiber Optic Hydrocarbon Sensors Based On Long Period Gratings", Journal of Microwaves and Optoelectronics,. **3**, 47-55 (2004)
19. Gustavo Rafael Collere Possetti, Marcia Muller and Jose Luis Fabris, "Refractometric optical fiber sensor for measurement of ethanol concentration in

ethanol-gasoline blend", (International Microwave & Optoelectronics Conference (IMOC), 2009)

20. Sumat Nanda, Nidhi Sharma and Sukhdev Roy, "Simple and Sensitive Fiber Optic Sensor to Detect Adulteration in Petrol and Diesel", (PHOTONICS-2008: International Conference on Fiber Optics and Photonics, IIT Delhi, India ,2008)

21. Vandana Mishra, Subhash C Jain, Nahar Singh, G C Poddar and Pawan Kapur , "Fuel adulteration detection using long period fiber grating sensor technology", Indian Journal of Pure & Applied Physics, **46,** 106-110 (2008).

22. Xianfeng Chen, Kaiming Zhou, Lin Zhang and Ian Bennion, "Dual-peak long-period fiber gratings with enhanced refractive index sensitivity by finely tailored mode dispersion that uses the light cladding etching technique", Appl. Opt. **46**, 451-455 (2007).

23. Sarfraz Khaliq, Stephen W. James and Ralph P. Tatam, "Fiber-optic liquid-level sensor using a long-period grating", Opt. Lett. **26**, 1224-1226 (2001)

24. Dankers J P, Lenhart J L, Kueh S R, van Zanten J H, Advani S G and Parnas R S, " Fiber optic flow and cure sensing for liquid composite molding", Opt. Lasers Eng. **35,** 91–104 (2001)

25. Kueh S R M, Parnas R S and Advani S G, "A methodology for using long-period gratings and mold-filling simulations to minimize the intrusiveness of flow sensors in liquid composite molding", Compos. Sci. Technol. **62,** 311–327 (2002)

26. Matthew P. DeLisa, Zheng Zhang, Mira Shiloach, Saeed Pilevar, Christopher C. Davis, James S. Sirkis and William E. Bentley, "Evanescent Wave Long-Period Fiber Bragg Grating as an Immobilized Antibody Biosensor", Anal. Chem. **72**, 2895-2900 (2000).

27. Jian Yang, Li Yang, Chang-Qing Xu, Chenglin Xu, Weiping Huang and Yingfu Li, "Long-period grating refractive index sensor with a modified cladding structure for large operational range and high sensitivity", Appl. Opt. **45**, 6142- 6147 (2006)

28. Joo Hin Chong, Ping Shum, H. Haryono, A. Yohana, M.K. Rao, Chao Lu and Yinian Zhu, "Measurements of refractive index sensitivity using long-period grating refractometer", Opt. Commun. **229**, 65–69 (2004)

29. Hou R, Ghassemlooy Z, Hassan A, Lu C and Dowker K P, " Modelling of long-period fiber grating response to refractive index higher than that of cladding", Meas. Sci. Technol. **12,** 1709–1713 (2001)

30. Lee B H, Liu Y, Lee S B, Choi S S and Jang J N, "Displacements of the resonant peaks of a long-period fiber grating induced by a change of ambient refractive index", Opt. Lett. **22,** 1769–1771 (1997)

31. Duhem O, Henninot J-F, WarenghemM and Douay M, " Demonstration of long-period grating efficient couplings with an external medium of a refractive index higher than that of silica", Appl. Opt. **37,** 7223–7228(1998)

32. Shu X and Huang D, "Highly sensitive chemical sensor based on the measurement of the separation of dual resonant peaks in a 100 μm period fiber grating", Opt. Commun. **171,** 65–69 (1999).

33. Allsop T, Zhang L and Bennion I, "Detection of organic aromatic compounds by a long period fiber grating optical sensor with optimised sensitivity", Opt. Commun. **191,** 181–190 (2001)

34. Stephen W James and Ralph P Tatam, "Optical fiber long-period grating sensors: characteristics and application", Meas. Sci. Technol. **14**, R49–R61(2003)

35. Gwandu B A L, Shu X, Allsop T D P, ZhangW, Zhang L and Bennion I, "Simultaneous refractive index and temperature measurement using cascaded long-period grating in double-cladding fiber", Electron. Lett. **38,** 695–696 (2002)

36. A N Vengsarkar, P J Lemaire, J B Judkins, V Bhatia, T Erdogan and J E Sipe, "Long-period fiber gratings as band-rejection filters", J. Lightwave Technol. **14**, 58-65 (1996).
37. X Shu, L Zhang and I Bennion, "Sensitivity characteristics of long-period fiber gratings", J. Lightwave Technol. **20**, 255-266 (2002).
38. V Bhatia, "Applications of long-period gratings to single and multi-parameter sensing", Opt. Express **4**, 457-466(1999).
39. V Bhatia and A M Vengsarkar, "Optical fiber long-period grating sensors", Opt. Lett. **21**, 692-694 (1996).
40. D B Stegall and T Erdogan, "Leaky cladding mode propagation in long-period fibre grating devices", IEEE Photon. Technol. Lett. **11**, 343–345 (1999).
41. R Hou, Z Ghassemlooy, A Hassan, C Lu, and K P Dowker, "Modelling of long-period fiber grating response to refractive index higher than that of cladding", Meas. Sci. Technol. **12**,1709-1713(2001).
42. K S Chiang, Y Liu, M N Ng and X Dong, "Analysis of etched long-period fiber grating and its response to external refractive index", Electron. Lett. **36**, 966-967 (2000).
43. Li-Yang Shao,Jian Zhao, Xinyong Dong, H. Y. Tam, C. Lu and Sailing He, "Long-period prating fabricated by periodically tapering standard single-mode fiber", Appl. Opt. **47**, 1549-1552 (2008)

Fiber optic sensor for determining relative humidity of the environment

5.1 Introduction

Water vapour is a natural component of air and the amount of water vapour in the air is described by the term "humidity." The mass of water vapour in a given volume of air (i.e. density of water vapour in a given volume, usually expressed in grams per cubic meter) is defined as *Absolute humidity* while ratio of the percentage of water vapour present in air at a particular temperature to the maximum amount of water vapour the air can hold at that temperature is called *relative humidity*. It is often expressed as a percentage using the following equation [1]

$$RH = \frac{P_W}{P_{WS}} \times 100\%$$

where P_W is the partial pressure of the water vapour and P_{WS} is the saturation water vapour pressure.

As humidity is a very common, continuously changing component of our environment, the measurement and control of humidity is necessary in a range of areas like air-conditioning, structural health monitoring, horticulture, meteorological services, chemical and food processing industry, paper and textile production, semiconductor manufacturing process etc [1]. The requirements for humidity monitoring may vary according to the application and hence various techniques from the simplest way of exploiting the expansion and contraction of materials such as human hair to the most sophisticated techniques, such as using a miniaturized electronic chip, have been explored over many years to obtain meaningful humidity measurements [1-4].

Generally, humidity sensors can be divided into two major groups namely electronic and optical, those that measure changes in electrical and optical properties of the sensing material upon interaction with moisture. Materials that have been studied for humidity sensing purposes include

polymer, composite and ceramic, each of which has its own merits and specific conditions of application. Since this subject has been studied for some time, excellent reviews can be found in the literature on the principles and preparation techniques of different humidity sensors [1-4].

Electronic humidity sensors are either capacitive or resistive type which works on the electrical properties of the sensing material. Capacitive humidity sensors consist of a substrate on which a thin film of polymer or metal oxide is deposited between two conductive electrodes. The sensing surface is coated with a porous metal electrode to protect it from contamination and exposure to condensation. The incremental change in the dielectric constant of a capacitive humidity sensor is proportional to the relative humidity (RH) of the surrounding environment. Capacitive sensors are characterized by low temperature coefficient, ability to function at high temperatures (up to 200°C), full recovery from condensation, and reasonable resistance to chemical vapours [2-7]. In capacitive type sensors the distance of the sensing element from the signal conditioning circuitry is limited due to the capacitive effect of the connecting cable with respect to the relatively small capacitance changes of the sensor.

Resistive humidity sensors measure the change in electrical impedance of a hygroscopic medium such as a conductive polymer, salt, or treated substrate. Resistive sensors usually consist of noble metal electrodes either deposited on a substrate by photo resist techniques or wire-wound electrodes on a plastic or glass cylinder. The substrate is coated with a salt or conductive polymer. Alternatively, the substrate may be treated with activating chemicals such as acid. The sensor absorbs the water vapour and ionic functional groups are dissociated, resulting in an increase in electrical conductivity. A distinct advantage of resistive RH sensors is their repeatability, which allows the electronic signal conditioning circuitry to be calibrated by a resistor at a fixed RH point. This eliminates the need for humidity calibration standards and hence resistive humidity sensors are generally field replaceable. In residential and commercial environments, the life expectancy of these sensors is greater than 5 years, but exposure to chemical vapours and other contaminants such as oil mist may lead to premature failure. Another drawback of some resistive sensors is their tendency to shift values when exposed to condensation if a water-soluble coating is used. Resistive humidity sensors have significant temperature

117

dependencies when installed in an environment with large (>10°F) temperature fluctuations [2-4,8-10].

The most important specifications to keep in mind when selecting a sensor are accuracy, repeatability, interchangeability, long-term stability, resistance to chemical and physical contaminants, size, packaging, cost effectiveness, field and in-house calibrations, and the complexity and reliability of the signal conditioning and data acquisition (DA) circuitry. Generally electronic sensors are inexpensive and have low power consumption, covering a wide humidity range with good repeatability but suffer from temperature dependency and cross-sensitivities to some chemical species. Their performance is limited owing to their inability to remote and distributed sensing, multiplexing, deployment in harsh environments, and their susceptibility to electromagnetic and radio frequency interference. Fiber optic type sensors can overcome these disadvantages and can be constructed by utilizing the humidity sensitive variation in optical properties of sensor materials. Optical fiber humidity sensors have been already used to facilitate the remote sensing and continuous monitoring of humidity in diverse applications such as the baking and drying of food, cigar storage, civil engineering to detect water ingress in soils or in the concrete in civil structures, medical applications and many other fields [1,11-22]. However, the limitations of the operating range and accuracy of the FO-based humidity sensors are some of the drawbacks which researchers are striving to continue to address.

Various fiber optic sensor techniques based on absorption [16,23,24], fluorescence [25,26], evanescent wave [14,18,21,27-29,30-35], fiber gratings [11-13,36-38] and interferometry [39,40] have been exploited over the years in the design and development of optical fiber RH sensors. Potential materials and chemical reagents like cobalt chloride ($CoCl_2$)[16,23,41,42] , cobalt oxide (Co_3O_4) [43], Rhodamine B [44] , titanium dioxide (TiO_2) [22,33,39,45], tin dioxide (SnO_2) [46], silicon dioxide (SiO_2) [20,47], calcium chloride ($CaCl_2$) [48] etc have been reported based on their humidity-dependent optical absorption properties. Zhou et al. [16] who have demonstrated an in-line absorption-based humidity sensor using a porous optical fiber segment doped with CoCl2. The use of the absorption characteristics of the same compound contained in a variety of materials such as gelatine and cellulose has also been discussed by various authors

[41,42]. Tao et al. [23] have demonstrated an active fiber core optical sensor (AFCOS) for humidity detection using an in-line absorption sensing concept. An air-gap design configuration with Rhodamine B (RB) and hydroxypropyl cellulose (HPC) coated fiber tip was reported by Otsuki et al. [44]. Titanium dioxide, also known as titania (TiO_2) , is the naturally occurring oxide of titanium and has been extensively investigated as a hygrosensitive material for humidity sensing applications. Humidity sensor based on TiO_2 overlay on side-polished fiber is reported by Alvarez-Herrero et.al [33]. Depending on the refractive index value of the overlay, the wavelength of the resonance shifts accordingly to fulfill the phase matching condition. This forms the basis of the sensing scheme and the sensor has shown a linear wavelength shift for 0 to 15%RH, with a sensitivity of 0.5 nm/%RH. A fiber optic humidity sensor with a response time of 5 sec and a dynamic range of 20%RH to 80%RH based on the moisture dependence absorption of light by the phenol red doped polymethylmethacrylate (PMMA) film was reported by Gupta et. al. [18].

The use of long period fiber grating (LPFG) for humidity sensing was first reported by Luo et al. [49] and in their work carboxymethylcellulose (CMC) hydrogel was covalently attached to cladding of a LPFG to form the humidity sensor. A similar LPFG-based humidity sensing scheme was demonstrated by Tan et al. [37] using a gelatine-coated LPFG and Konstantaki et al. [38] proposed a LPFG humidity sensor utilizing polyethylene oxide (PEO)/$CoCl_2$ hybrid overlay as the moisture sensitive coating. An optical fiber humidity sensor based on LPFG coated with a silicon dioxide (SiO_2) nanosphere film was reported by Viegas et.al [20]. Studies by Venugopalan et al. [13,50] have shown the use of polyvinyl alcohol (PVA) film as a sensing material for LPFG-based humidity detection. A long-period fiber grating coated with hydrogel for humidity measurement was developed by LiweiWang et al. [51].

Although various materials are used as humidity sensitive coatings in fiber optic humidity sensors, polymer film based sensors have attracted a great deal of interest due to their inherent advantages. They are compatible with oxides and ceramics, low-cost, flexible, light weight, easily processibile and can be used at room temperatures. In general, polymers provide useful mechanical properties to the sensor design and hygroscopic polymers like Poly-aniline [52,53], PVA [13,17,32,50], Chitosan [54,55],

119

polyethyleneoxide [56], PMMA [18] Polyimide (PI) [57].etc are being used in optical sensors.

Gaston et al. [32] have proposed an evanescent wave type humidity sensor based on a single mode, side-polished fiber with a PVA overlay and got a linear response in the RH range 70% to 90%. The humidity sensitivity of PVA was successfully utilized for the construction of LPFG based humidity sensors [13,50]. The commercial polyimide-recoated FBGs were found to respond linearly over a wide humidity range [57]. The sensor was reported to respond well to a humidity range of 10–90%RH and display good repeatability. Razat Nohria et.al. [52]worked on Humidity sensor based on ultrathin polyaniline film deposited using layer-by-layer nano-assembly. They used layer-by-layer (LbL) nano-assembly for deposition of ultrathin poly(anilinesulfonic acid) (SPANI) films and the change in electrical sheet resistance of the sensing film was monitored as the device was exposed to humidity. In their work on Humidity sensors based on polymer thin films, Sakai et.al. [59] had explained the humidity sensing behaviour of hydrophilic polymers like poly-(2-acrylamido- 2-methylpropane sulfonate) and poly-(2-hydroxy-3-methacryloxypropyi trimethylammonium chloride) impregnated in microporous polyethylene film.. A humidity sensor with nanostructure Co dispersed in polyaniline deposited as a clad, having quick response of 8 s (20–95%RH) and recovery time of 1 min (95–20%RH) was reported [53]. Effect of changes in relative humidity and temperature on ultrathin chitosan films were studied by Murray et al. [54] while Jinesh et al [55] was successful in constructing a fiber optic evanescent wave based humidity sensor using chitosan as the clad and macro bend fiber coated with Poly (ethylene oxide) [56].

Chitosan is a natural polysaccharide formed by alkaline deacetylation of the second most abundant naturally occurring chitin of crab and shrimp shells [60]. Since it is inexpensive, non-toxic and possesses potentially reactive amino functional groups, chitosan has been evaluated for numerous applications, including medicine, food, cosmetics and wastewater treatment [61] and has also showed its potential as hygroscopic coating for fiber optic humidity sensor [54,55]. Though the response of the chitosan coated evanescent wave sensor is linear its humidity sensitivity is found to be poor. Poly (vinyl alcohol) is a non-toxic, water-soluble synthetic polymer that has good film forming ability. It has a large number of hydroxyl groups which

allows it to react with many types of functional groups. This advantage makes it suitable for biocompatible materials and has found use in the fabrication of fiber optic humidity sensors [13,17,32,50]. The PVA coated humidity sensor has shown better sensitivity but the operating range is 50% - 90% RH [32].

The humidity sensitivity of polymers depends on the availability of hydrophilic head groups and their degree of swelling. Developement of membranes with both sensitivity and mechanical strength has been deemed extremely difficult. The mechanical strength of PVA can be enhanced by acetalization. However, the degree of water absorption is considerably lessened along with the increase in mechanical strength. Therefore, it is extremely difficult to obtain polymer membranes which are satisfactory in water sorbtion and mechanical strength. Addition of chitosan to PVA improves hydrophilic head groups along with the improvement in mechanical strength. If the proportion of chitosan is less than 10% , the beneficial effect achievable by addition of chitosan will be significantly reduced. On the other hand if the proportion becomes more than 60%, any additional effects will hardly be obtained. Moreover chitosan will be leached away in an acidic medium if the membrane is higher in its chitosan content. Chitosan/PVA blend has been found to be miscible in all composition and El-Hefian et.al [62] has shown that the blend with 50% PVA has maximum degree of swelling compared with pure polymers.

It is observed that the presence of metal oxide ions increases the humidity sensitivity of hydrophilic polymers. Khijwania et. al. [19] have reported a RH sensor based on U-shaped probe coated with anhydrous $CoCl_2$ and PVA. It has a response time of 1 sec with a sensing range of 1.6% RH to 92% RH. Recently an optical fiber humidity sensor based on TiO_2-nanoparticle doped nanostructured thin film as the fiber sensing cladding was reported by R Aneesh et.al.[22]. Stannic oxide (SnO2) nanoparticles suspended polyvinyl alcohol (PVA) matrix was used for humidity sensing by Hatamie et.al. [63]. Enhancement of the humidity-sensing properties of poly(methyl methacrylate) (PMMA) with the addition of alkali salts (KOH and K_2Co_3) was reported by Su et.al [64]

In this work we have tried to find out the humidity sensing behavior of PVA-chitosan blend by coating the polymer over an exposed core region of a plastic clad silica fiber. The response of the evanescent wave fiber optic

121

humidity sensor thus constructed is presented. Also we have tried to improve the sensitivity and operational range by dispersing TiO_2 in the PVA-chitosan blend. The fabricated sensor exhibits good characteristics, such as sensitivity, range and time response.

5.2 Chitosan and PVA

Chitosan is a biopolymer derived primarily from deacetylation of chitin, found in the shells of crustaceans and insects [60,61,65-67]. Structurally, both chitosan and chitin are linear polymers composed of 2-amino-2-deoxy-(1,4)-β-D-glucopyranose with different degrees of *N*-acetylation, which differentiates them. The molecular structure of chitosan is shown in figure 5.1.
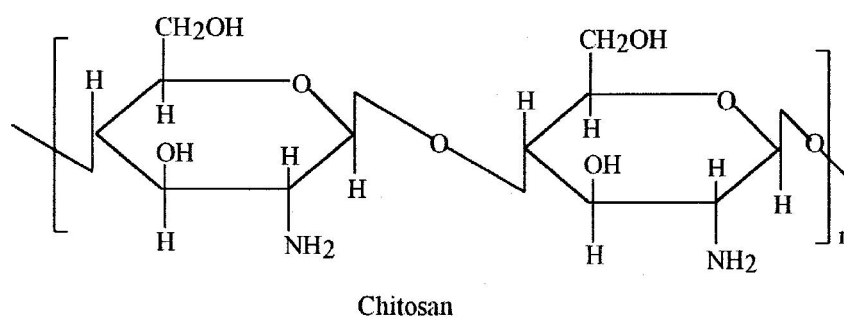
Figure 5.1 Molecular structure of Chitosan

Alkali treatment of chitin replaces the acetyl side group on the chitin repeat units with an amine group, converting them to chitosan. The degree of *N*-acetylation in chitin, is the ratio of 2-acetamido-2-deoxy-D-glucopyranose to 2-amino-2-deoxy-D-glucopyranose structural units. Chitosan is the universally accepted non-toxic *N*-de acetylated derivative of chitin. In chitin, the acetylated units prevail (degree of acetylation typically 0.90). Chitosan is the fully or partially *N*-deacetylated derivative of chitin with a typical degree of acetylation of less than 0.35. Thus the percentage of repeat units with acetyl side groups is specified as the degree of acetylation (DA), with pure chitin corresponding to DA-100% and pure chitosan corresponding to DA-0% [65-67]. The degree of deacetylation (DD) is defined as DD=100-DA. Chitosan is insoluble in water at neutral pH but it can be dissolved in weakly

acidic aqueous solutions and be made into hydrogels. The hydrogel form of chitosan can absorb up to 2000% of its own weight in water. For applications that require mechanical rigidity and improved stability with respect to changes in relative humidity, it is preferable to convert chitosan to chitin, and this is typically accomplished by exposing the chitosan to acetic anhydride. Unfortunately, the toxic nature of acetic anhydride makes the chemical conversion of chitosan to chitin environmentally unfriendly.

To improve mechanical properties and pursue the wider utilities of chitosan, poly(vinyl alcohol) (PVA) is mixed with chitosan which cause an increase in the Young's modulus [68].

Poly (vinyl alcohol) (PVA) is a nontoxic, watersoluble, biocompatible, and biodegradable synthetic polymer, which is widely used in biochemical and biomedical applications [69]. PVA is a hydrophilic and good fiber-forming polymer which adsorbs moisture from the environment [32]. The molecular structure of PVA is shown in figure 5.2.

$(CH_2 \ CHOH)_n$
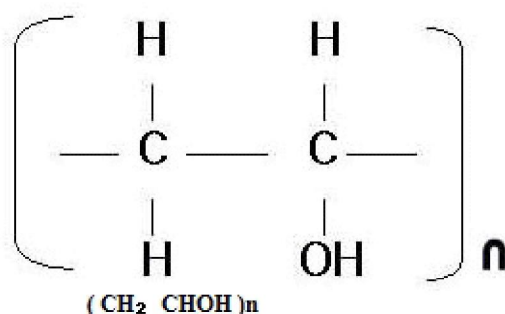
Figure 5.2 Molecular structure of poly vinyl alcohol (PVA)

Blends of chitosan and poly vinyl alcohol (PVA) with good miscibility have been reported to provide good mechanical properties and have biomedical applications [68,70,71].The schematic of intermolecular and intramolecular hydrogen bonds that occurred after blending PVA with chitosan is shown in figure 5.3
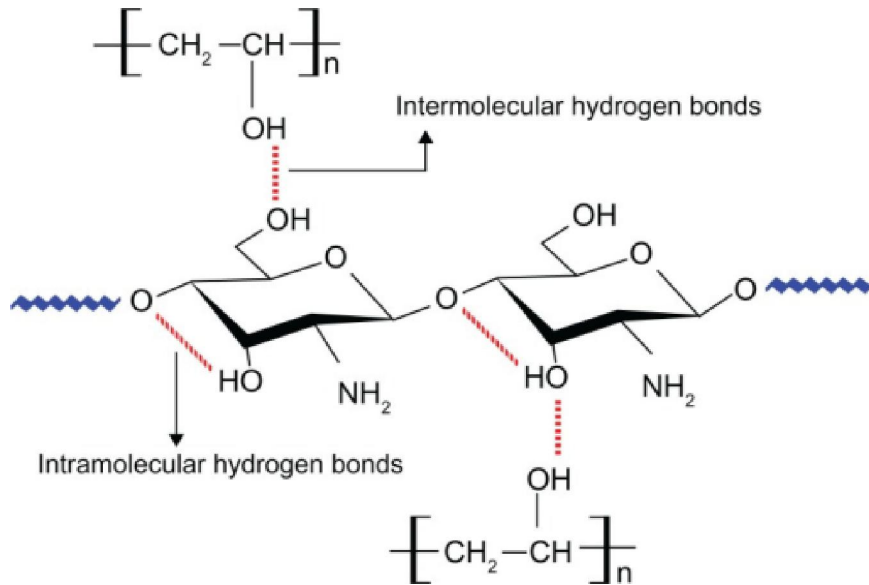
Figure 5.3 Molecular structure of chitosan/PVA blend

5.3 Experimental

The fiber used for the sensor element fabrication is a multimode, step index, plastic clad silica fiber of core diameter 400 μm with a numerical aperture of 0.37. In order to have efficient light coupling from the source to the fiber and the fiber to the detector, fiber ends were prepared properly to get optically flat end faces, perpendicular to the axis of the fiber. The ends of the fibers are wet polished with 600-grain sandpaper and alumina powder to maximize the optical power coupling to the fiber probe. Since evanescent wave is to be used, 5 cm length of the cladding was removed from the central portion of the fiber.

Since the optic fiber is immune to the relative humidity, a moisture sensitive polymer need to be coated onto the fiber as a transducer material to convert the chemical relative humidity into a physical phenomena which the fiber can sense. PVA and chitosan are two polymers whose refractive index is found to be dependant on the amount of water trapped in the polymer matrix.

The degree of swelling for pure chitosan and pure PVA films are 89% and 674% respectively while that of the chitosan/PVA blended films

ranges from 1047% to 2117% [62]. This is because PVA is a water-soluble polymer and the blending of chitosan with PVA tends to increase the water intake due to the increasing of hydrophilic groups (-OH) in the blends. Also, the PVA chains are physically entangled with the chitosan chains leading to the formation of a hydrogel network [62,71]. Thus the chitosan/PVA blend is a better transducer for humidity than pure polymers and it is shown that the blend containing 50% each of chitosan and PVA has the highest degree of swelling. So in this work we have used a blend polymer film containing equal concentration of chitosan and PVA.
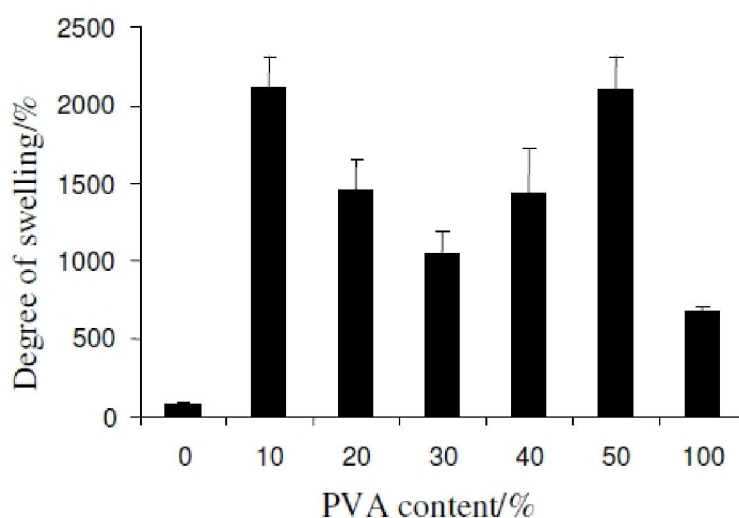
Figure 5.4 Degree of swelling for chitosan PVA blend, reproduced from [62]

Chitosan with a degree of deacetylation (DD) of 96% was purchased from a commercial source. PVA with an average molecular weight of 195 x 103 g mol-1 was also used in this work. Distilled water was used to prepare all solutions. All chemicals were used without further purification and freshly prepared solutions were used in all experiments.

A 10 gm L^{-1} solution of chitosan was prepared by dissolving 5 gm of chitosan in 500 mL acetic acid (0.1 M) followed by stirring and heating at 40°C for 6 hours. A similar 10 gmL^{-1} solution of PVA was prepared by dissolving 5 gm of PVA in 500 mL of preheated ultra pure water. The solution was then stirred and kept at about 60°C for 2 hours. The aqueous PVA solution was added drop by drop to the chitosan solution, under continuous stirring at around 60°C and stirring was allowed to continue for

30 min after mixing. Proper amount of amorphous TiO_2 powder is then incorporated into this chitosan/PVA matrix and stirred continuously for 30 minutes to form the polymer composite. Air bubbles were eliminated by keeping the solutions at room temperature for two hours and figure 5.5 shows the entire process as a flow chart.

```
┌─────────────────────────────────┐
│  Dissolving chitosan in acetic acid │
└─────────────────────────────────┘
                 ⇓
┌─────────────────────────────────┐
│     Dissolving PVA in water       │
└─────────────────────────────────┘
                 ⇓
┌─────────────────────────────────┐
│  Mixing chitosan and PVA solution │
└─────────────────────────────────┘
                 ⇓
┌─────────────────────────────────┐
│        Dissolving TiO₂ in          │
│      chitosan/PVA solution         │
└─────────────────────────────────┘
                 ⇓
┌─────────────────────────────────┐
│   Removing cladding of PCS fiber  │
└─────────────────────────────────┘
                 ⇓
┌─────────────────────────────────┐
│   Dipcoating the unclad region of │
│      PCS fiber with the prepared   │
│         polymer composite          │
└─────────────────────────────────┘
```
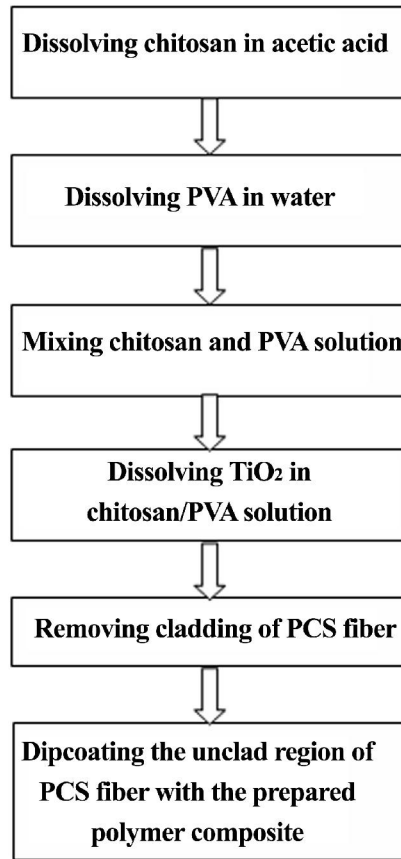
Figure 5.5 The fabrication of fiber probe

Before coating with the sensing material, the fiber needed to be caliberated and hence the fiber behavior towards exterior refractive index change was gathered. The fiber was fixed straight and a diode laser output was coupled to one end while the other end was connected to a power meter. The power meter was interfaced with a computer to record time varying output. Different oils and ethylene-glycol-water mixtures were used as mediums to

126

vary the refractive index around the decladded region of the fiber. An Abbe refractometer was used to measure the refractive index of the prepared solutions. The output power was recorded by embedding the decladded region with the prepared liquids. After taking the reading for first liquid the recording was stopped. The decladded region was cleaned using iso-propanol and then the reading was continued with second liquid. The outputs were recorded for all the prepared refractive index samples. The out put was converted in to dB scale and is shown in figure 5.6. Figure 5.7 depicts the optical power loss in decibels versus the refractive index of the medium around the fiber.
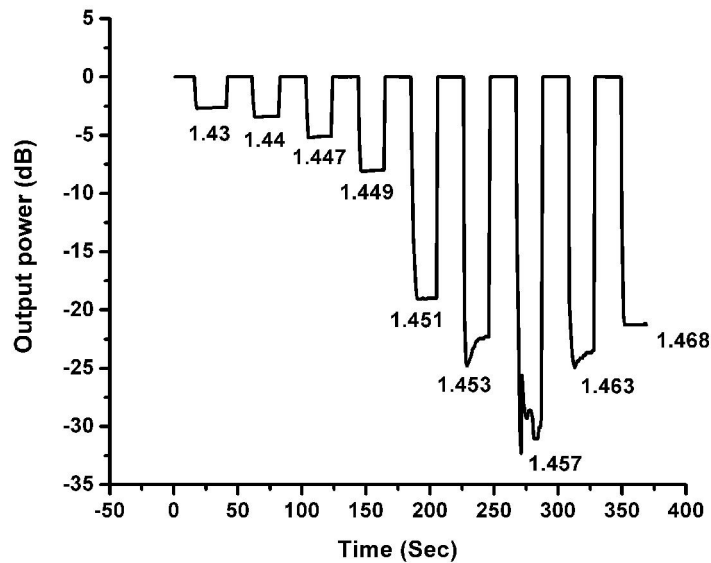
Figure 5.6 Loss in coupled power for various ambient refractive indices

Once the characterization of the prepared fiber was done, it was considered ready for the next step in sensor fabrication viz the deposition of a suitable polymeric layer. The dip coating method was used to deposit the TiO_2 immobilized polymer film onto the bare fiber core. The decladded fibers are dipped in the prepared polymer solutions and pulled out at a constant speed using computer controlled set-up. The probes were then dried at room temperature for two days and were thoroughly washed with NaOH solution

127

and water. After drying, good homogeneous films firmly adhered to the fiber were obtained.
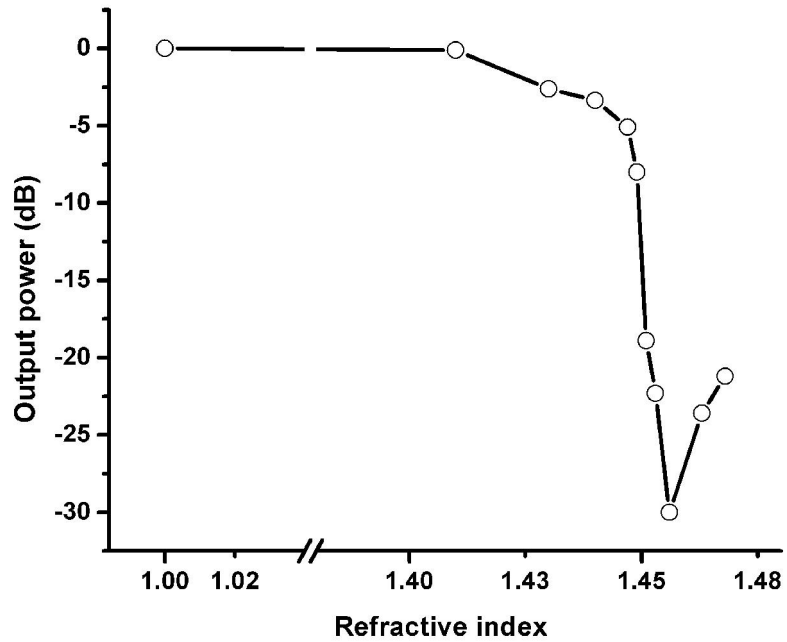
Figure 5.7 Fiber output as a function of ambient refractive index
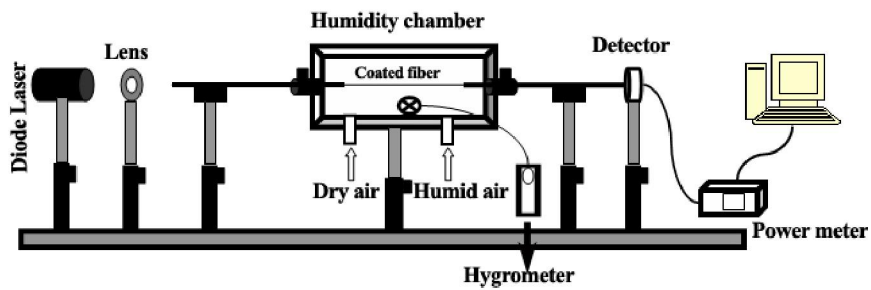
Figure 5.8 Experimental setup to determine humidity sensitivity

This polymer composite coated probe was then fixed in an in-house-made plexi-glass humidity chamber in such a way that the sensing region was in the middle of the chamber. The chamber had provisions for passing the dry and moist air into it. A commercial moisture sensor was used for calibration and its sensor head was fixed inside the chamber. The schematic diagram of the experimental setup for humidity measurement is shown in Figure. 5.8. In order to change the humidity inside the chamber to different levels, an aerator was used to pump air into the chamber via ethylene glycol (dry air) or water (humid air). Air bubbled through water will create a humid environment in the chamber while dehumidification is achieved by passing air through ethylene glycol. One end of the fiber was coupled to a diode laser operating at 632.8 nm while the other end was coupled to a low power silicon photo detector (Newport 818-IR). Outputs of the power meter (Newport, Model 1815C) were monitored in a real time using a computer based data acquisition system developed using Lab View. A constant temperature of 25 °C was maintained throughout the experimental investigations for all sensing probes.

5.3 Theory

We have used polymers as humidity sensitive transducer for which refractive index varies upon adsorption of water molecules. The amount of water molecules adsorbed is proportional to its concentration and hence the refractive index change is proportional to ambient humidity of the surrounding volume.

Thus the moisture mass in unit volume of the polymer, C_m is proportional to ambient humidity H,

$$C_m = S.H \tag{5.1}$$

where S is the moisture solubility of the polymer.

The variation in the refractive index (n) of these swelling polymers with respect to humidity (H) is given by [72]

$$\frac{\delta n}{\delta H} = \frac{\left(n^2 + 2\right)^2}{6n} k_m S\left(1 - \frac{f}{f_c}\right) \tag{5.2}$$

where k_m is the molar refraction divided by the molecular weight of water, S is the moisture solubility of the polymer, parameter f ($0<f<1$) is the fraction of the absorbed moisture that contributes to an increase in polymer volume.

129

In the case of f=0, the polymer exhibits no change in its volume as it sorbs moisture. On the other hand, in the case of f=1, the volume of the polymer increases by the same amount as that of the sorbed moisture. f_c is a critical value which defines the variation in refractive index. when f<f_c , the refractive index, n increases as H increases, while n decreases as H increases when f>f c . If n_p is the refractive index of the polymer without any moisture and ρ_m density of water f_c is defined by the relation [72]

$$f_c = k_m \rho_m \frac{n_p^2 + 2}{n_p^2 - 1} \qquad (5.3)$$

When light propagates in an optical fiber, a fraction of the radiation extends a short distance from the guiding region into the medium of lower refractive index that surrounds it. This is the evanescent field and the evanescent energy may interact with analytes that attenuate it by means of refractive index changes, absorption or scattering.

The output power (*P*out) of the optical fiber sensor head with respect to the refractive index (*n*) of sensing layer is given by [73,74]

$$P_{out} = P_{in} \frac{n_1^2 - n^2}{n_1^2 - n_2^2} \qquad (5.4)$$

where n_1 is the refractive index of the core, n_2 is the refractive index of the cladding, P_{in} represents the total power injected into the guided modes of the fiber from the source. It is evident from this equation that power coupled to the fiber after the sensing region decreases linearly with the increase in n^2.

The amplitude *E(x)* of the evanescent field decreases exponentially with the distance *x* from the core–cladding interface according to the equation

$$E(x) = E_0 e^{-x/d_p} \qquad (5.5)$$

where *d*p is the penetration depth.

The penetration depth describes the distance from the interface where the intensity of the evanescent field has decreased to 1/e of the initial intensity E_0.

The magnitude of the penetration depth is given by [73,74]

$$d_p = \frac{\lambda}{2\pi n_1 \left[\sin^2 \theta - \left(\dfrac{n_2}{n_1} \right)^2 \right]^{\frac{1}{2}}} \tag{5.6}$$

where λ is the vacuum wavelength, θ is the angle of incidence and $n1$, $n2$ are the refractive index values of the core and the cladding, respectively. From equation 5.6 it is clear that the penetration depth dp increases with the cladding refractive index, indicating an increase in the magnitude of the electric field present in the cladding medium and thus a reduction in the electric field within the core.

The normalized frequency (fiber V-parameter) is given by [73,74]

$$V = \frac{2\pi a}{\lambda} \sqrt{n_1^2 - n_2^2} \tag{5.7}$$

where a is the core radius.

This equation shows that the V-parameter decreases when the cladding refractive index increases. Since the number of modes N propagating within the fiber is proportional to the square of the normalized frequency, it can be inferred that increasing the refractive index of the cladding reduces the number of modes propagating within the fiber.

5.4 Results and Discussion

Humidity response of PVA was studied by Gaston et al. [32] and he did his experiments using a side polished fiber coated with PVA. It was explained that PVA has a refractive index of 1.53 which is higher than that of the fiber cladding. Upon increase in humidity, the refractive index of PVA starts to decrease and hence the output decreases first and once the refractive index drops below that of cladding, the output starts to increase. A similar type of response (i.e. decrease in refractive index with respect to increase in humidity) is observed by Venugopal [13] by coating PVA over an LPFG. Chitosan as a humidity sensitive polymer for fiber optic sensors was studied by Jinesh et. al [55]. It was observed that upon increase in humidity the coupled power increases.

We have evaluated the response of Chitosan/PVA composite layer as a function of change in relative humidity. The polymer coated fiber probe was placed in the humidity chamber and the humidity level inside the

chamber was brought down to 45% RH by bubbling air through ethylene glycol. We were not able to bring the relative humidity below 45% due to the limitation of our setup. A constant temperature of 25 °C was maintained throughout the experimental investigations for all sensing probes. Afterwards the humidity was slowly increased to the maximum possible value by bubbling air through water and the output power was recorded using a PC at fixed time intervals of 1 sec. The result thus obtained is depicted in figure 5.9
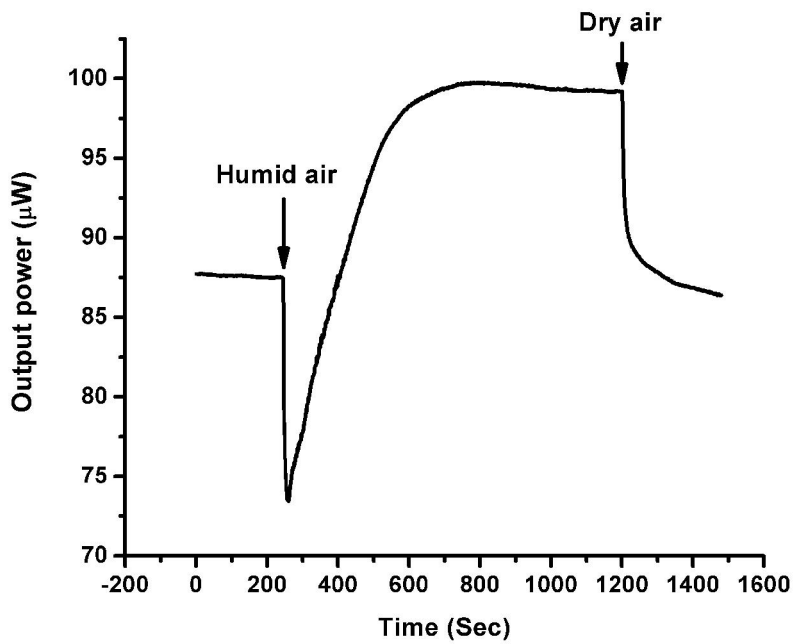
Figure 5.9. Response of PVA-chitosan blend as a function of relative humidity

As can be observed from this result, initially fiber output decreases as the humidity increases within the chamber. On further increase in humidity, the output starts to raise and reach a saturation level. On the introduction of dry air, it is evident from the graph that the output power drops along with humidity. At 45% RH, the optical output reaches the same value as before

but it can be observed that the reverse response is different from the forward path. The dip observed during the forward path is abscent in the reverse path.

To check whether the initial drop in output power is due to optical absorption, we measured the absorption characteristics of the film. The polymer blend was coated on a glass slide and using an absorption spectrometer we took the absorption spectrum of the film. The glass slide was then kept in a humid environment and repeated the absorption measurement. The result obtained is depicted in figure 5.10 and is obvious that the trapping of water molecules in the polymer matrix has very little effect on optical absorption.

It has been shown that the blend contains 50% each of chitosan and PVA has the highest degree of swelling on adsorption of water molecules [62]. This volume expansion of the polymer, when exposed to humidity, induces a strain effect on the fiber. Since the strain sensitivity of a bare fiber is very small, this cannot be a reason for the drop in intensity.
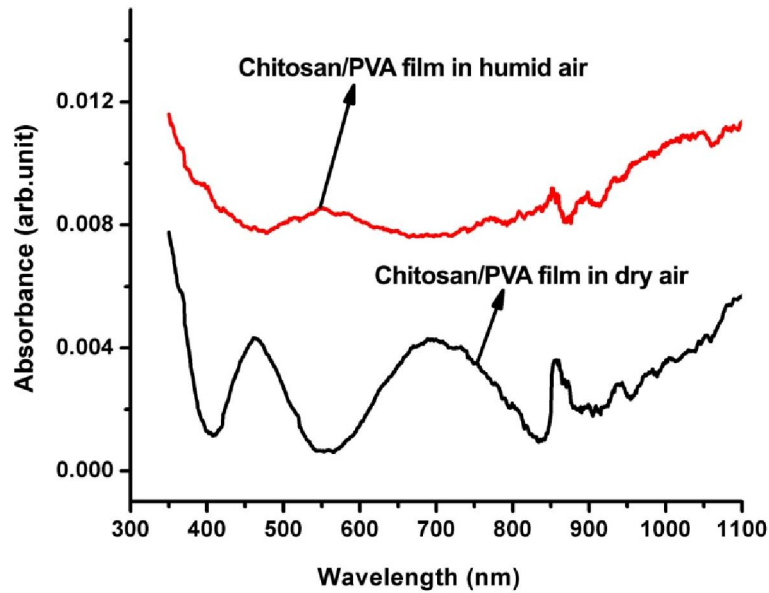
Figure 5.10 . Absorption spectrum of PVA-chitosan blend film in dry
state and upon adsorption of water

The evanescent type fiber optic sensors have been extensively studied and the transmitted optical power depends on the refractive index of the material in contact with the decladded region. The general shape of this variation is similar to the one shown in Figure. 5.7 for the fiber sample used in the experiments. It is evident that the maximum change in output occurs when the external refractive index varies between 1.4 and 1.5. Minimum transmittance occurs when the external refractive index matches the value of the fiber core, a situation in which the guiding conditions are lost.

Under dry conditions the polymer chains tend to curl up into a compact, coil form. On the other hand, at high humidity, polymer adsorbs water molecules and gets hydrated uncurling of the compact, coil form into straight chains that are aligned with respect to one another. This in turn contributes towards the change in refractive index. Watanabe et.al [72] did studies on humidity dependence of the refractive index of polymethylmethacylate (PMMA) and found that the refractive index of PMMA increases as humidity increases at room temperature, while it decreases as humidity increases at temperatures higher than 60 °C. As mentioned in equation 5.2 and 5.3, if the f parameter of the polymer is less than f_c , the refractive index, n increases with increase in humidity (RH), while n decreases as RH increases when f>f c. It has been shown by Gaston et.al[32] and Venugopalan et al [13] that the refractive index of PVA decreases with the increase in ambient humidity, which means it has the f parameter greater than fc. A higher value of f indicates a larger volume increase. Since the degree of swelling of PVA-chitosan blend is much higher than that of pure PVA [62], it can be deduced that the f parameter of PVA-chitosan blend is greater than fc and hence its refractive index decreases with increase in humidity.

Refractive index of chitosan/PVA blended film is around 1.5 [71] in its dry state and hence the fiber coated with the film acts as a lossy medium. As humidity increase water molecules diffuse into the polymer matrix and get adsorbed in the pores. This causes a reduction in refractive index and hence the output decreases till the refractive index reaches that of the core. It is evident from figure 5.4 that a further decrease in polymer refractive index increases the output. Since the response of chitosan/PVA blend is not linear for humidity variation, it cannot be effectively used for humidity sensor.

134

Titanium Dioxide itself is a hygrosensitive material and has been used by many authors in different ways as humidity sensors. We tried to evaluate the effect of TiO_2 on the humidity sensitivity of polymers like PVA and PVA-Chitosan blend.

The titanium dioxide (TiO_2) embedded PVA film was then estimated for its humidity response in a similar way mentioned earlier. The response thus obtained for a titanium dioxide concentration of 1g/L in PVA is shown in figure 5.11.
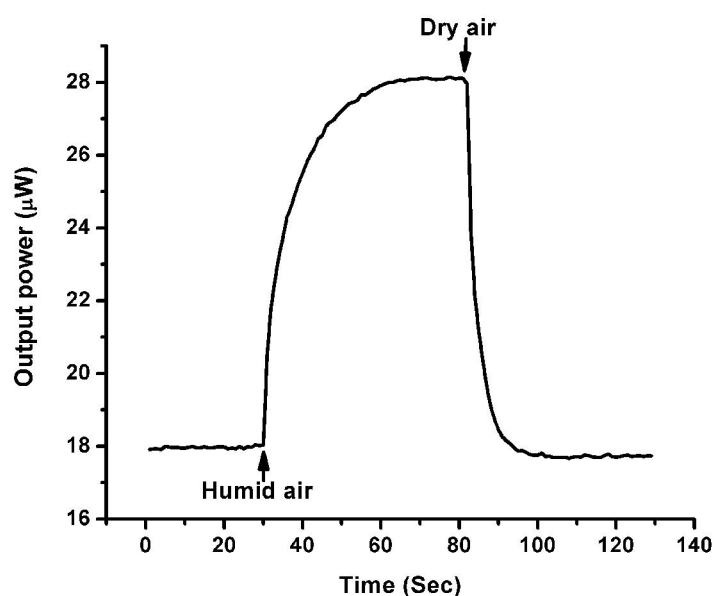
Figure 5.11. Response of TiO_2- PVA composite film as a function of relative humidity

Unlike in the case of pure chitosan-PVA film, the output starts to increase with the introduction of humid air. The coupled power increases till the ambient humidity reach saturation and on the introduction of dry air the output drops and reaches the initial value.

As we did before, the absorption spectrum of the TiO_2 embedded PVA film was taken in its dry state and after keeping it in humid environment. The result obtained is shown in figure 5.12. It is evident that absorption is

135

meager for 632 nm (wavelength of the laser used) and hence it can be concluded that the variation in output is due to change in refractive index.
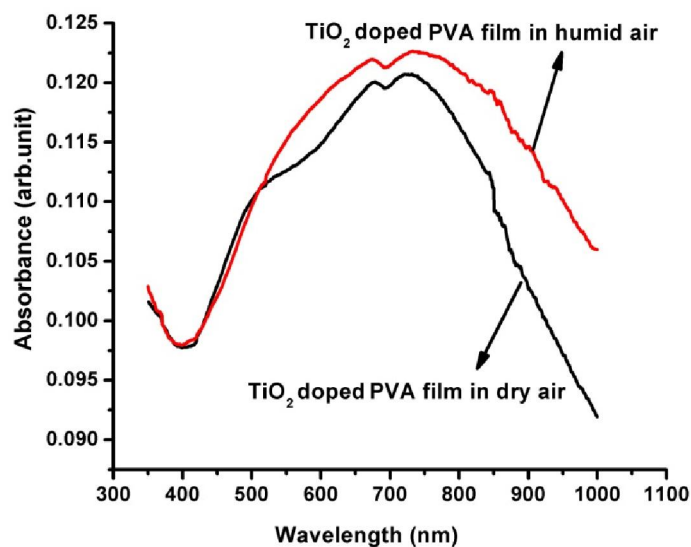
Figure 5.12 Absorption spectrum of TiO_2- PVA composite film in dry state and upon adsorption of water

The humidity response of TiO_2 embedded chitosan/PVA film was then evaluated. Titanium dioxide powder was added to chitosan/PVA mix containing 50% each of chitosan and PVA to produce film with 1 gm/L TiO_2 concentration. Humidity inside the chamber was recorded using a commercial hygrometer, and the fiber output corresponding to a particular value of RH% was noted manually. Humid air was pumped into the chamber for a short interval and humidity was allowed to stabilize to a specific value. The process is continued till the humidity reached 95% and then dry air was blown at various steps to reduce humidity. During this process the power output from the coated fiber probe was recorded continuously and is reproduced in figure 5.13 while the sensor output as a function of relative humidity is shown in figure 5.14. It is clear from the graph that the sensor response is linear and reversible in the range 50% to 95% RH with a

sensitivity of 0.1 μW/%RH. We were not able to record the response below 48% RH due to technical hurdles.
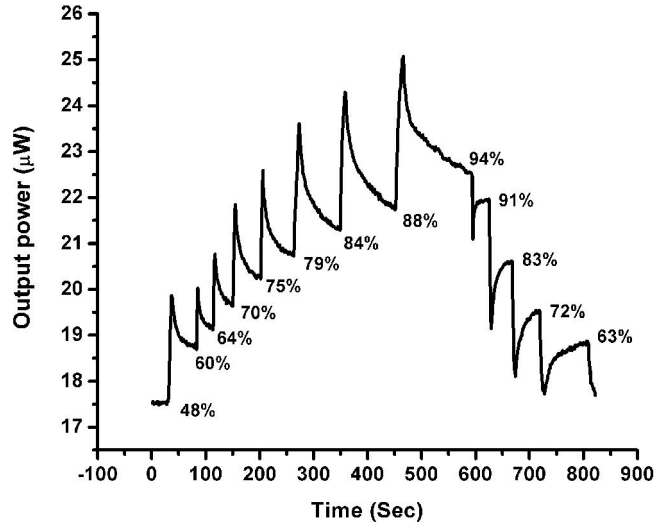
Figure 5.13 Output power of TiO_2- PVA-chitosan composite film for different ambient humidity
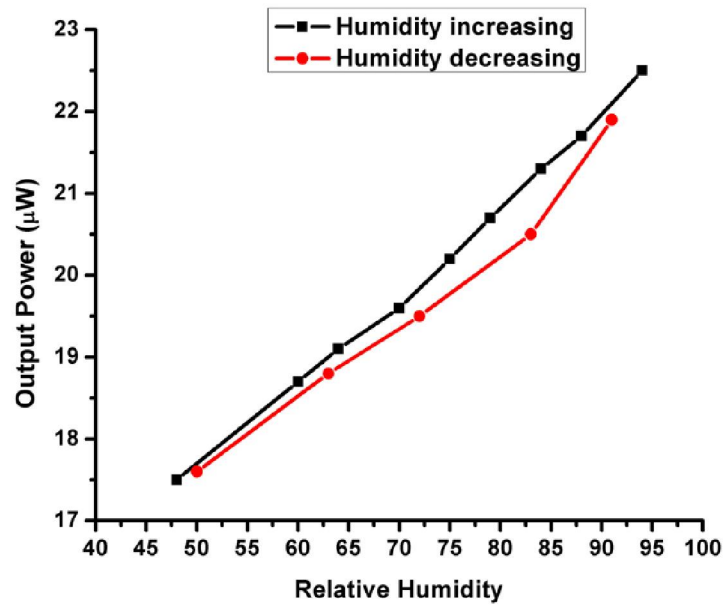
Figure 5.14 Output power of TiO_2- PVA-chitosan composite film as a function of relative humidity

137

The effect of titanium dioxide on the humidity sensitivity of PVA and Chitosan/PVA blend is compared. The polymer coated fibers were fixed in the chamber. After bringing down the humidity of chamber to 45%, humid air was pumbed. The variation in output was recorded and Figure 5.15 shows the comparison of humidity response of TiO_2 -Chitosan/PVA composite with that of TiO_2-PVA composite for a TiO_2 concentration of 1 gm/L. It is evident that, with equal concentration of TiO_2, the PVA-Chitosan blend film shows better sensitivity than TiO_2 embedded pure PVA film. The fiber output as a function of relative humidity for the two probes is presented in figure 5.16.
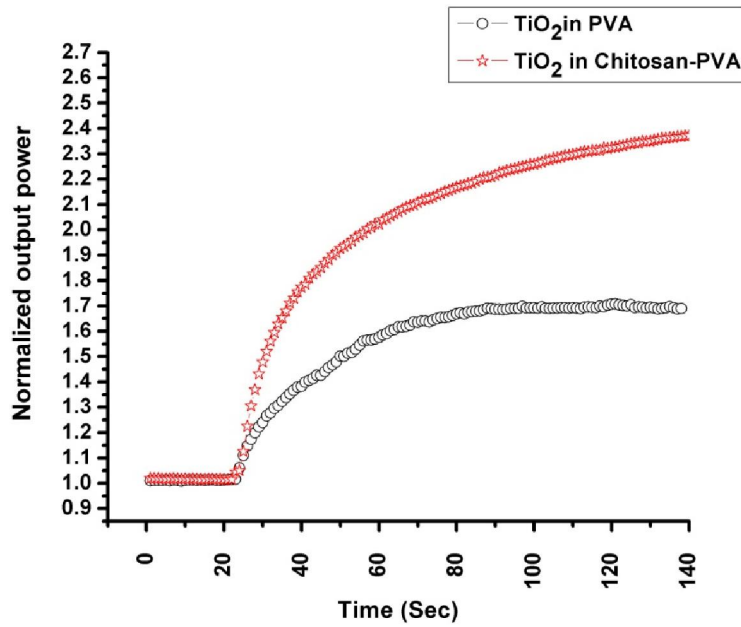
Figure 5.15 Response of TiO_2- PVA composite film and TiO_2-chitosan/PVA composite film as a function of relative humidity
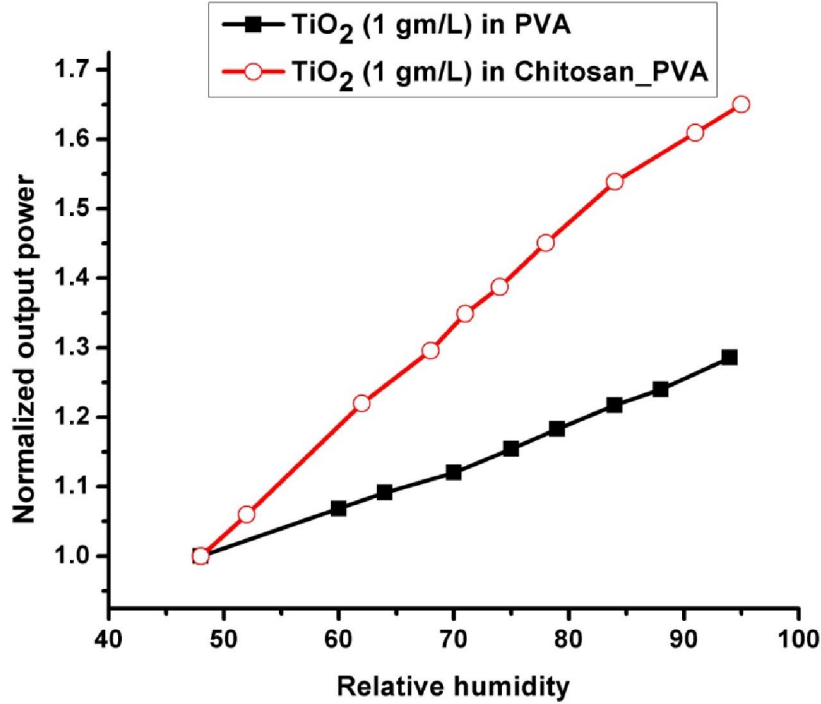
Figure 5.16 Fiber output as a function of relative humidity for TiO_2- PVA composite film and TiO_2- chitosan/PVA composite film

It is obvious that the initial drop in intensity observed in the case of pure PVA-chitosan blend is absent in the case of TiO_2-PVA-chitosan composite. The addition of TiO_2 might have reduced the refractive index of the polymer composite below that of the fiber cladding. From the characterization response shown in figure 5.7, it is obvious that if the coating refractive index is less than that of cladding the output increases linearly with decrease in coating refractive index.

Shadie Hatamie [63] et al. have carried out studies on Stannic oxide (SnO_2) nanoparticles suspended in polyvinyl alcohol (PVA) matrix and have shown that the bonds of PVA does not alter after the formation of the composite film. Thus in the case of titanium dioxide polymer composites too, it can be assumed that the film formed was merely by embedding the TiO_2 particles in the polymer matrix, homogeneously. The TiO_2 particles are attached to the polymer chain by weak Vander Waal's force of attraction.

The presence of the titanium dioxide molecules in the polymer matrix thus increases hydrophilic head groups and hence stimulates the rate of adsorption. Figure 5.17 shows the output power for TiO_2 embedded chitosan/PVA film for titanium dioxide concentrations of 1 gm/L and 0.1 gm/L. It is obvious that the polymer with higher titanium dioxide concentration shows a better sensitivity.
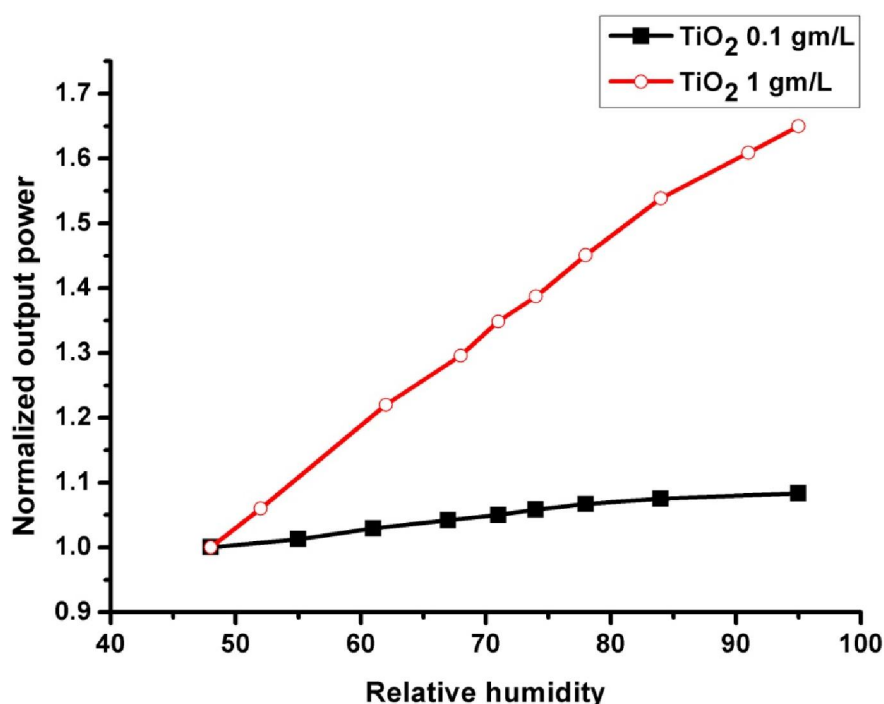
Figure 5.17 Fiber output as a function of relative humidity for TiO_2- PVA-chitosan composite film for different concentrations of TiO_2

The higher sensitivity of TiO_2 embedded chitosan/PVA blend film can be attributed to the fact that the chitosan addition to PVA increases hydrophilic head groups available per unit volume of the polymer. It is clear that the Chitosan/PVA blend film absorbs more water than pure PVA film and thus increases the sorption capacity of the film. Titanium dioxide too is hydrophilic and its addition to the polymer also helps in the enhancement of available hydrophilic head groups per unit volume. This enhancement in

140

hydrophilic heads helps in adsorbtion of more water molecules which in turn causes a larger shift in refractive index and hence more output.

Conclusions

The design and fabrication of fiber optic humidity sensors using polymers like poly vinyl alcohol and chitosan blended poly vinyl alcohol as hygrosensitive coatings are discussed. The hygroscopic properties of PVA, chitosan and TiO_2 are discussed elaborately and the preparation and characterization of polymer and fiber probes are explained. Both PVA and chitosan/PVA blend are sensitive to humidity and their refractive index is found to decreases with increase in ambient humidity. Blending of PVA in chitosan helps to improve its mechanical strength and the available hydrophilic head groups per unit volume. Though found sensitive to humidity, the humidity response of the chitosan/PVA blend is not linear. Addition of titanium dioxide to the polymer produces a linear output variation for change in humidity. The TiO_2 particles added to the polymer does not alter the bonds and are attached to the polymer chain by weak Vander Waal's force of attraction. Blending of titanium dioxide increases hydrophilic heads and increases humidity sensitivity. TiO_2 embedded Chitosan/PVA blend gives better humidity sensitivity than TiO_2 embedded pure PVA. The humidity sensitivity is found to increase with increase in TiO_2 concentration.

References

1. T.L. Yeo , T. Sun and K.T.V. Grattan, "Fiber-optic sensor technologies for humidity and moisture measurement", Sens. Actuators, A **144**, 280–295(2008)
2. Z.M. Rittersma, "Recent achievements in miniaturised humidity sensors-a review of transduction techniques", Sens. Actuators, A **96**, 196-210, (2002)
3. Zhi Chen and Chi Lu, "Humidity Sensors: A Review of Materials and Mechanisms", Sens. Lett. **3**, 274–295 (2005)
4. Noboru Yamazoe and Yasuhiro Shimizu, "Humidity sensors: Principles and applications", Sens. Actuators **10**, 379 – 398 (1986)
5. Celine Laville and Claude Pellet, "Comparison of Three Humidity Sensors for a Pulmonary Function Diagnosis Microsystem", IEEE Sens. J. **2**, 96-101 (2002).
6. M. Matsuguchi, S. Umeda, Y. Sadaoka and Y. Sakai, "Characterization of polymers for a capacitive-type humidity sensor based on water sorption behavior", Sens. Actuators, B **49**, 179–185 (1998)
7. Wenmin Qu , Jorg-Uwe Meyer, "A novel thick-film ceramic humidity sensor", Sens. Actuators, B **40**, I75-I82 (1997)

8. Weon-Pil Taia and Jae-Hee Oh, "Fabrication and humidity sensing properties of nanostructured TiO_2-SnO_2 thin films", Sens. Actuators, B **85**, 154-157 (2002)

9. Qin Kuang, Changshi Lao, Zhong Lin Wang, Zhaoxiong Xie, and Lansun Zheng, "High-Sensitivity Humidity Sensor Based on a Single SnO2 Nanowire", J. Am. Chem. Soc. **129**, 6070-6071 (2007).

10. Kan-Sen Chou, Tzy-Kuang Lee and Feng-Jiin Liu, "Sensing mechanism of a porous ceramic as humidity sensor", Sens. Actuators, B **56**, 106–111 (1999).

11. F.J. Arregui, I.R. Matıas, K.L. Cooper and R.O. Claus, "Simultaneous measurement of humidity and temperature by combining a reflective intensity-based optical fiber sensor and a fiber Bragg grating", IEEE Sens. J. **2**, 482–487 (2002).

12. T.L. Yeo, D. Eckstein, B. McKinley, L.F. Boswell, T. Sun and K.T.V. Grattan, "Demonstration of a fiber-optic sensing technique for the measurement of moisture absorption in concrete", Smart Mater. Struct. **15**, N40–N45 (2006).

13. T. Venugopalan, Teck L. Yeo, Tong Sun, and Kenneth T. V. Grattan, "LPG-Based PVA Coated Sensor for Relative Humidity Measurement", IEEE Sens. J. **8**, 1093-1098 (2008)

14. A.P. Russell and K.S. Flectcher, "Optical sensor for determination of moisture", Anal. Chem. Acta., **170**, 209-216 (1985).

15. D.S. Ballantine, "Optical waveguide humidity sensor", Anal. Chem. **58**, 2883-2885 (1986).

16. Q. Zhou, M.R. Shahriari, D. Kritz and G.H. Sigel, "Porous fiber-optic sensor for high-sensitivity humidity measurement", Anal. Chem. **60**, 2317-2320 (1988).

17. A. Gaston, I. Lozano, F. Perez, F. Auza, and J. Sevilla, "Evanescent wave optical-fiber sensing (Temperature, Relative Humidity, and pH Sensors)", IEEE Sens. **3**, 806-811 (2003).

18. B.D. Gupta and Ratnanjali, "A novel probe for a fiber optic humidity sensor," Sens. Actuators B **80**, 132-135 (2001).

19. S.K. Khijwania, K.L. Srinivasan and J.P. Singh, "Performance optimized optical fiber sensor for humidity measurement" Opt. Eng. **44**, 34401(1-7) (2005).

20. D. Viegas, J. Goicoechea, J.L. Santos, F.M. Araujo, L.A. Ferreira, F.J. Arregui and I.R. Matias, "Sensitivity improvement of a humidity sensor based on Silica Nanosphers on a Long-Period Fiber grating", Sensors **9**, 519-527 (2009).

21. S. Muto, O. Suzuki, T. Amano and M. Morisawa, "A plastic optical fiber sensor for real-time humidity monitoring" Meas. Sci. Technol. **14**, 746-750 (2003).

22. R. Aneesh and Sunil K. Khijwania, "Titanium dioxide nanoparticle based optical fiber humidity sensor with linear response and enhanced sensitivity", Appl. Opt. **51**, 2164-2171 (2012)

23. S. Tao, C.B. Winstead, R. Jindal and J.P. Singh, "Optical-fiber sensor using tailored porous sol–gel fiber core", IEEE Sens. J. **4**, 322–328 (2004).

24. T.E. Brook, M.N. Taib and R. Narayanaswamy, "Extending the range of a fibre-optic relative humidity sensor", Sens. Actuators B, **38–39**, 272– 276 (1997).

25. H.E. Posch and O.S. Wolfbeis, "Fiber-optic humidity sensor based on fluorescence quenching", Sens. Actuators **15**, 77–83 (1988).

26. M. Bedoya, M.T. Diez, M.C. Moreno-Bondi and G. Orellana, "Humidity sensing with a luminescent Ru(II) complex and phase-sensitive detection", Sens. Actuators B **113**, 573–581 (2006).

27. A. Kharaz and B. Jones, "A distributed fibre optic sensing system for humidity measurement", Meas. Contr. **28**, 101–103 (1995).

28. R. Jindal, S. Tao, J.P. Singh and P.S. Gaikwad, "High dynamic range fiber optic relative humidity", Opt. Eng. **41**, 1093–11093 (2002).
29. F.J. Arregui, Z. Ciaurriz, M. Oneca and I.R. Matias, "An experimental study about hydrogels for the fabrication of optical fiber humidity sensors", Sens. Actuators B **96**, 165-172 (2003).
30. C. Bariain, I.R. Matias, F.J. Arregui and M. Lopez-Amo, "Optical fiber humidity sensor based on a tapered fiber coated with agarose gel", Sens. Actuators B **69**, 127–131 (2000).
31. J.M. Corres, J. Bravo and I.R. Matias, "Nonadiabatic tapered single-mode fiber coated with humidity sensitive nanofilms", IEEE Photonics Technol. Lett. **18**, 935–937 (2006).
32. A. Gaston, F. Perez and J. Sevilla, "Optical fiber relative humidity sensor with polyvinyl alcohol film", Appl. Opt. **43**, 4127–4132 (2004).
33. A. Alvarez-Herrero, H. Guerrero and D. Levy, "High-sensitivity sensor of a low relative humidity based on overlay on side-polished fibers", IEEE Sens. J. **4**, 52–56 (2004).
34. K. Ogawa, S. Tsuchiya and H. Kawakami, "Humidity sensing effects of optical fibers with microporous SiO_2 cladding", Electron. Lett. **24**, 42–43 (1988)
35. L. Xu, J.C. Fanguy, K. Soni and S. Tao, "Optical fiber humidity sensor based on evaenscent wave scattering", Opt. Lett. **29**, 1191–1193 (2004).
36. P. Kronenberg, P.K. Rastogi, P. Giaccari and H.G. Limberger, "Relative humidity sensor with optical fiber Bragg grating", Opt. Lett. 27, 1385–1387 (2002).
37. K.M. Tan, C.M. Tay, S.C. Tjin, C.C. Chan and H. Rahardjo, "High relative humidity measurements using gelatin coated long-period grating sensors", Sens. Actuators B **110**, 335–341 (2005).
38. M. Konstantaki, S. Pissadaki, S. Pispas, N. Madamopoulous and N.A. Vainos, "Optical fiber long period grating humidity sensor with PEO/CoCl2 coating", Appl. Opt. **45**, 4567–4571 (2006).
39. F. Mitschke, "Fiber optic sensor for humidity", Opt. Lett. **14**, 967–969 (1989).
40. F.J. Arregui, Y. Liu, I.R. Matias and R.O. Claus, "Optical fiber humidity sensor using a nano Fabry–Perot cavity formed by the ionic self-assembly method", Sens. Actuators B **59**, 54–59 (1999).
41. S. Otsuki and K. Adachi, "Humidity dependence of visible absorption spectrum of gelatin films containing cobalt chloride", J. Appl. Polym. Sci. **45**, 1557–1564 (1993).
42. F. Boltinghouse and K. Abel, "Development of an optical relative humidty sensor. Cobalt chloride optical absorbency sensor study", Anal. Chem. **61**, 1863–1866 (1989).
43. M. Ando, T. Kobayashi and M. Harutu, "Humidity-sensitive optical absorption of Co_3O_4 film", Sens. Actuators B **32**, 157–160 (1996).
44. S. Otsuki, K. Adachi and T. Taguchi, "A novel fiber-optic gas sensing arrangement based on an air gap design and an application to optical detection of humidity", Anal. Sci. **14**, 633–635 (1998).
45. Pi-Guey Su, Lin-Nan Huang, "Humidity sensors based on TiO2 nanoparticles/ polypyrrole composite thin films", Sens. Actuators B **123**, 501–507 (2007).
46. T.M. Racheva and G.W. Critchlow, "SnO_2 thin films prepared by the sol-gel process", Thin Solid Films **292**, 299-302 (1997).
47. Jesus M. Corres, Ignacio R. Matias, Miguel Hernaez, Javier Bravo, Francisco J. Arregui, "Optical Fiber Humidity Sensors Using Nanostructured Coatings of SiO2 Nanoparticles", IEEE Sens. J. **8**, 281-285 (2008)

143

48. D.V. Andreev, L.L. Makarshin and V.N. Parmon, "Sorption and Sensing Characteristics of Polyvinyl Alcohol Films Impregnated with $CaCl_2$", React.Kinet.Catal.Lett. **80**, 181-188 (2003).

49. S. Luo, Y. Liu, A. Sucheta, M. Evans and R. van Tassell, "Applications of LPG fiber optical sensors for relative humidity and chemical warfare agents monitoring", Proc. SPIE **4920**, 193-204 (2002)

50. T. Venugopalan, T. Sun, K.T.V. Grattan, "Long period grating-based humidity sensor for potential structural health monitoring", Sens. Actuators, B **148**, 57–62(2008)

51. LiweiWang, Yang Liu, Min Zhang, Dongsheng Tu, Xianhui Mao and Yanbiao Liao, "A relative humidity sensor using a hydrogel-coated long period grating", Meas. Sci. Technol. **18**, 3131–3134 (2007).

52. Razat Nohria, Rajneek K. Khillan, Yi Su, Rohit Dikshit, Yuri Lvov and Kody Varahramyan, "Humidity sensor based on ultrathin polyaniline film deposited using layer-by-layer nano-assembly", Sens. Actuators, B **114**, 218–222 (2006).

53. Anu Vijayan, Madhavi Fuke, Ranjit Hawaldar, Milind Kulkarni, D. Amalnerkar, R.C. Aiyer, "Optical fiber based humidity sensor using Co-polyaniline clad", Sens. Actuators, B **129**, 106–112 (2008)

54. Christopher A. Murray and John R. Dutcher, "Effect of Changes in Relative Humidity and Temperature on Ultrathin Chitosan Films", Biomacromolecules **7**, 3460-3465 (2006)

55. Jinesh Mathew, K. J. Thomas, V. P. N. Nampoori and P. Radhakrishnan, "A Comparative Study of Fiber Optic Humidity Sensors Based on Chitosan and Agarose", Sensors & Transducers Journal **84**, 1633-1640 (2007)

56. Jinesh Mathew, YuliyaSemenova, GinuRajan, PengfeiWang, GeraldFarrell, "Improving the sensitivity of a humidity sensor based on fiber bend coated with a hygroscopic coating", Opt. Laser Technol. **43**, 1301–1305 (2011).

57. X.F. Huang, D.R. Sheng, K.F. Cen and H. Zhou, "Low-cost relative humidity sensor based on thermoplastic polyimide-coated fiber Bragg grating", Sens. Actuators, B **127**, 518–524 (2007).

58. Madhavi V. Fuke, Anu Vijayan, Prajakta Kanitkar and R. C. Aiyer, "Optical Humidity Sensing Characteristics of Ag-Polyaniline Nanocomposite", IEEE Sens. J. **9**, 648-653 (2009).

59. Y. Sakai, Y. Sadaoka, M. Matsuguchi, "Humidity sensors based on polymer thin films", Sens. Actuators, B **35-36**, 85-90 (1996).

60. Pradip Kumar Dutta, Joydeep Dutta and V S Tripathi, "Chitin and chitosan: Chemistry, properties and applications", J. Sci. Ind. Res. 63, 20-31 (2004).

61. Marguerite Rinaudo, "Chitin and chitosan: Properties and applications", Prog. Polym. Sci. **31**, 603–632 (2006).

62. Esam A. El-Hefian, Mohamed Mahmoud Nasef and Abdul Hamid Yahaya, "The Preparation and Characterization of Chitosan / Poly (Vinyl Alcohol) Blended Films", E-J. Chem. **7,** 1212- 1219 (2010).

63. Shadie Hatamie , Vivek Dhas , B.B. Kale , I.S. Mulla and S.N. Kale, "Polymer-embedded stannic oxide nanoparticles as humidity sensors Mater. Sci. Eng., C **29**, 847–850 (2009).

64. Pi-Guey Su , Yi-Lu Sun, Chu-Chieh Lin, "Humidity sensor based on PMMA simultaneously doped with two different salts", Sens. Actuators, B **113**, 883–886 (2006)

65. Majeti N.V. Ravi Kumar, "A review of chitin and chitosan applications", React. Funct. Polym. **46**, 1–27 (2000)

66. C.K.S. Pillai,Willi Paul and Chandra P. Sharma," Chitin and chitosan polymers: Chemistry, solubility and fiber formation", Prog. Polym. Sci. **34**, 641–678 (2009).
67. M. Dash, F. Chiellini, R.M. Ottenbrite, E. Chiellini, "Chitosan—A versatile semi-synthetic polymer in biomedical applications", Prog. Polym. Sci. **36**, 981–1014 (2011).
68. Yumiko Nakano, Yuezhen Bin, Mami Bando, Teruo Nakashima, Tsumuko Okuno, Hiromichi Kurosu and Masaru Matsuo, "Structure and Mechanical Properties of Chitosan/Poly(Vinyl Alcohol) Blend Films", Macromol. Symp. **258**, 63–81 (2007).
69. Hua Zheng, Yumin Du, Jiahui Yu, Ronghua Huang and Lina Zhang, "Preparation and Characterization of Chitosan/Poly(vinyl alcohol) Blend Fibers", J. Appl. Polym. Sci. **80**, 2558–2565 (2001)
70. Ezequiel S. Costa-Junior, Edel F. Barbosa-Stancioli, Alexandra A.P. Mansur, Wander L. Vasconcelos and Herman S. Mansur, "Preparation and characterization of chitosan/poly(vinyl alcohol) chemically crosslinked blends for biomedical applications", Carbohydr. Polym.**76**, 472–481(2009).
71. H.M.P. Naveen Kumar, M.N. Prabhakar, C. Venkata Prasad, K. Madhusudhan Rao, T.V. Ashok Kumar Reddy, K. Chowdoji Rao, M.C.S. Subha, "Compatibility studies of chitosan/PVA blend in 2% aqueous acetic acid solution at 30 ∘C", Carbohydr. Polym. **82** ,251–255 (2010)
72. Toshio Watanabe, Naoki Ooba, Yasuhiro Hida, and Makoto Hikita, "Influence of humidity on refractive index of polymers for optical waveguide and its temperature dependence", Appl. Phys. Lett. **72**, 1533-1535 (1998).
73. Bishnu P. Pal, Fundamentals of Fiber Optics in Telecommunication and Sensor Systems (New Age Publishers, New Delhi, 1992)
74. M Sheeba, M Rajesh, C P G Vallabhan, V P N Nampoori and P Radhakrishnan, "Fiber optic sensor for the detection of adulterant traces in coconut oil", Meas. Sci. Technol. **16**, 2247–2250 (2005)

Conclusions and Future Prospects

Fiber optic sensor is a vital topic and for the past four decades, rigorous research in this area has been undertaken around the globe. A wide variety of fiber optic sensors were reported and many of them have been commercialized. Though fiber optic sensors have inherent advantages over other sensing technologies, in terms of commercialization they face competition in terms of cost. So it is worthwhile to develop less expensive fiber optic sensors and in this thesis the design and development of some fiber optic sensors for quality evaluation is discussed.

The design and fabrication of a fiber optic sensor probe for detection of critical mole fraction and purity of alcohol is discussed first. The intensity modulated extrinsic optical fiber sensor probe is fabricated by chemically etching a plastic clad silica fiber using hydro fluoric acid. The probe couples light through the tapered region and the theory of working was verified using simulation results. The added use of the probe as a water level detector is also explained. The probe was used for the measurement of critical concentration of binary mixtures of alcohol and water. The critical mole fractions obtained using the robust and inexpensive probe for methanol, ethanol, 2-propanol and tert-butanol agrees well with the values obtained using methods like neutron diffraction studies and microwave analysis. Unlike lower alcohols like methanol, ethanol and propanol, micellization occurs in tert-butanol water mixtures and the results obtained using this probe also give an evidence for the phenomenon. The probe can be effectively used for concentration detection of alcohol water mixtures, which has applications in food and beverage industries.

We demonstrate the fabrication and characterization of long period fiber gratings. The fabrication process of LPFGs in SMF 28 using fusion splicer and carbon dioxide (CO_2) laser is explained. The fabrication methods discussed using arc and CO_2 laser are found to be much more flexible and cost effective than the UV laser exposure technique. The possible mechanisms of refractive index modulations in the fabricated asymmetric LPFGs are due to residual stress relaxation and physical deformation. The

temperature sensitivities of the three types of LPFGs namely, arc induced, CO_2 laser induced and UV induced, are determined and compared in the temperature range 25^0C to 80^0C. The periodically tapered LPFG fabricated using electric arc from fusion splicer is found to be insensitive to temperature in the range of experimental studies. For many telecommunication applications spectral stability is of prime importance, and an LPFG with temperature insensitive attenuation band is an attractive feature. The fabricated LPFG is also attractive for fabricating temperature-insensitive sensors.

The effective application of LPFG's in determining the quality of ethanol blended petrol is presented. The response of the fabricated LPFG's namely UV, electric arc and CO_2 induced long period fiber gratings towards ambient refractive indices are studied. Though the UV induced LPFG shows better refractive index sensitivity near the cladding refractive index, the arc induced LPFG has a better sensitivity in the 1 to 1.4 refractive index region. Besides being insensitive to temperature, the periodically tapered arc induced LPFG shows better sensitivity among the three LPFG's in determining the purity of ethanol blended petrol. The periodically tapered arc induced LPFG can be successfully utilized as a temperature insensitive transducer for quality evaluation of ethanol blended petrol.

We have also demonstrated the design of polymer coatings which can be effectively used in fiber optic sensors. Humidity sensors are designed using polymers like poly vinyl alcohol and chitosan blended poly vinyl alcohol as hygrosensitive coatings. Both PVA and chitosan/PVA blend are sensitive to humidity and their refractive index is found to decrease with increase in ambient humidity. Blending of chitosan in PVA helps to improve its mechanical strength and the available hydrophilic head groups per unit volume. Though found sensitive to humidity, the humidity response of the chitosan/PVA blend is not linear. A better and linear response towards humidity is obtained by blending titanium dioxide with the polymer. Blending of titanium dioxide powder in the polymer matrix is found to give better sensitivity towards humidity than bare polymer due to the increase in available hydrophilic heads. The humidity sensitivity is found to increase when titanium dioxide is blended in chitosan/PVA matrix compared to pure PVA. The humidity sensitivity is found to increase with increase in titanium dioxide concentration.

Future prospects

The works detailed in this thesis can form the basis for the development of a variety of sensors and improvements can also be done on the technologies explained. A list of few possible future works is given below

- The thermal insensitivity of arc induced long period fiber grating (LPFG) can be studied in detail over a large temperature range.
- The TiO_2 embedded chitosan/PVA film can be further analyzed for its effectiveness as coating material for fiber optic alcometer
- The variation in humidity sensitivity can be studied by embedding nano TiO_2 instead of bulk TiO_2 material.
- LPFG coated with TiO_2 embedded chitosan/PVA film can be studied for its humidity sensitivity.